

## 8. Experimentelle Tests der Quantenchromodynamik

8.1 QCD-Tests in  $e^+e^-$ -Kollisionen

8.2 QCD-Effekte in der tief-inelastischen Lepton-Nukleon-Streuung

8.3 Test der QCD in Proton-Antiproton-Kollisionen

8.4 Bestimmung der starken Kopplungskonstanten  $\alpha_s$

8.5 Eigenschaften der Gluonen (Spin, Selbstkopplung)

# 8.1 QCD-Tests in $e^+e^-$ - Kollisionen

1977: DESY macht die Gluonen sichtbar

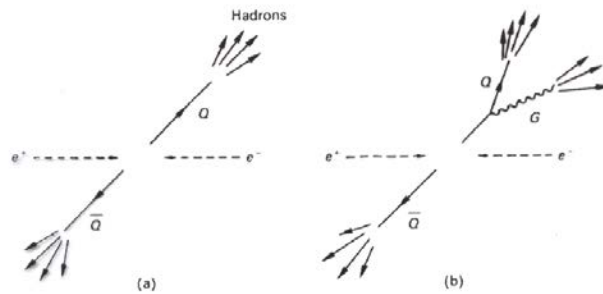
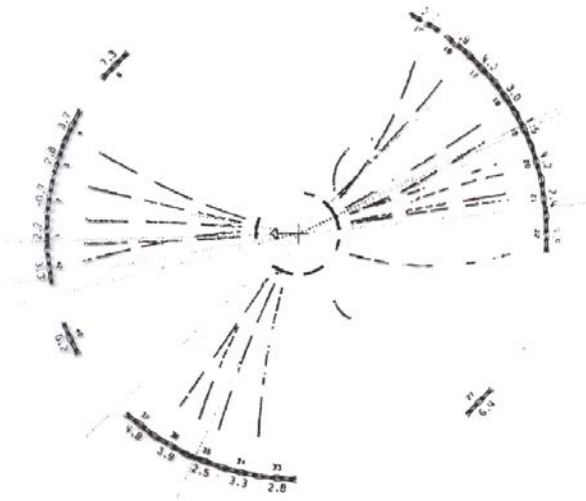


Fig. 8.27



**Table 3.**  $e^+e^-$  colliders and experiments.

Facility	Location	$\sqrt{s}$ [GeV]	Experiments
ACO [84]	LAL Orsay	$\approx 1$	M3N [85, 86]
ADONE [87]	INFN Frascati	1 – 3	Boson [88], $\mu\pi$ [89], $\gamma\gamma$ [90], $\gamma\gamma 2$ [91], MEA [92]
VEPP-2 [93]	Novosibirsk	1 – 1.5	VEPP-2 [93]
CEA [94]	Cambridge, MA	4	BOLD [95]
SPEAR [96]	SLAC Stanford	2 – 8	SLAC-LBL [97, 98], MARK I [99], MARK II [100]
PEP [101]	SLAC Stanford	29	MARK II [102], HRS [103], TPC/ $2\gamma$ [104, 105], MAC [106]
DORIS [107, 108]	DESY Hamburg	3 – 11	PLUTO [109], DASP [110, 111], LENA [112], DH(HM) [113, 114]
CESR [115]	Cornell, Ithaca	10 – 11	CLEO [116, 117], CUSB [118, 119]
→ PETRA [120]	DESY Hamburg	12 – 47	CELLO [121], JADE [122], MARK J [123], PLUTO [109], TASSO [110, 124]
TRISTAN [125]	KEK Tsukuba	50 – 64	TOPAZ [126], VENUS [127], AMY [128]
SLC [129]	SLAC Stanford	$\approx 91$	MARK II [102], SLD [130]
→ LEP [131]	CERN Geneva	88 – 209	ALEPH [132, 133], DELPHI [134, 135], L3 [136], OPAL [137]

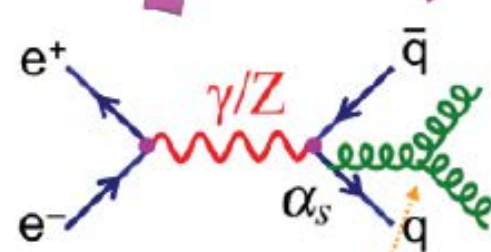
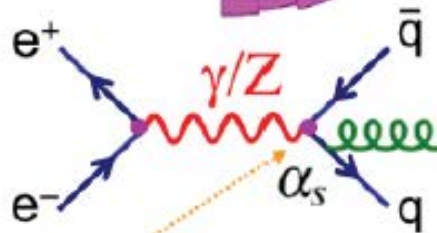
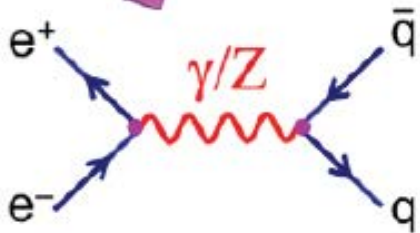
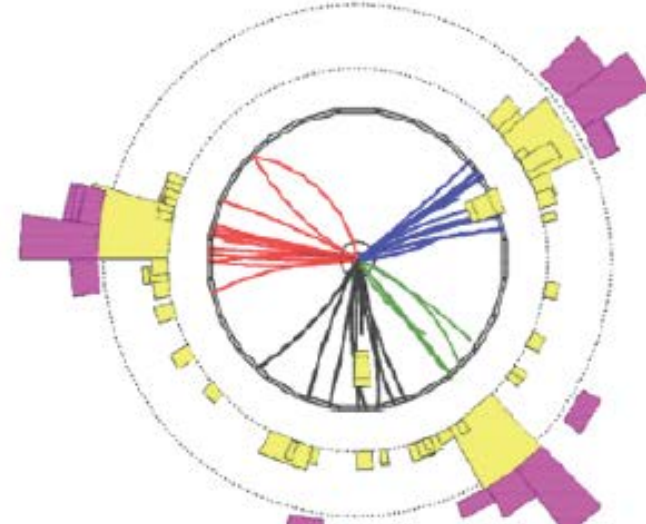
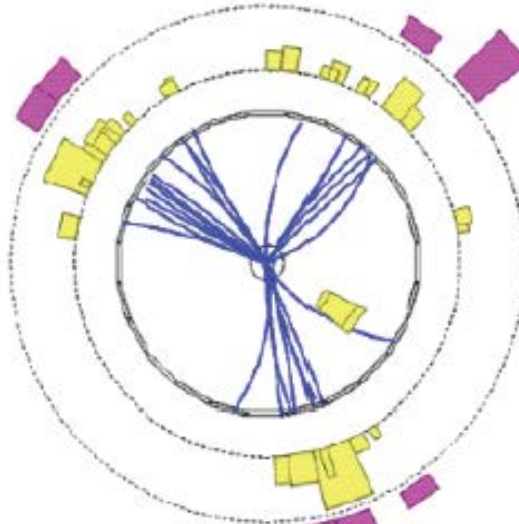
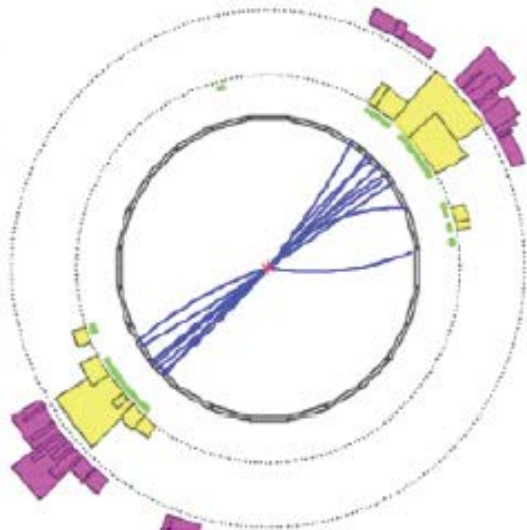
★  $e^+e^-$  colliders are also a good place to study gluons

$$e^+e^- \rightarrow q\bar{q} \rightarrow 2\text{jets}$$

$$e^+e^- \rightarrow q\bar{q}g \rightarrow 3\text{jets}$$

$$e^+e^- \rightarrow q\bar{q}gg \rightarrow 4\text{jets}$$

OPAL at LEP (1989-2000)



**Experimentally:**

- Three jet rate → measurement of  $\alpha_s$
- Angular distributions → gluons are spin-1
- Four-jet rate and distributions → QCD has an underlying SU(3) symmetry

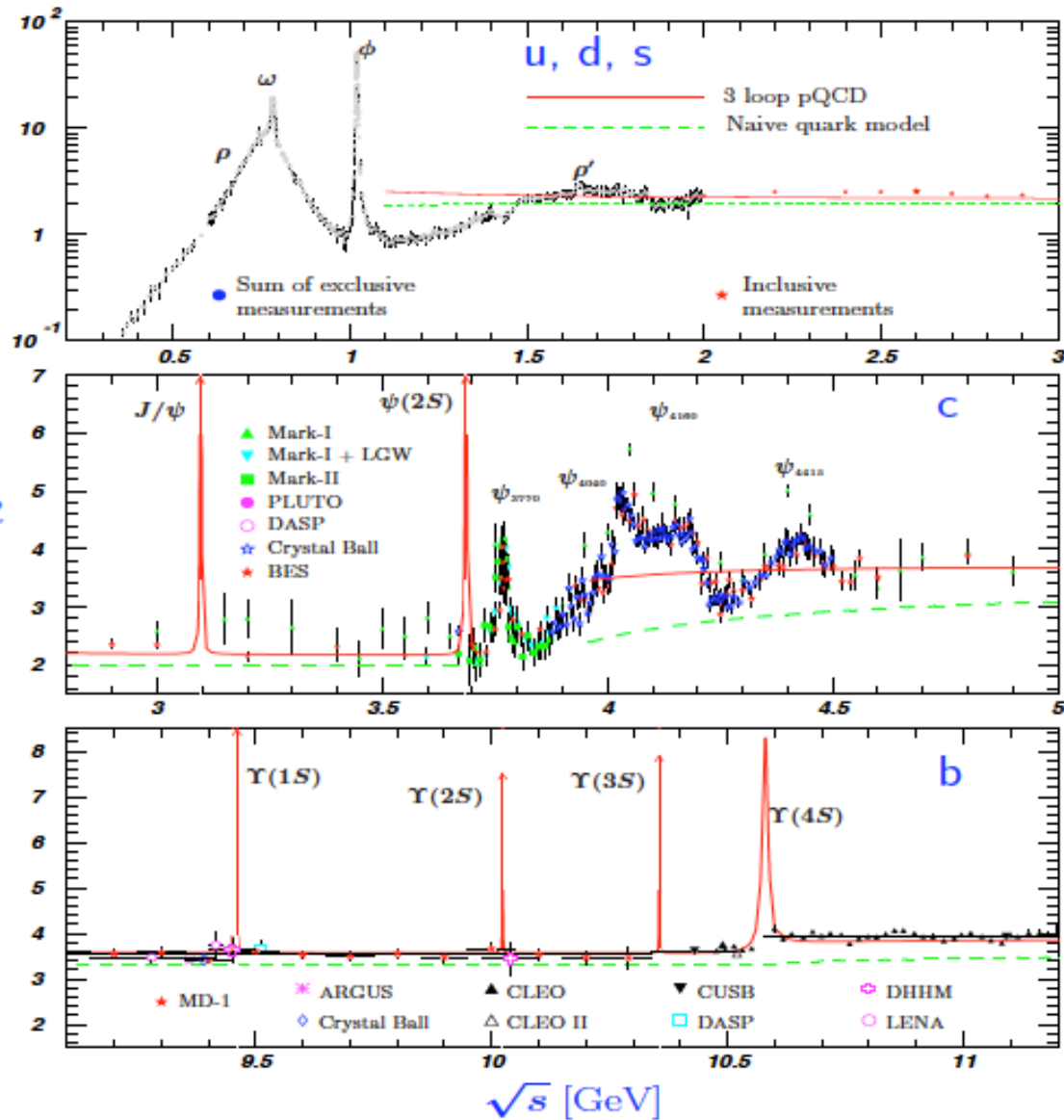
$$R = \frac{e^+e^- \rightarrow \text{Hadrons}}{e^+e^- \rightarrow \mu^+\mu^-}$$

$$\sigma(e^+e^- \rightarrow \text{Hadrons}) \propto \sigma(e^+e^- \rightarrow \mu^+\mu^-)$$

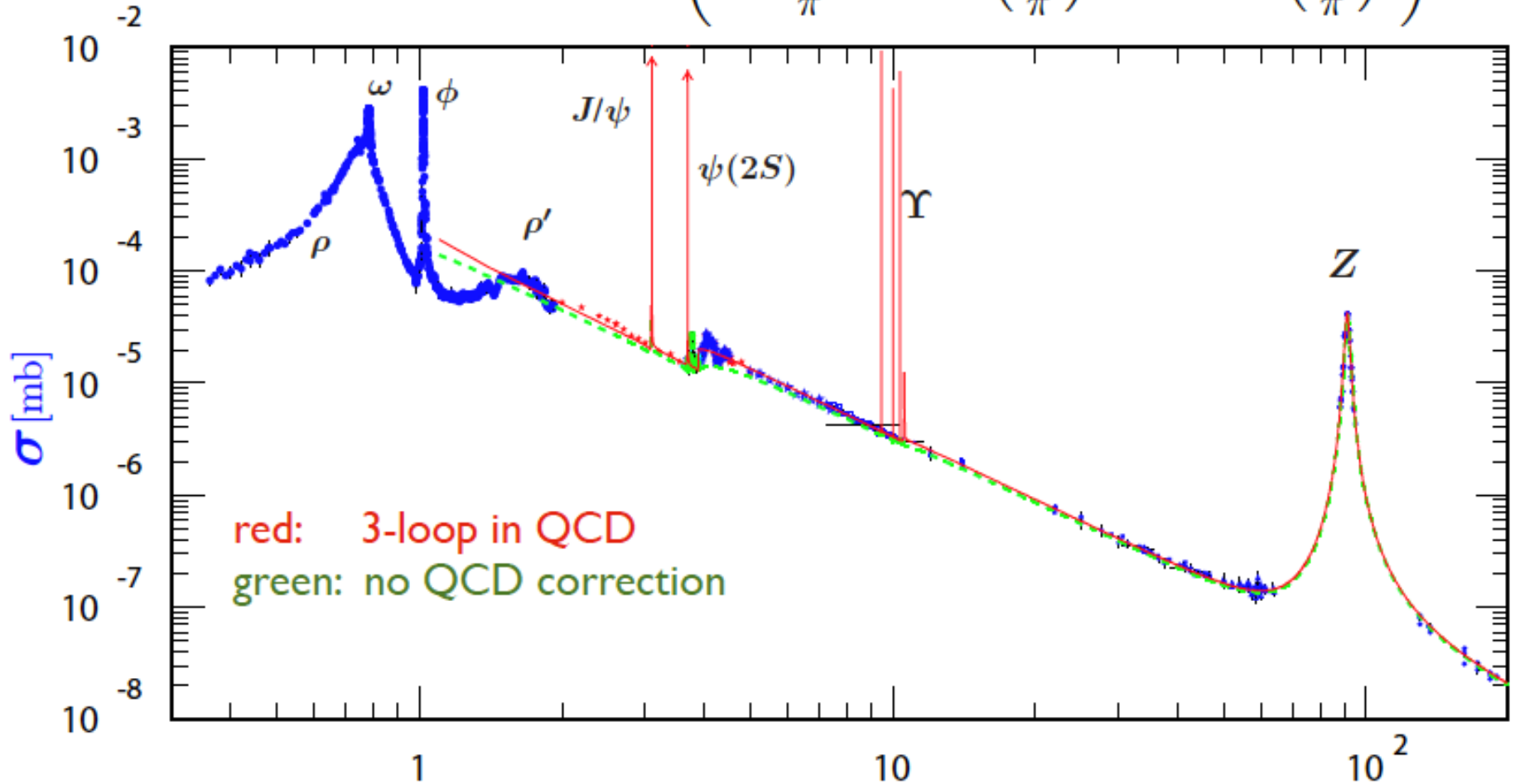
$$R = N_c \sum_{q=u,d,\dots} e_q^2$$

$$R = \begin{cases} \frac{2}{3}N_c & (u, d, s), \\ \frac{10}{9}N_c & (u, d, s, c), \\ \frac{11}{9}N_c & (u, d, s, c, b), \end{cases}$$

The R measurements are compatible with  $N_c=3$  (outside of the resonance region).



$$\sigma(e^+e^- \rightarrow \text{hadrons}) = \sigma_0 \left( 1 + \frac{\alpha_s}{\pi} + 1.409 \left( \frac{\alpha_s}{\pi} \right)^2 - 12.805 \left( \frac{\alpha_s}{\pi} \right)^3 \right)$$



# QCD – Korrekturen zum Prozess $e^+e^- \rightarrow$ Hadronen

$$\delta_{\text{QCD}}(Q) = \sum_{n=1}^{\infty} c_n \cdot \left( \frac{\alpha_s(Q^2)}{\pi} \right)^n$$

The first four terms in the  $\alpha_s$  series expansion are then to be found in Refs. 17, 18

$$c_1 = 1, \quad c_2 = 1.9857 - 0.1152n_f, \quad (9.9a)$$

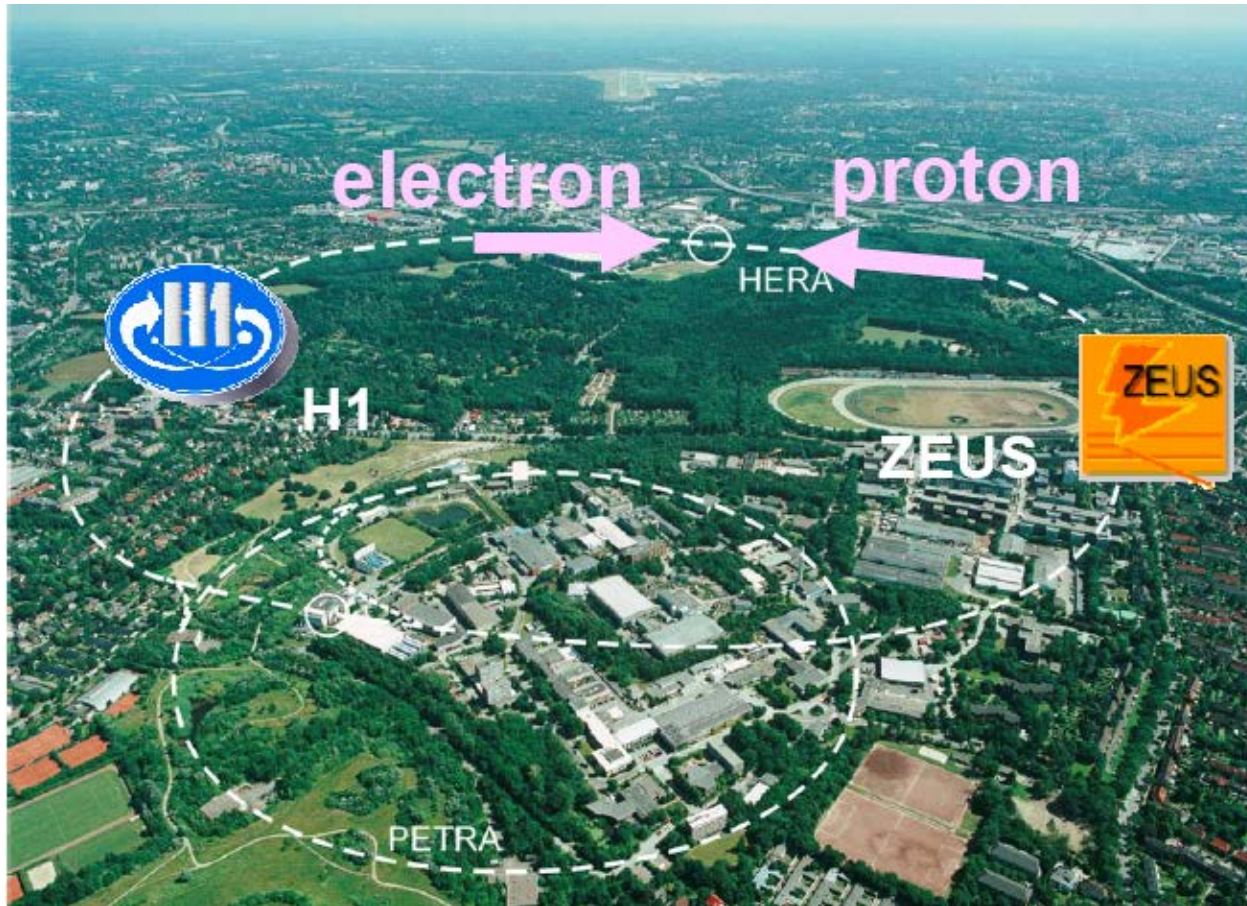
$$c_3 = -6.63694 - 1.20013n_f - 0.00518n_f^2 - 1.240\eta \quad (9.9b)$$

$$c_4 = -156.61 + 18.77n_f - 0.7974n_f^2 + 0.0215n_f^3 + C\eta, \quad (9.9c)$$

with  $\eta = (\sum e_q)^2 / (3 \sum e_q^2)$  and where the coefficient  $C$  of the  $\eta$ -dependent piece in the  $\alpha_s^4$  term has yet to be determined. For corresponding expressions including also  $Z$  exchange and finite-quark-mass effects, see Refs. 19, 20.

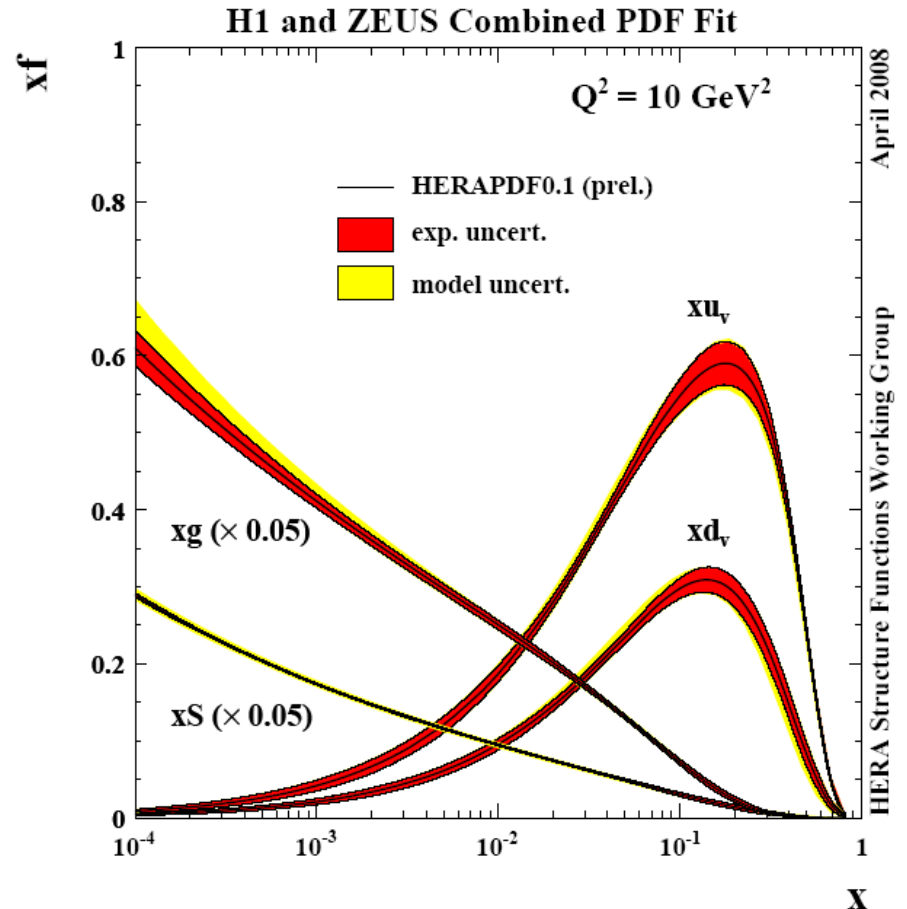
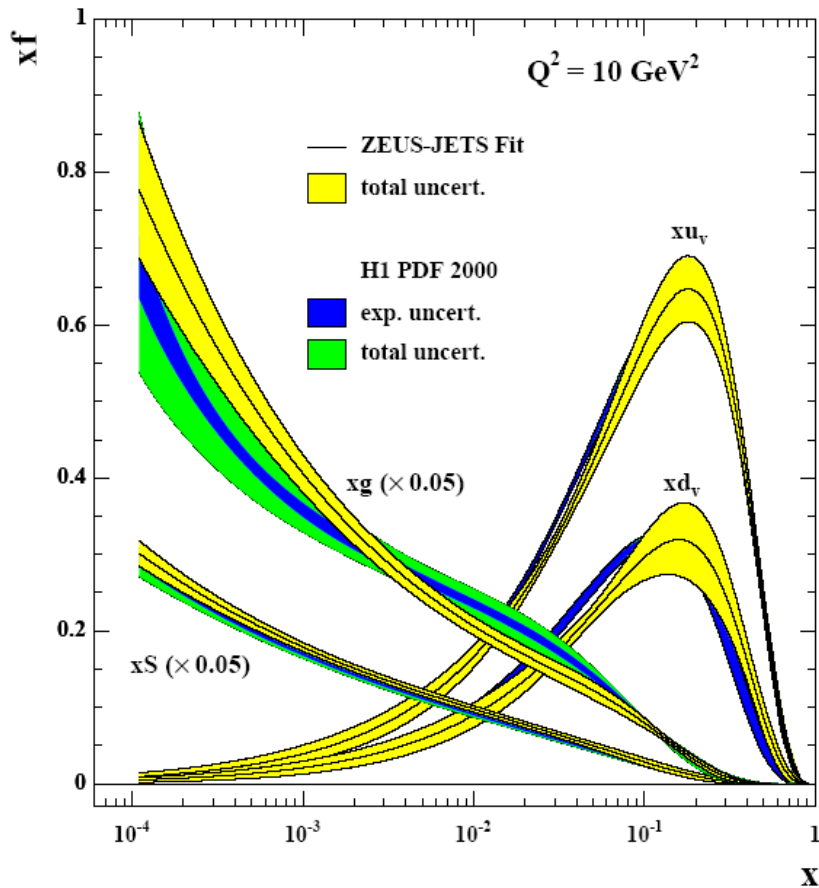
(from Rev. Particle Properties, Particle Data Group, PDG (2012))

## 8.2 Test der QCD in der tief inelastischen Lepton-Nukleon-Streuung

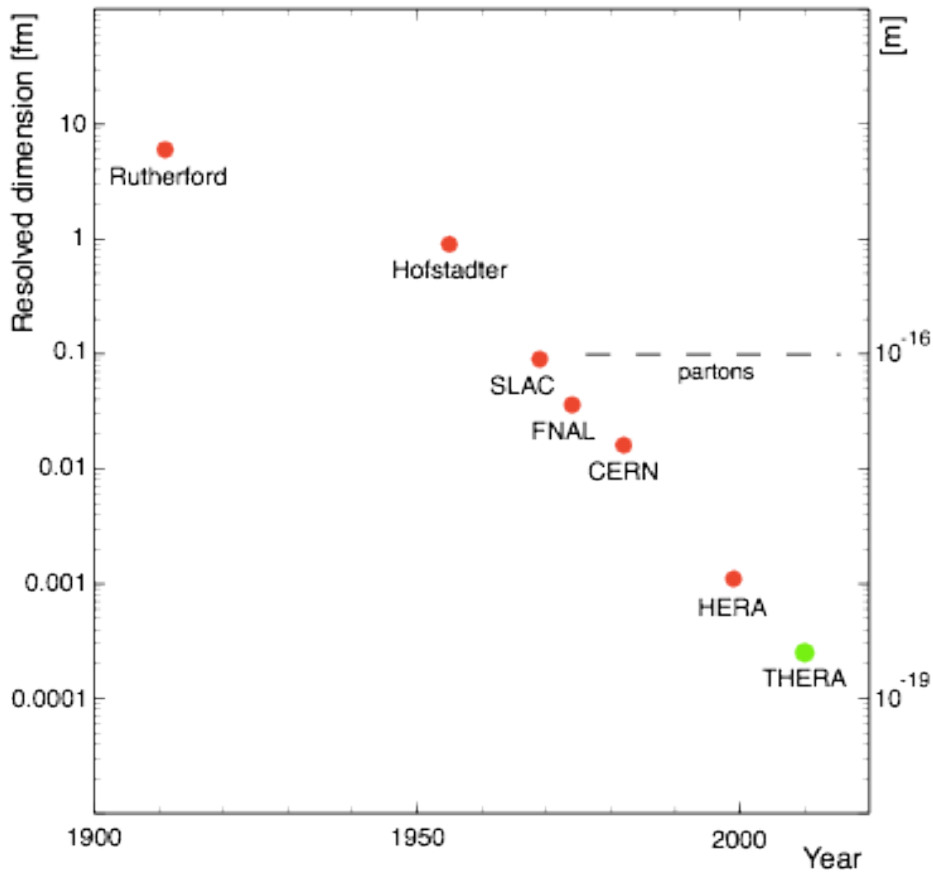
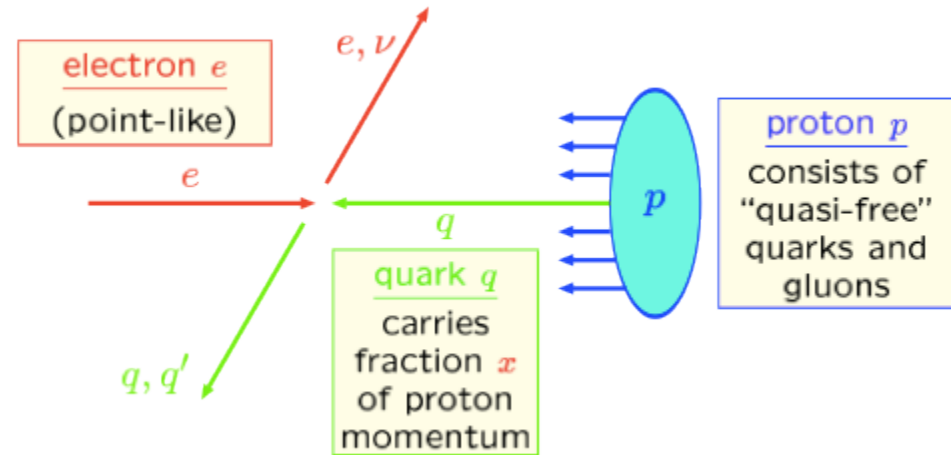


HERA-Beschleuniger am DESY in Hamburg (1990 – 2007:)  
Elektron/Positron-Proton Kollisionen: 30 GeV  $e^\pm$  auf 920 GeV p

# Parton Distribution functions (pdf)



# History of Deep Inelastic Scattering (DIS) experiments



**THERA** is an idea of an ep collider with a c.m.s. energy of 1 TeV,

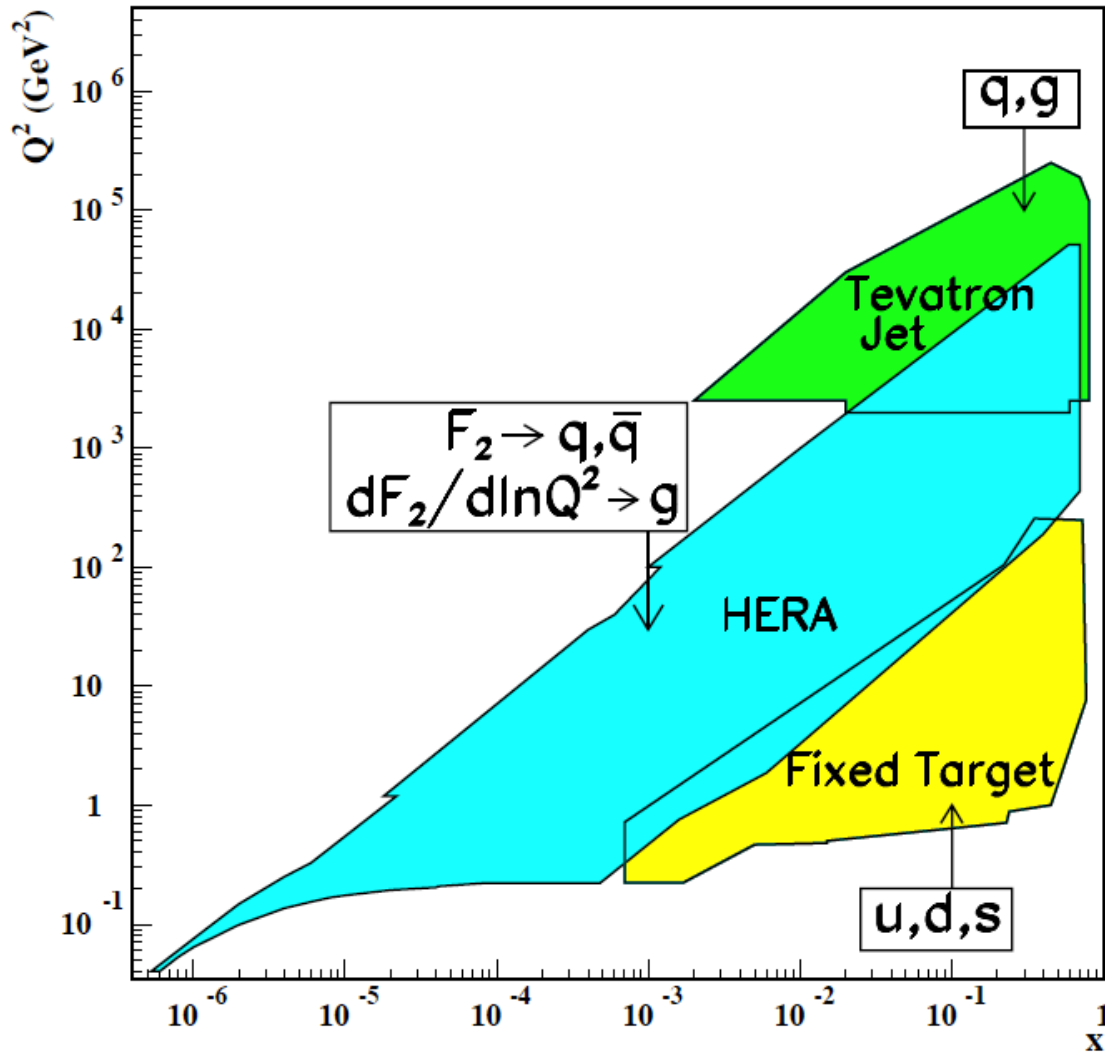
e.g. extend the LHC to collide electrons and protons

- The measurements of the parton distribution functions is the domain of Deep Inelastic Scattering (DIS) experiments

(BCDMS, NMC, ..., HERA)

- In addition, many processes measured at hadron colliders contribute

<u>Other experimental data:</u>		
reaction	subprocess	information
$p\bar{p} \rightarrow W + X$	$q\bar{q} \rightarrow W$	$u, d, u/d$
$\nu N \rightarrow \mu^+ \mu^- + X$	$\nu s \rightarrow \mu c$	$s$
$pp, pN \rightarrow \ell^+ \ell^- + X$	$q\bar{q} \rightarrow \ell^+ \ell^-$	$\bar{d}/\bar{u}$
$hh \rightarrow \gamma + X$	$qg \rightarrow q\gamma$	$g$
$p\bar{p} \rightarrow \text{jets} + X$	$gg \rightarrow gg$	$g, (q)$
	$gq \rightarrow gq$	
	$qq \rightarrow qq$	



Kinematic domains in  $x$  and  $Q^2$  probed by fixed-target and collider experiments, shown together with the constraints they make on the various parton distributions (from Particle Data Group).

deep inelastic  $ep$  scattering (DIS) =  
incoherent sum of elastic  $eq$  scattering:

$$\sigma(ep) = \sum_{q, \bar{q} \text{ in } p} f_{q|p} \cdot \sigma(eq)$$

parton distribution  $f_{q|p}(x)$ :

probability distribution  
to find a parton  
of flavor  $q$  with  
momentum fraction  $x$   
in the proton

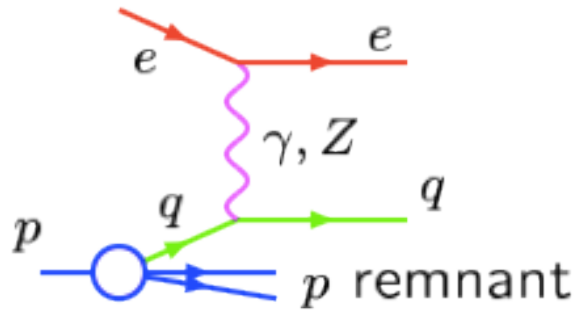
$\sigma(eq)$ :

differential  
 $eq$  cross section  
(depends on  
scattering angle and  
 $eq$  center-of-mass energy)

So, if parton distributions are known, the cross sections can be predicted,  
or vice versa: from a measurement of the cross sections, the parton distributions  
can be inferred

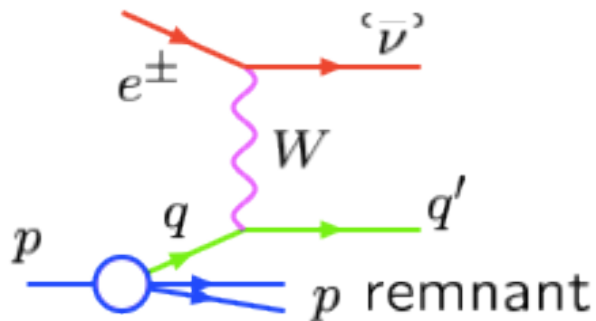
Important:  $Q^2$  dependence, QCD effects

# DIS Signatures



## Neutral Current (NC)

- Scattered electron  
⇒ isolated  
⇒ energy  $\gtrsim 10$  GeV
- One or more  
"central" jets
- Proton remnant  
energy deposition  
around beam pipe  
in  $p$  direction

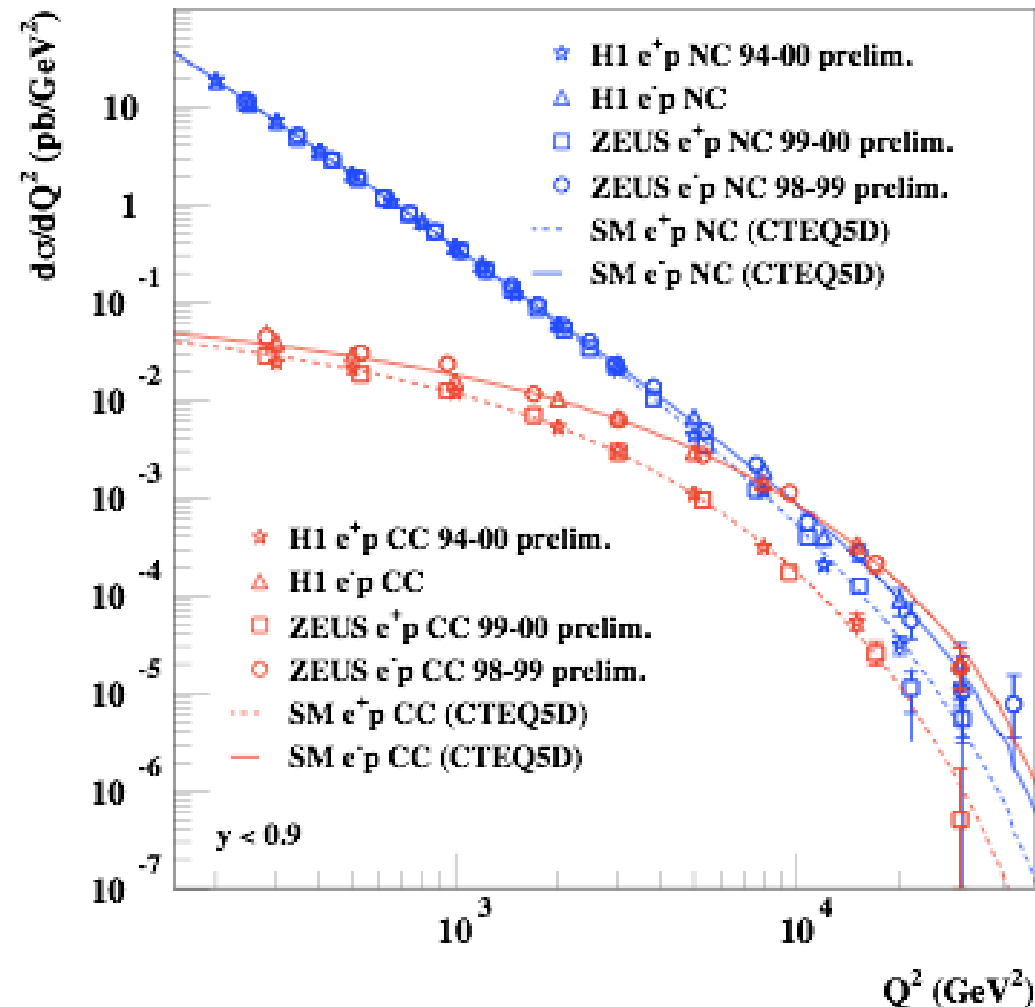


## Charged Current (CC)

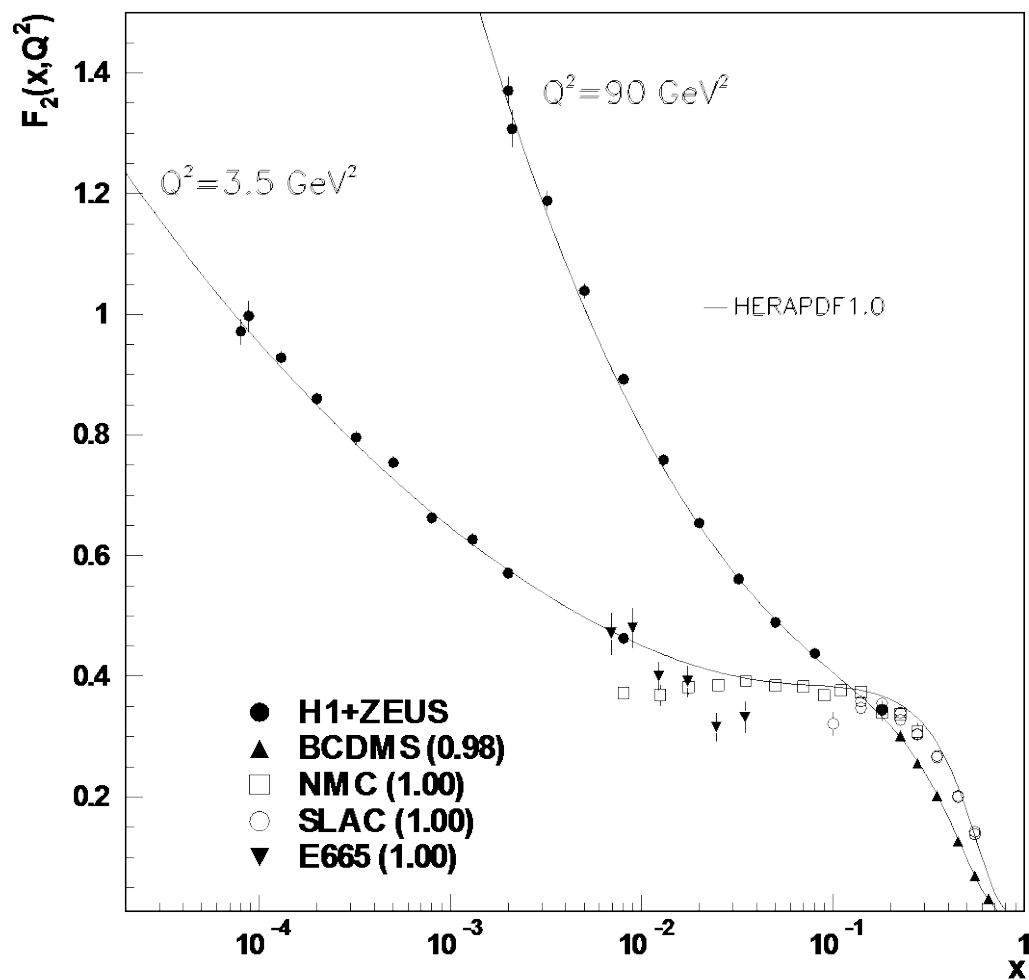
- Scattered neutrino  
⇒ invisible  
⇒ causes missing  
transverse  
momentum
- Hadronic final state  
⇒ as in NC reactions

# NC and CC cross sections

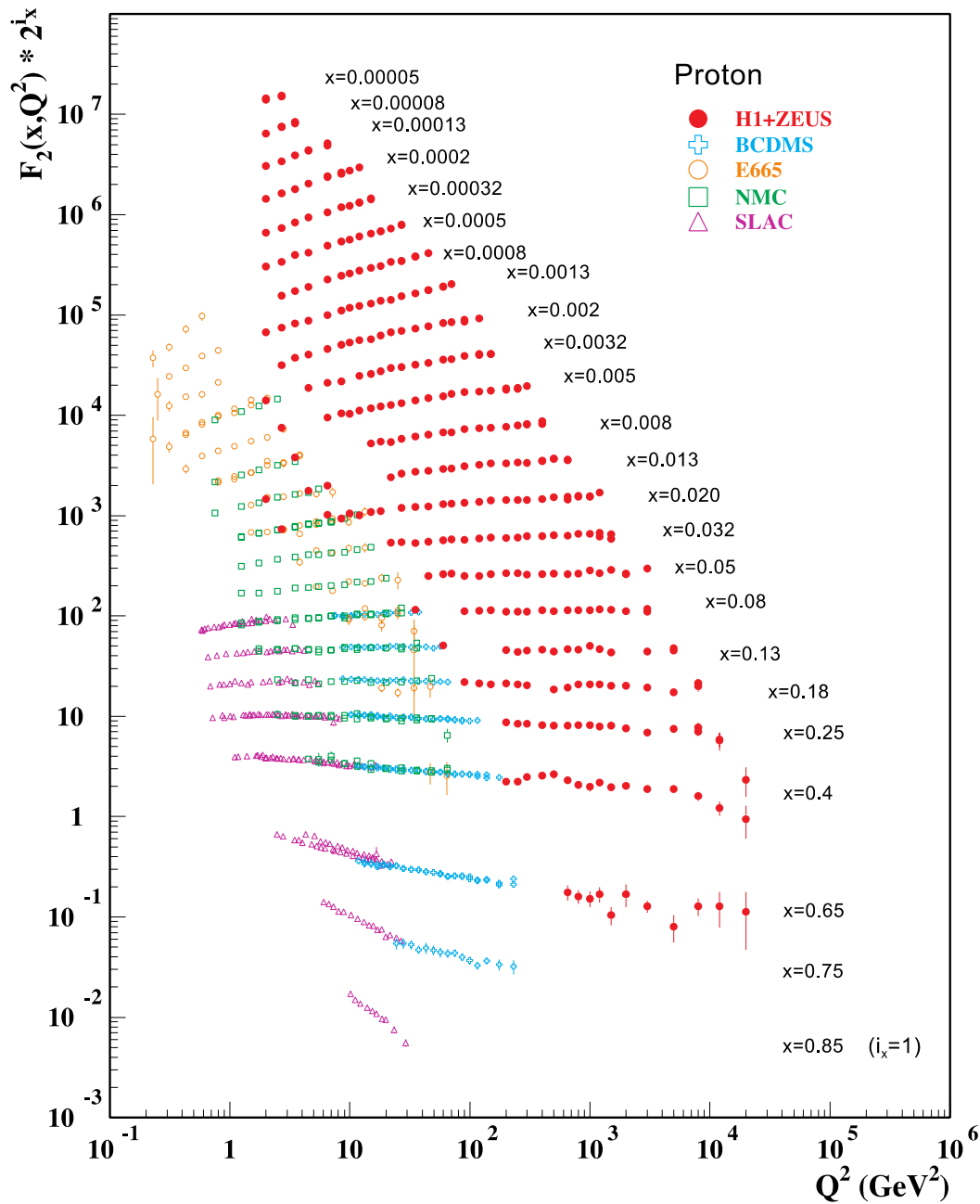
## Measurements of $d\sigma/dQ^2$ at HERA:



- HERA: first simultaneous measurements of NC and CC reactions,  $e^+p$  and  $e^-p$  in the same experiment.
- For  $Q^2 \gtrsim M_{W,Z}^2$  we have  $d\sigma/dQ^2(\text{NC}) \sim d\sigma/dQ^2(\text{CC})$  (electroweak unification).
- Cross sections vary by many orders of magnitude, measurements still statistics-dominated at high  $Q^2$ .



# The legacy of HERA



An enormous extension of the kinematic range both to high  $Q^2$  and to low  $x$

- low  $x$ : significant constraints on the gluon
- high  $Q^2$ :  $W/Z$  exchange and probe of the electroweak sector.

# The principle of the pdf determination

- The parton distribution functions cannot be described from first principles. A parametrization is performed at a reference scale  $Q_0$  as a function of  $x$

For  $p = u_v, d_v, \sum_q (q + \bar{q}), g$  and also for  
 $p = \bar{u} + \bar{d}, \bar{u} - \bar{d}, s$  :

$$xp(x, Q_0^2) = A_p x^{a_p} (1-x)^{b_p} P(x; c_p, \dots)$$

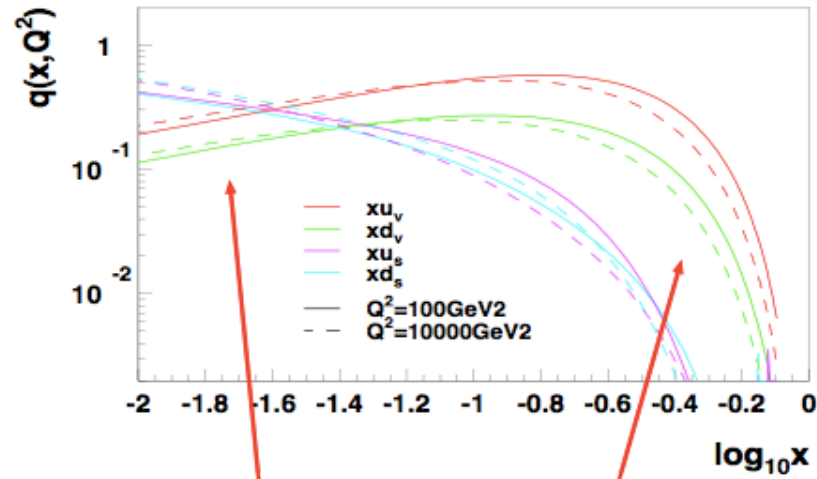
characterizes  
PDFs at  $x = 0$   
(sea:  $a_p < 0$ , pole;  
valence:  $a_p > 0$ )

characterizes  
PDFs at  $x = 1$   
( $b_p > 0$  for all  
PDFs)

weakly  
 $x$ -dependent  
function  
("fine tuning")

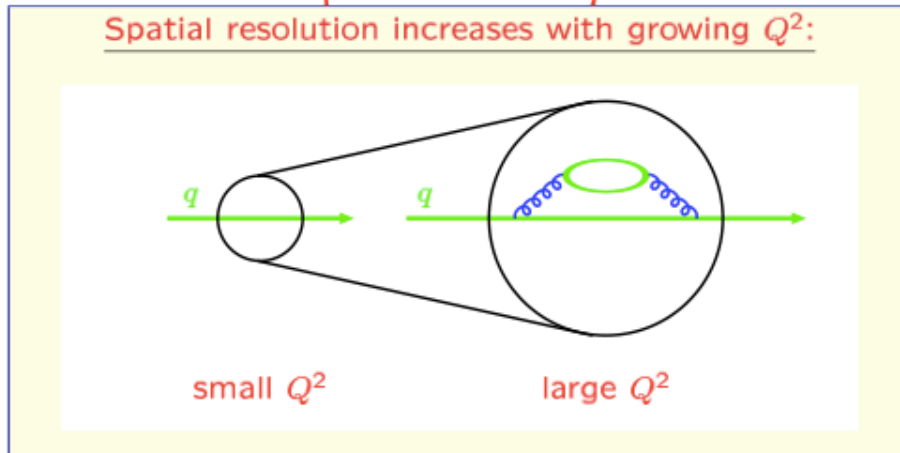
- The QCD evolution (DGLAP) is used to calculate the pdfs at a higher  $Q^2$  scale (up to NLO, partly NNLO precision)
- Predictions for experimental observables (cross sections, structure functions, ...) are calculated
- pdf parameters are determined from a  $\chi^2$  fit to the experimental data
- Fits are performed by several groups: CTEQ, MRST, ....

# Scaling violations via QCD effects

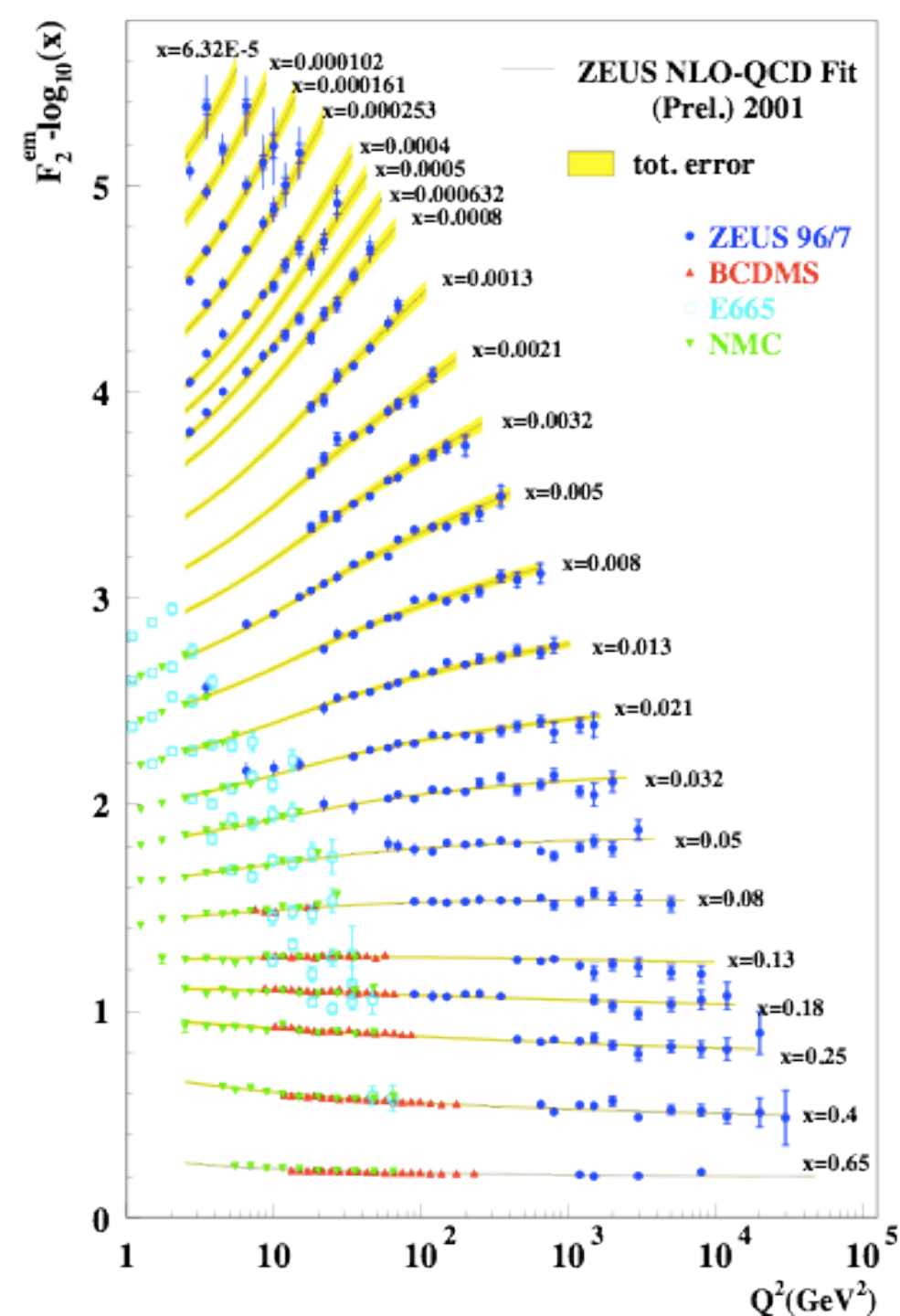


small  $x$ :  
PDFs increase  
with  $Q^2$

large  $x$ :  
PDFs decrease  
with  $Q^2$



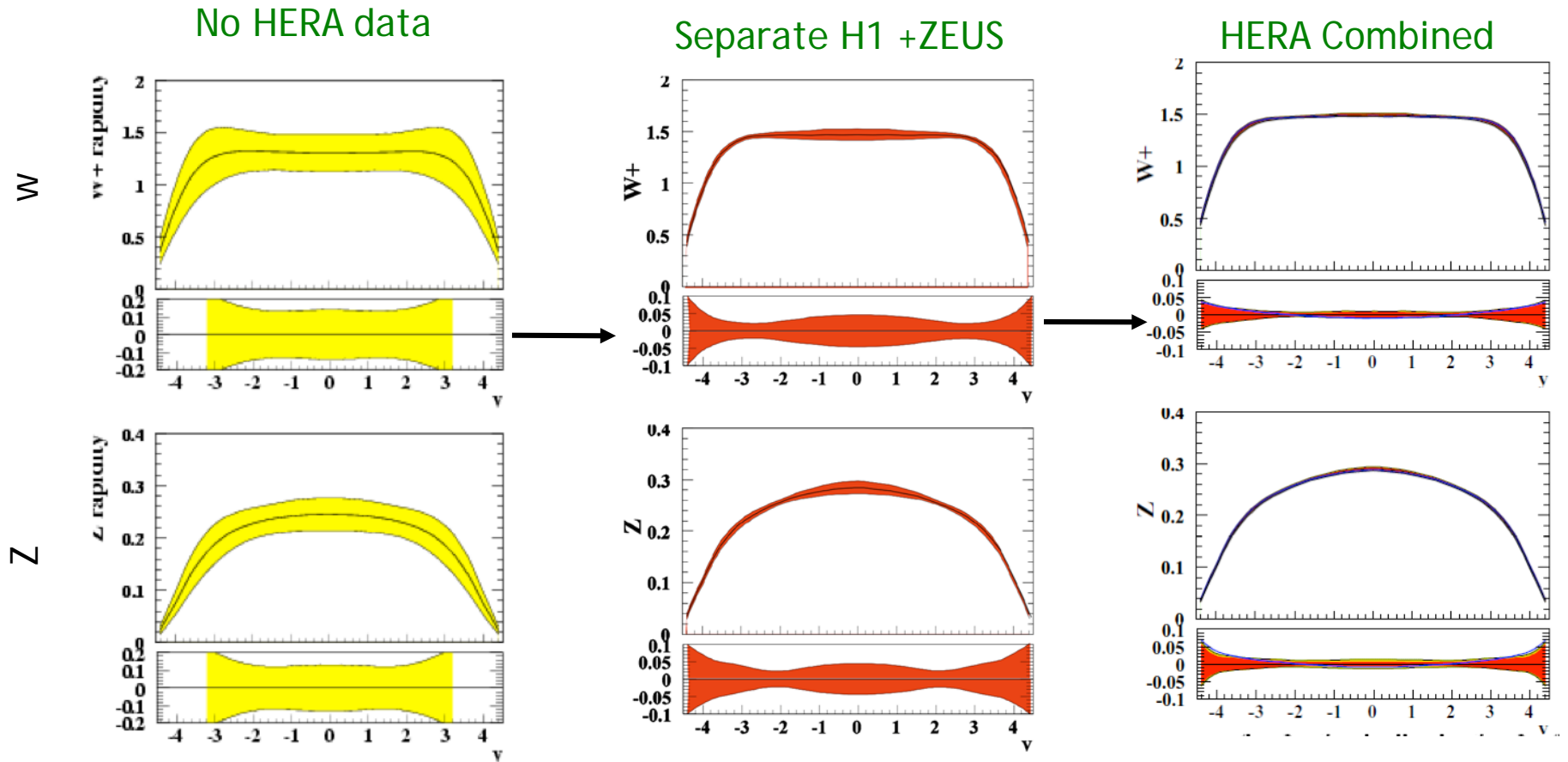
# QCD fits to data



## NC and CC DIS data

- Fixed target experiments: measurements of structure functions (different target nuclei)  
 NC: BCDMS, NMC, E665, SLAC, ...  
 CC: CCFR, CDHS(W), CHARM, BEBC, ...
- Structure functions and cross sections from ZEUS and H1

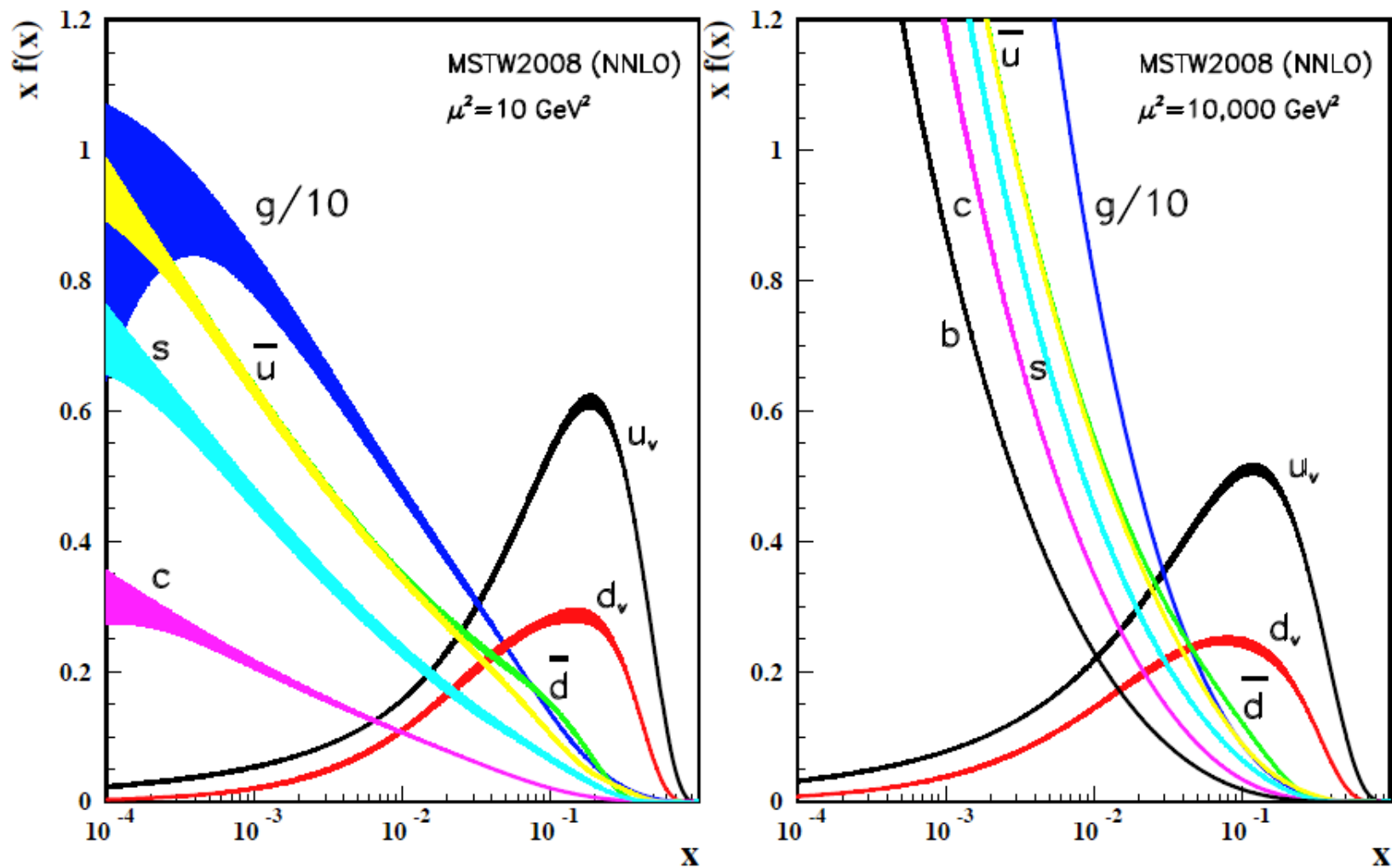
# Impact of HERA data on the LHC: W/Z production as an example



W and Z production cross sections and rapidity distributions are much more precisely known

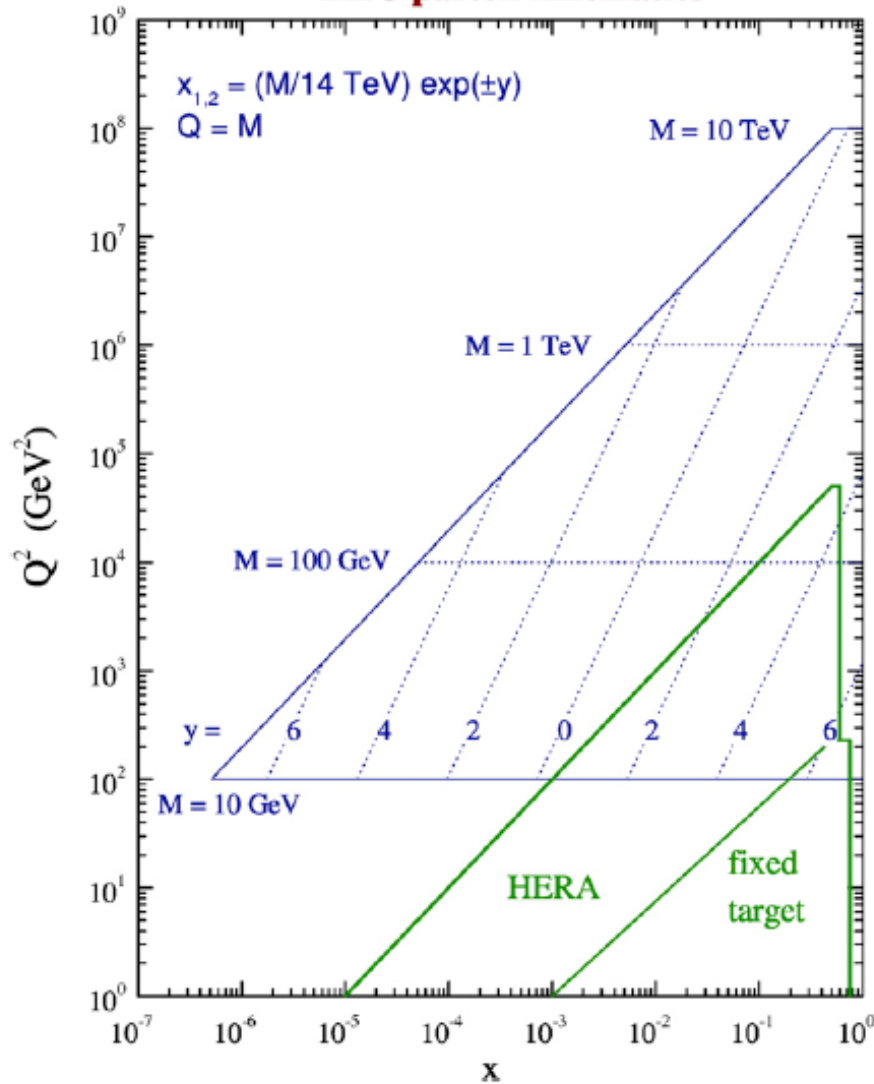
(mainly due to better constrained low-x region (gluons), due to  $gq \rightarrow Wq$  and  $g \rightarrow qq\bar{q}$  splitting contributions producing the necessary antiquarks (sea))

# Parton distribution functions (2010)



Distributions of  $x$  times the parton distributions  $f(x)$ , where  $f = u_v, d_v, \bar{u}, \bar{d}, s, b, g$  and their associated uncertainties using the NNLO MRST2008 parametrization at a scale  $\mu^2 = 20 \text{ GeV}^2$  and  $\mu^2 = 10.000 \text{ GeV}^2$ .

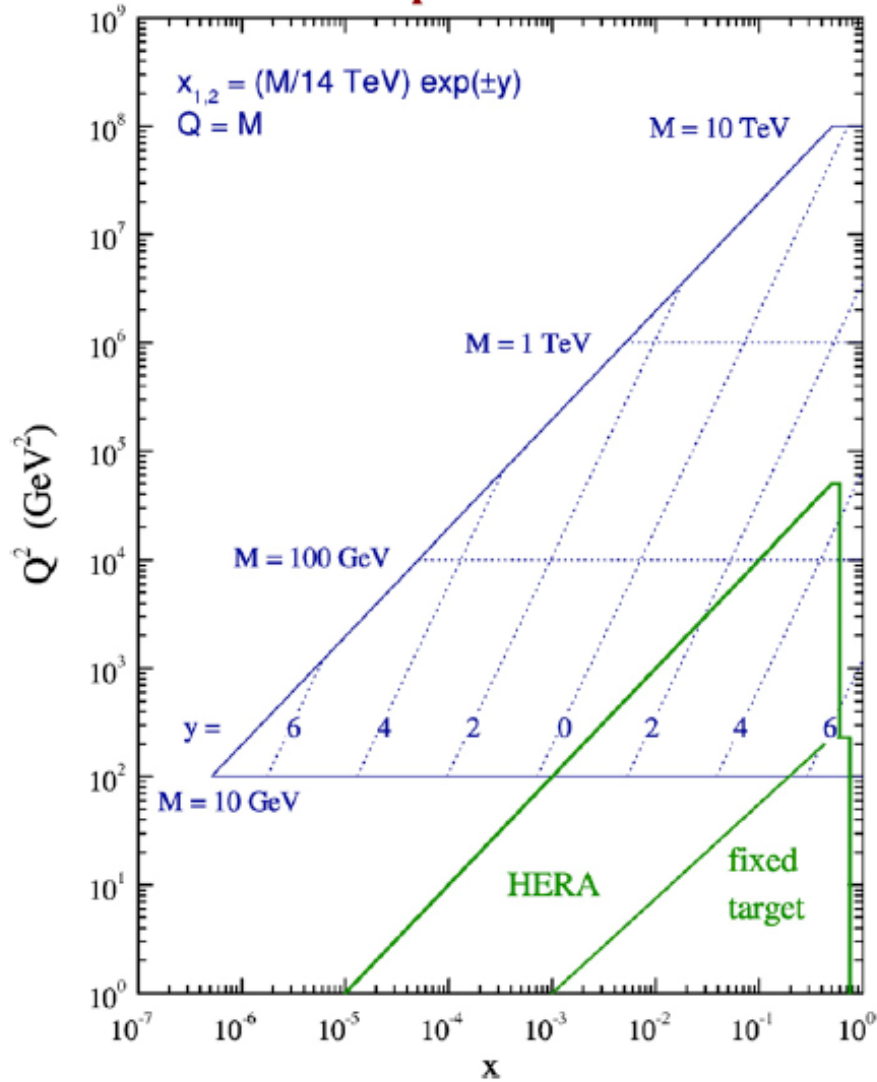
## LHC parton kinematics



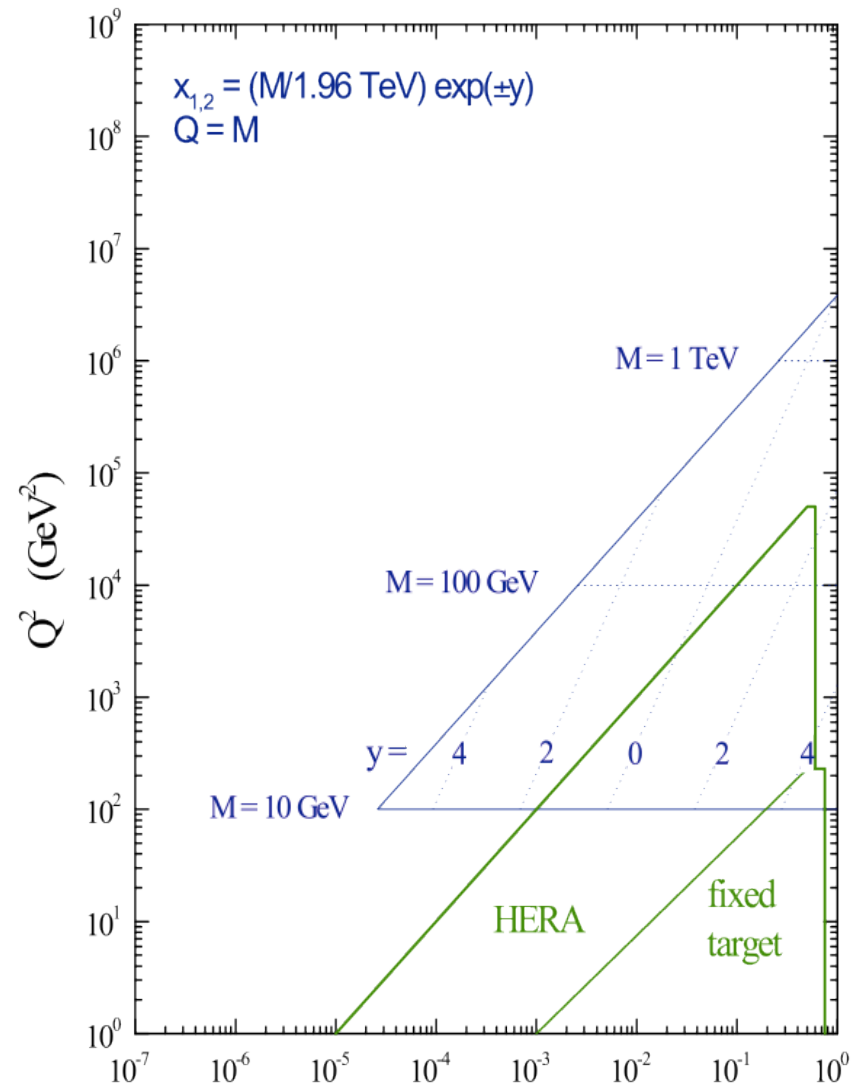
Graphical representation of the relationship between parton ( $x, Q^2$ ) variables and the kinematic variables corresponding to a final state of mass  $M$  with rapidity  $y$  at the LHC with  $\sqrt{s} = 14 \text{ TeV}$

# Comparison between the Tevatron and the LHC (14 TeV)

## LHC parton kinematics

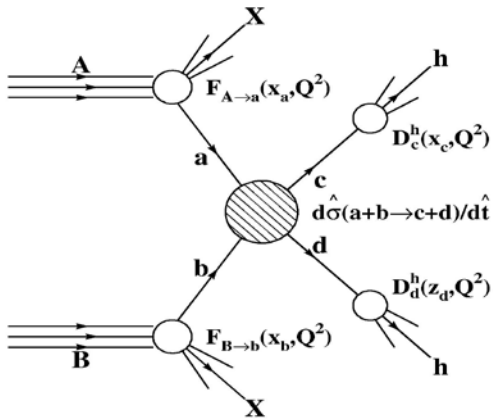


## Tevatron parton kinematics

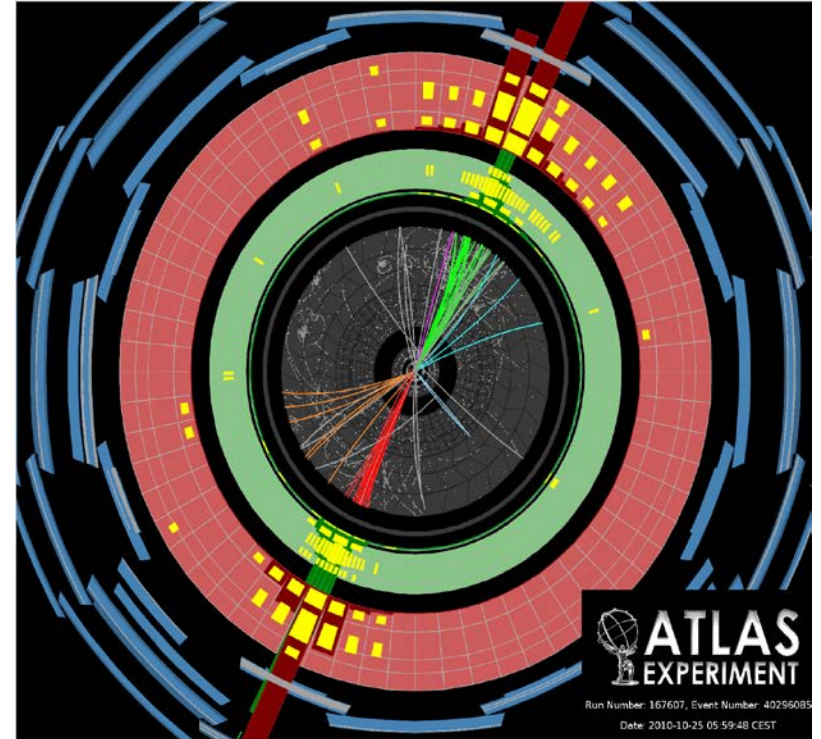


For the same masses (e.g. 100 GeV):  $x$ -values about 10 times lower at the LHC

## 8.3 Test der QCD in Proton-Proton-Kollisionen



- Jet-Produktion
- Produktion von W- und Z-Bosonen
- Produktion von Top-Quarks



## 8.3.1 Important kinematic Variables in pp collisions

## (i) Rapidity $y$

Usually the beam direction is defined as the  $z$  axis (Transverse plane:  $x$ - $y$  plane).

The rapidity  $y$  is defined as:

$$y = \frac{1}{2} \ln \left( \frac{E + p_z}{E - p_z} \right) = \tanh^{-1} \left( \frac{p_z}{E} \right)$$

Under a **Lorentz boost** in the  $z$ -direction to a frame with velocity  $\beta$

the rapidity  $y$  transforms as:  $y \rightarrow y - \tanh^{-1} \beta$

Hence the shape of the rapidity distribution  $dN/dy$  is invariant, as are differences in rapidity.

## (ii) Pseudorapidity $\eta$

Rapidity: 
$$y = \frac{1}{2} \ln \left( \frac{E + p_z}{E - p_z} \right) = \tanh^{-1} \left( \frac{p_z}{E} \right)$$

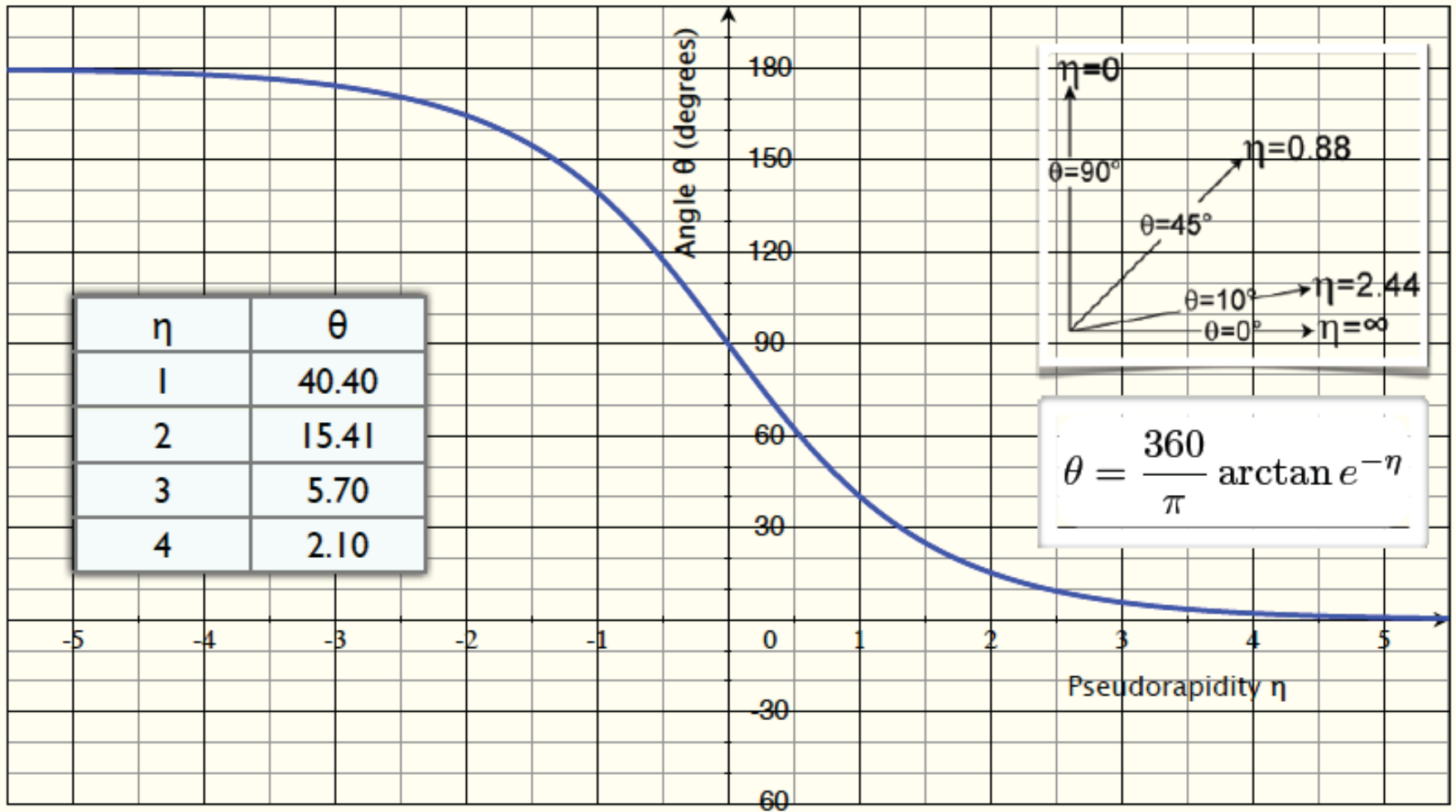
For  $p \gg m$ , the rapidity may be expanded to obtain

$$y = \frac{1}{2} \ln \frac{\cos^2(\theta/2) + m^2/4p^2 + \dots}{\sin^2(\theta/2) + m^2/4p^2 + \dots}$$
$$\approx -\ln \tan(\theta/2) \equiv \eta$$

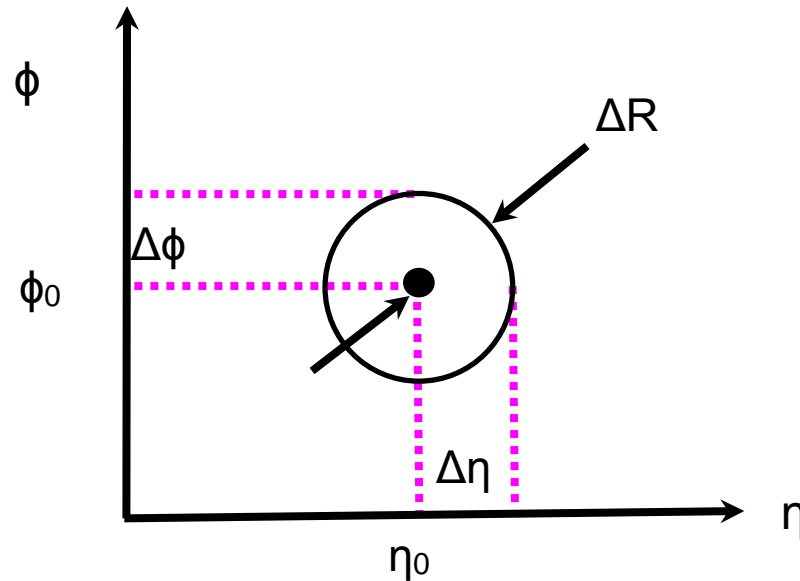
where  $\cos \theta = p_z/p$ .

**Identities:**  $\sinh \eta = \cot \theta$  ,  $\cosh \eta = 1/\sin \theta$  ,  $\tanh \eta = \cos \theta$

# Relation between pseudorapidity $\eta$ and polar angle $\theta$



(iii) Distance in  $\eta$   $\phi$  space:



Rapidity  $y$ :  $y = 1/2 \ln[(E + p_z)/(E - p_z)]$

Pseudorapidity  $\eta$ :  $\eta = -\ln \tan(\theta/2)$

Distance in  $\eta$ - $\phi$ :  $\Delta R = \sqrt{\Delta \eta^2 + \Delta \phi^2}$

## (iv) Transverse Energy

At hadron colliders, a significant and unknown proportion of the energy of the incoming hadrons in each event escapes down the beam-pipe. Consequently if invisible particles are created in the final state, their net momentum can only be constrained in the plane transverse to the beam direction. Defining the z-axis as the beam direction, this net momentum is equal to the missing transverse energy vector

missing transverse energy

$$\mathbf{E}_T^{\text{miss}} = - \sum_i \mathbf{p}_T(i)$$

where the sum runs over the transverse momenta of all visible final state particles.

## (v) Momenta of invisible particles

Consider a single heavy particle of mass  $M$  produced in association with visible particles which decays to two particles, of which one (labelled particle 1) is invisible. The mass of the parent particle can be constrained with the quantity  $M_T$  defined by

Transverse mass

$$\begin{aligned} M_T^2 &\equiv [E_T(1) + E_T(2)]^2 - [\mathbf{p}_T(1) + \mathbf{p}_T(2)]^2 \\ &= m_1^2 + m_2^2 + 2[E_T(1)E_T(2) - \mathbf{p}_T(1) \cdot \mathbf{p}_T(2)] \end{aligned}$$

where

$$\mathbf{p}_T(1) = \mathbf{E}_T^{\text{miss}}$$

This quantity is called the **transverse mass**.

# Transverse mass

$$\begin{aligned} M_T^2 &\equiv [E_T(1) + E_T(2)]^2 - [\mathbf{p}_T(1) + \mathbf{p}_T(2)]^2 \\ &= m_1^2 + m_2^2 + 2[E_T(1)E_T(2) - \mathbf{p}_T(1) \cdot \mathbf{p}_T(2)] \end{aligned}$$

where  $\mathbf{p}_T(1) = \mathbf{E}_T^{\text{miss}}$

The distribution of event  $M_T$  values has an end-point at

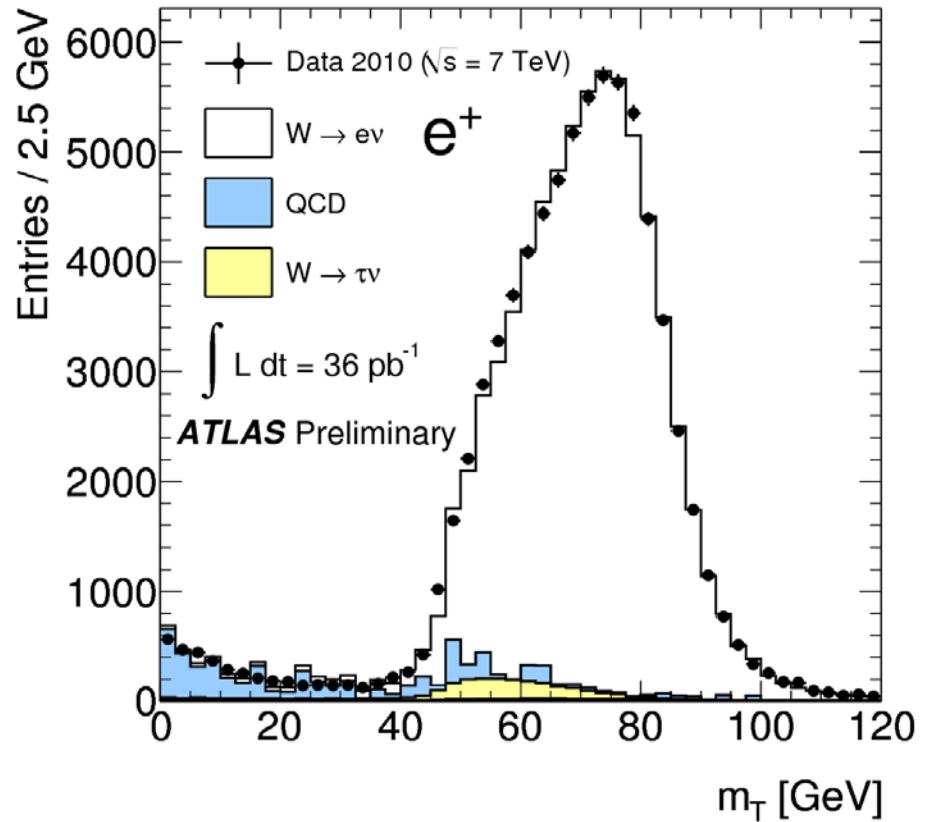
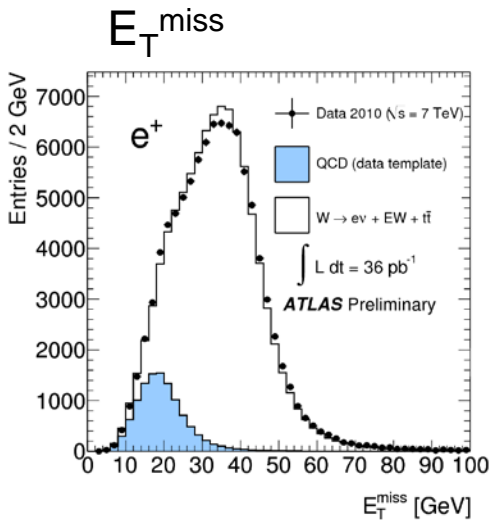
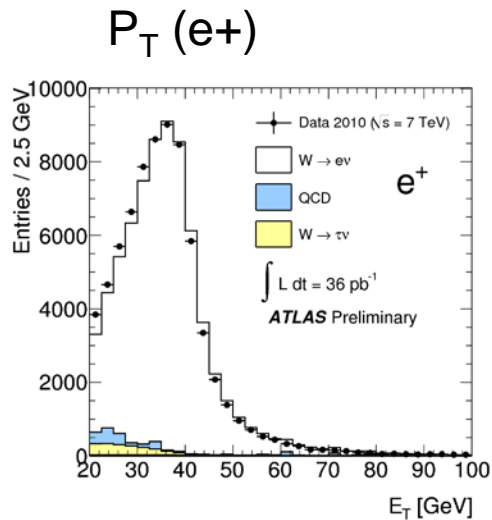
$$M_T^{\text{max}} = \bar{M}.$$

If  $m_1 = m_2 = 0$

$$M_T^2 = 2|\mathbf{p}_T(1)||\mathbf{p}_T(2)|(1 - \cos \phi_{12})$$

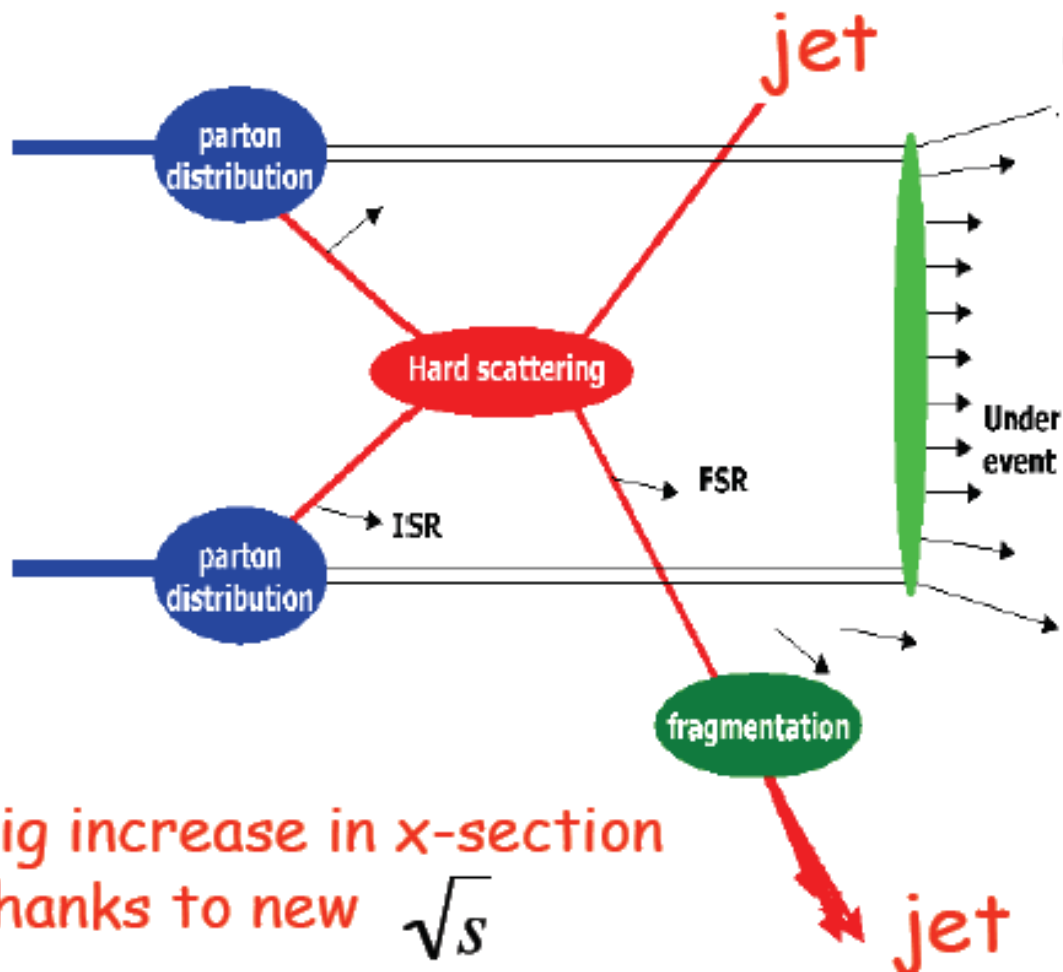
where  $\phi_{ij}$  is defined as the angle between particles  $i$  and  $j$  in the transverse plane.

# Example: Transverse mass of the W boson



$$m_T = \sqrt{2P_T(e)E_T^{\text{miss}}(1 - \cos \Delta\phi)}$$

(see previous slide)



# Hard scattering formalism

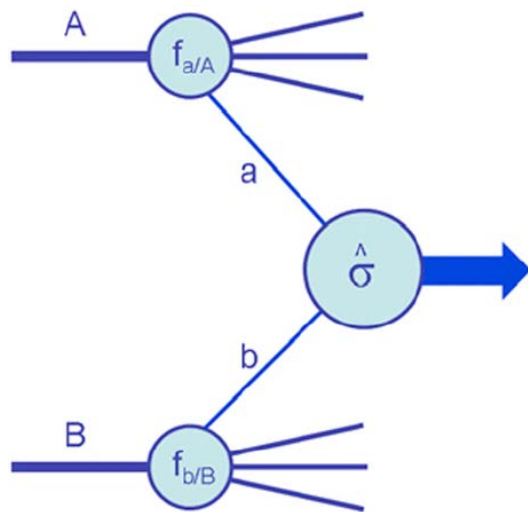
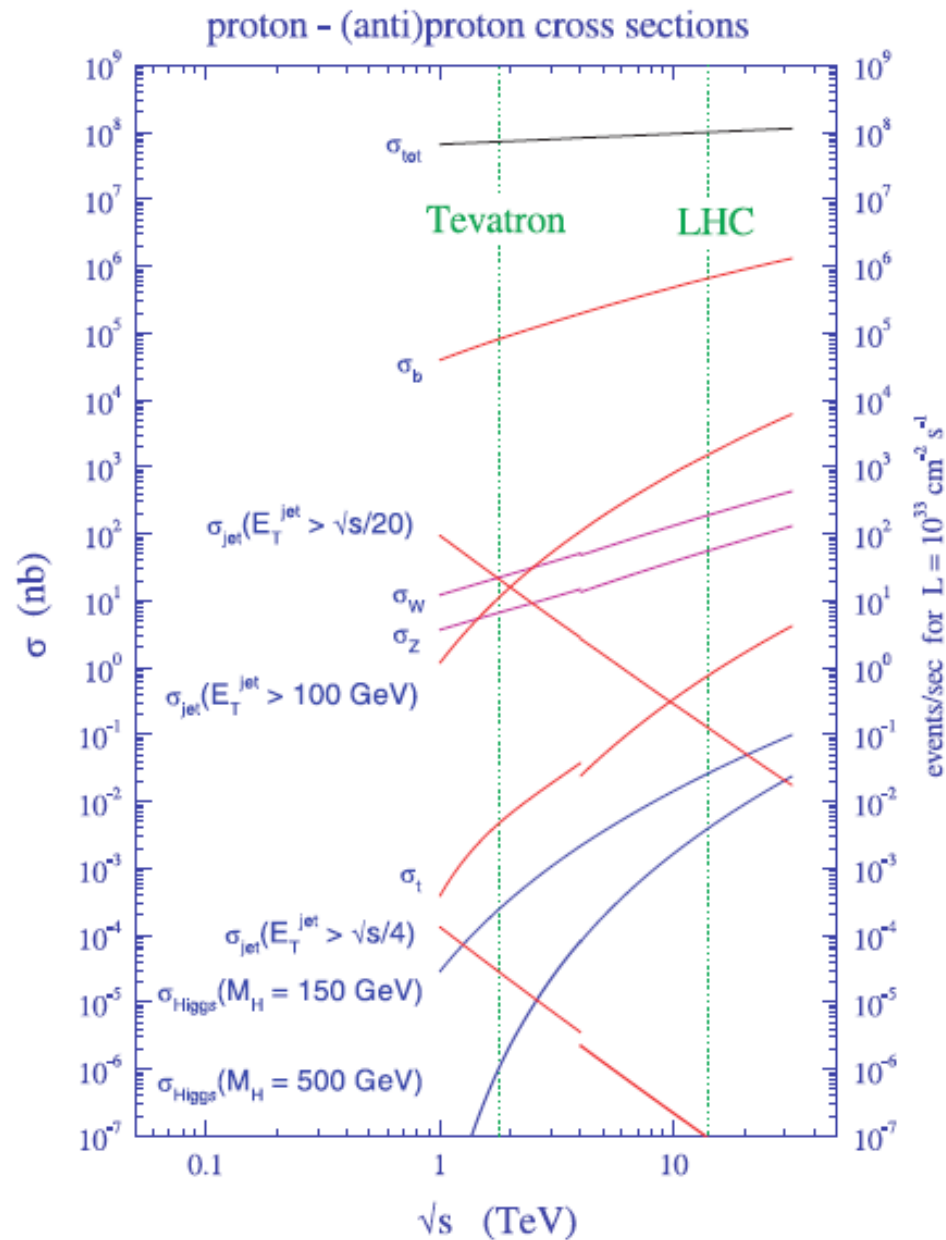
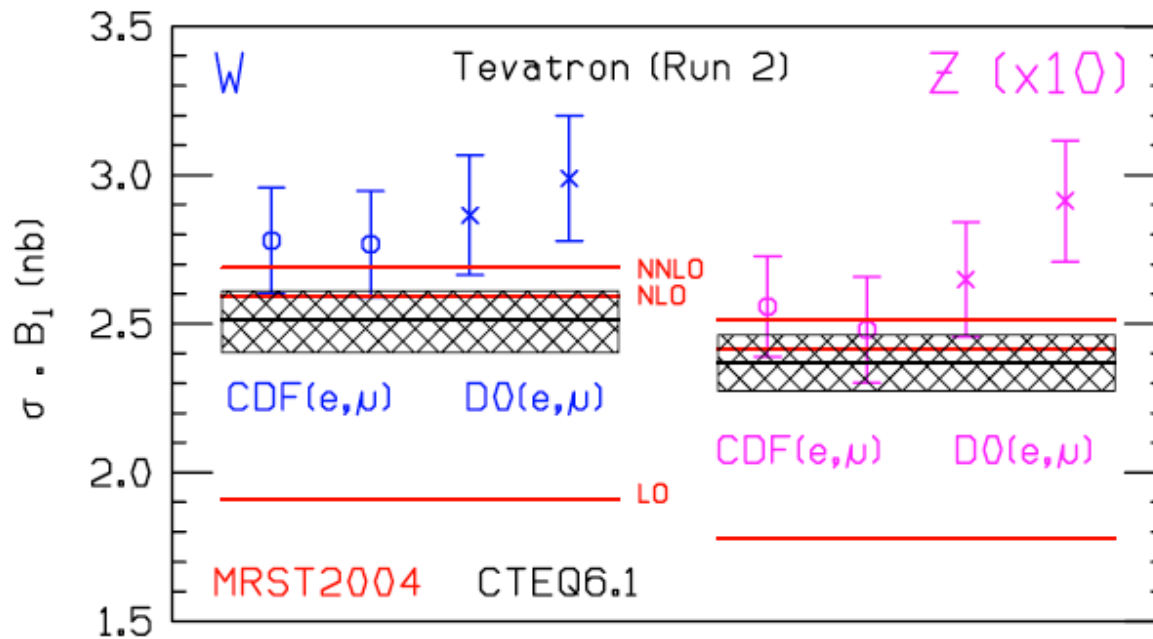


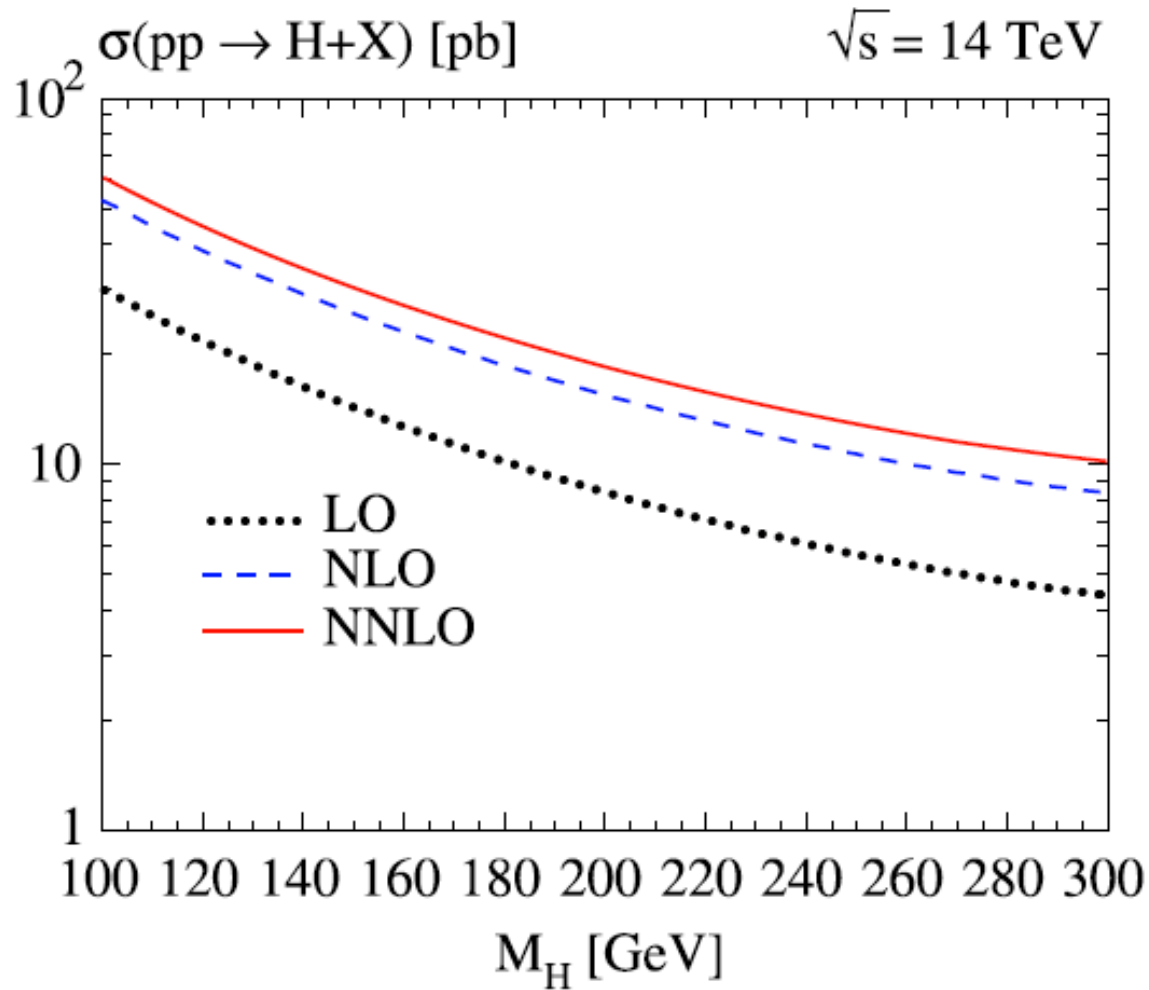
Illustration of a hard proton-proton interaction



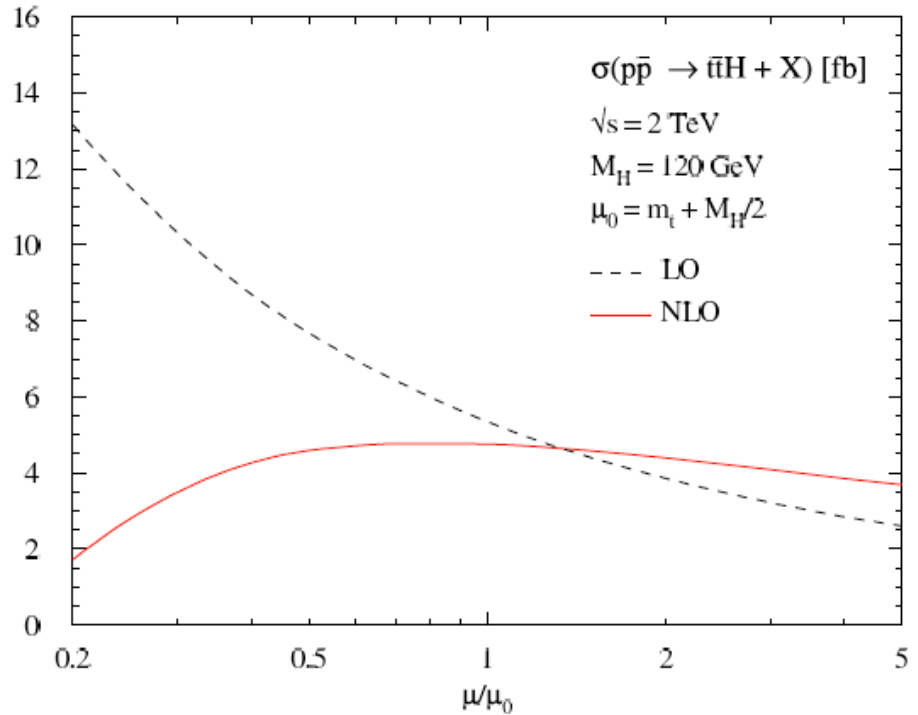
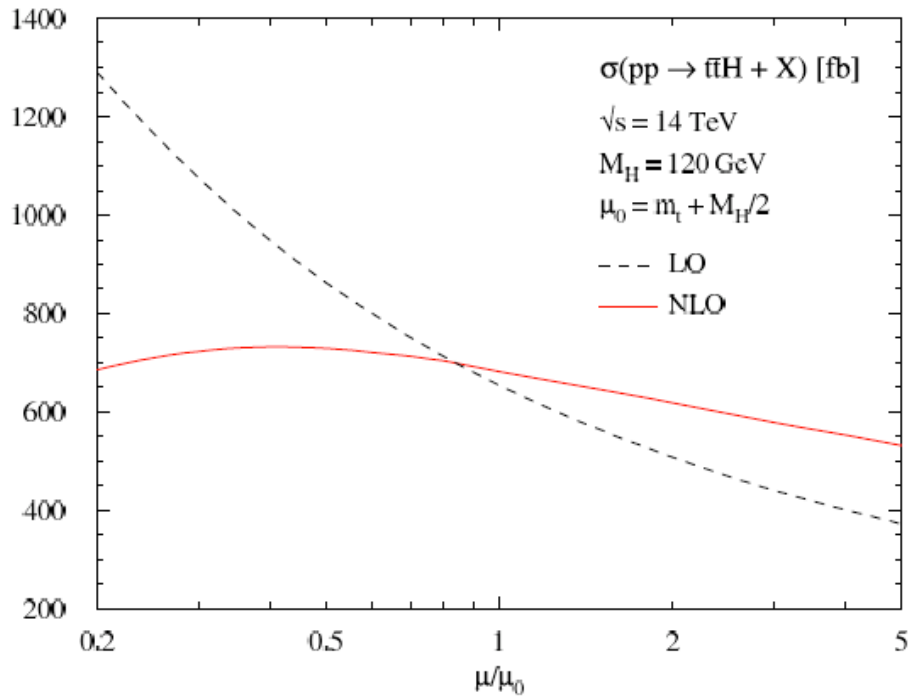
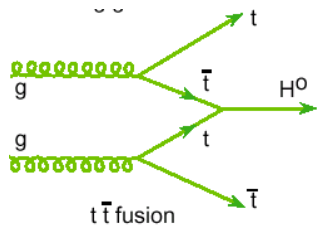
Cross sections for important hard scattering Standard Model processes at the Tevatron and the LHC colliders



Predictions for the W and Z total cross section at the Tevatron, using MRST2004 and CTEQ6.1 pdfs, compared with measurements from the CDF and D0 experiments. The MRST predictions are shown at LO, NLO and NNLO. The CTEQ6.1 NLO predictions are shown together with the accompanying error band resulting from pdf uncertainties.

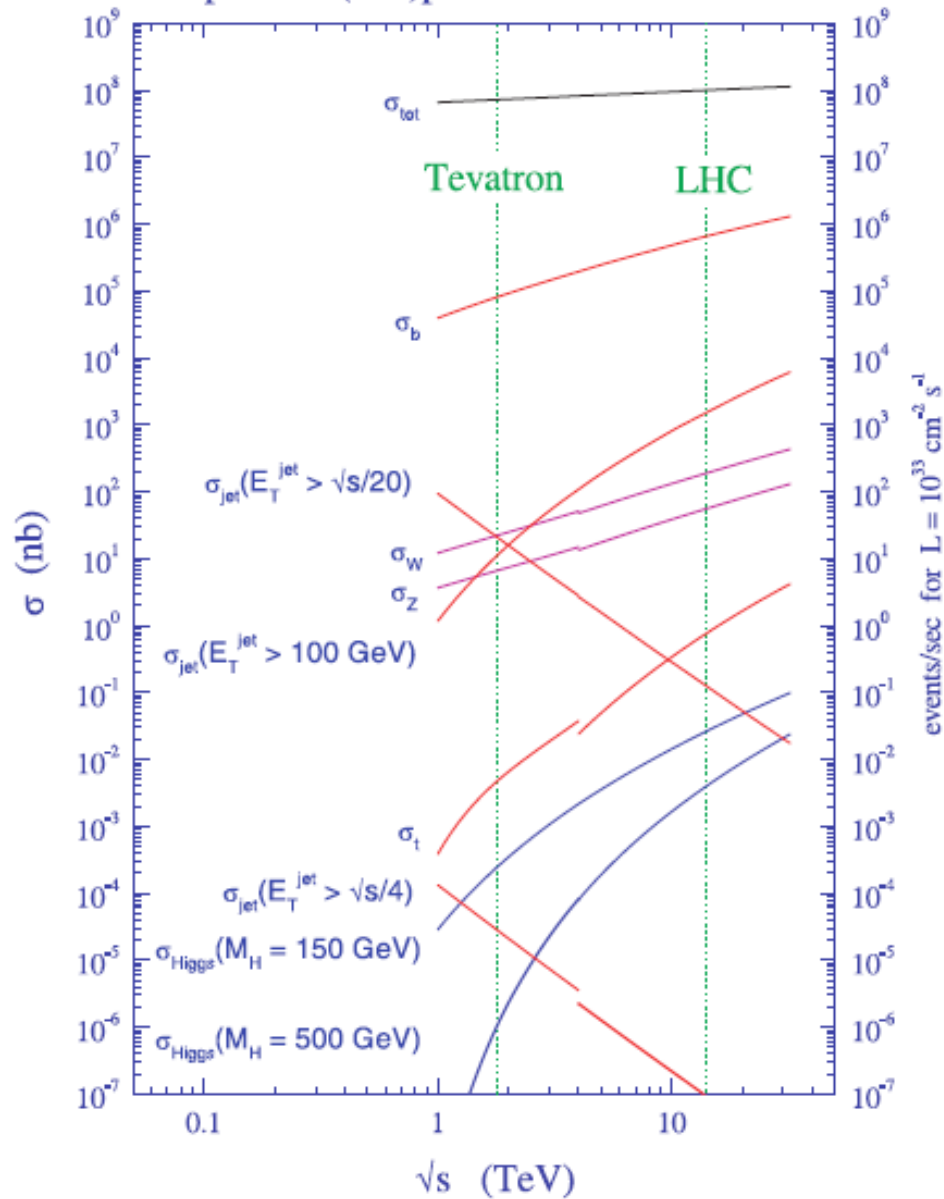


The inclusive Higgs boson production cross section as a function of the Higgs boson mass at LO, NLO and NNLO.



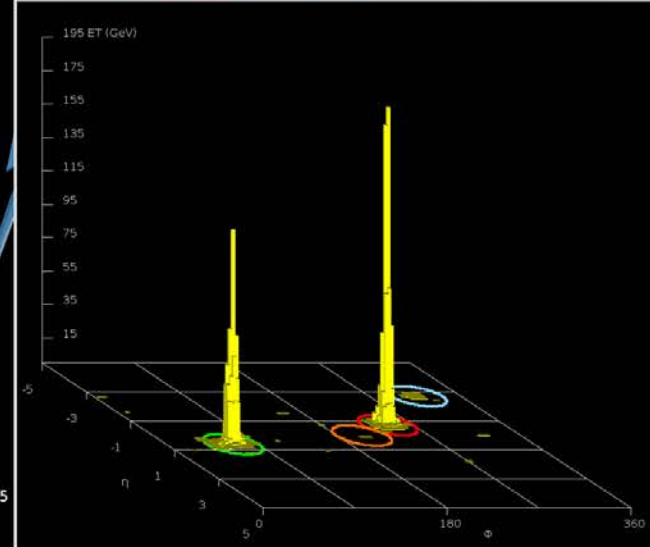
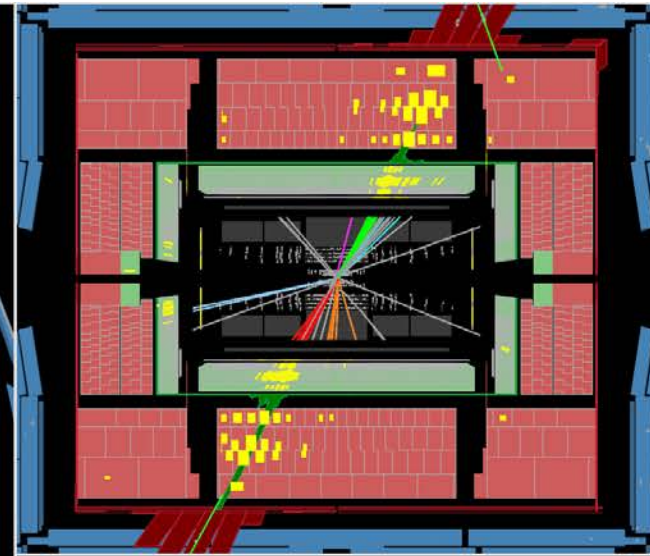
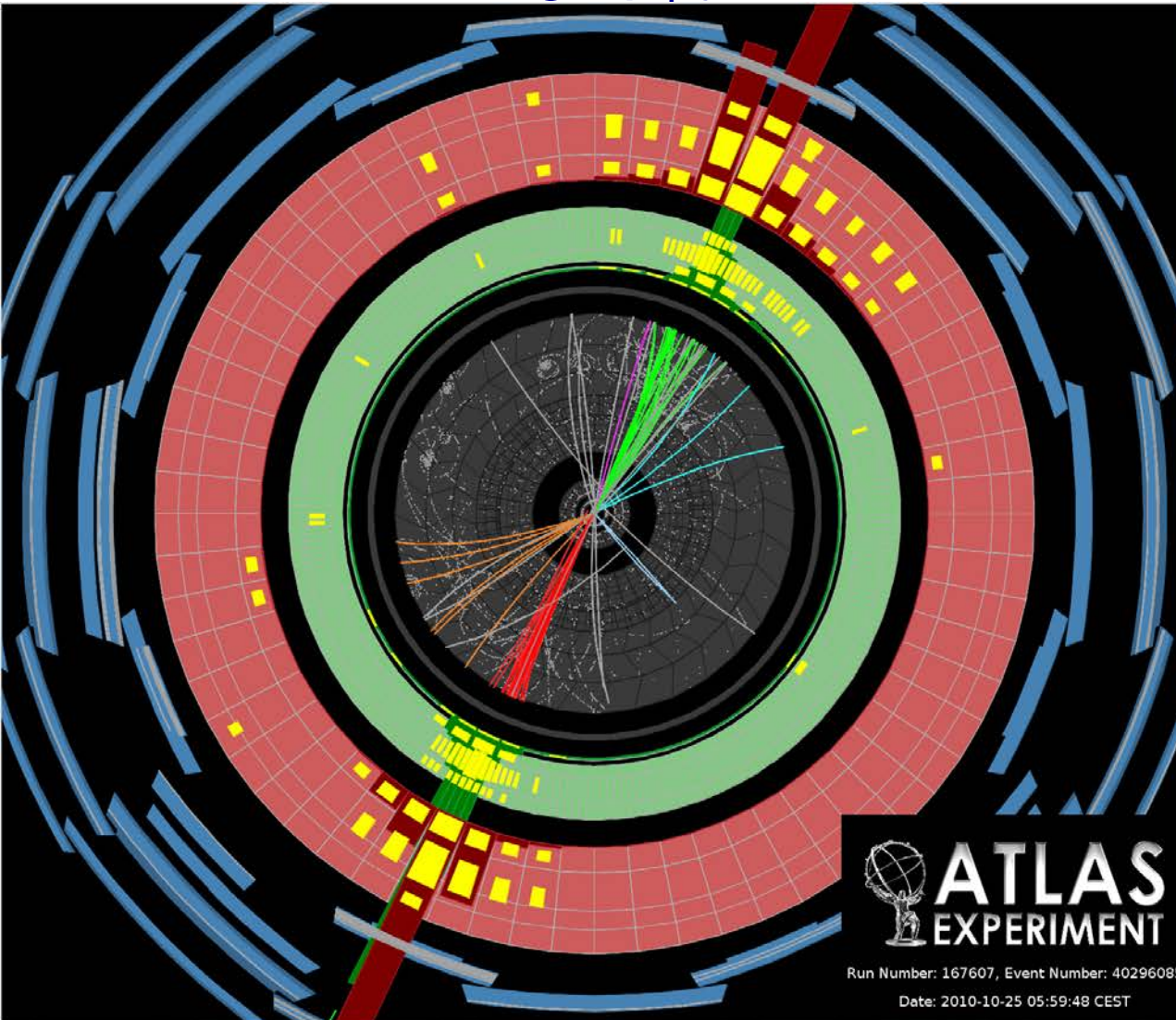
Variation of the  $t\bar{t}H$  production cross section at the LHC 14 TeV  $pp$  collider (left) and at the Tevatron 2 TeV  $p\bar{p}$  collider (right) with the renormalization and factorization scale  $\mu = \mu_R = \mu_F$ , varied around the value  $\mu_0 = m_t + m_H / 2$ .

### proton - (anti)proton cross sections



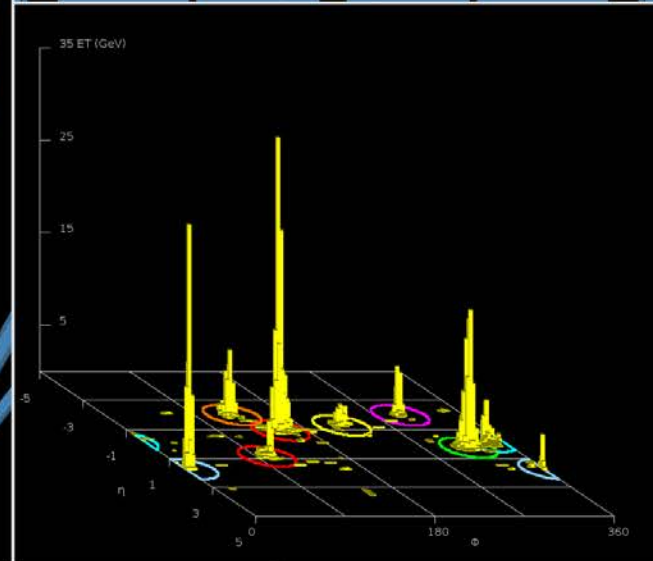
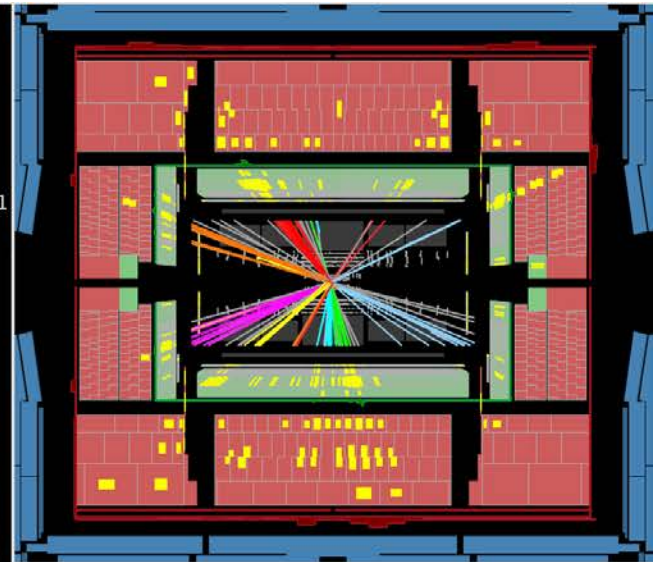
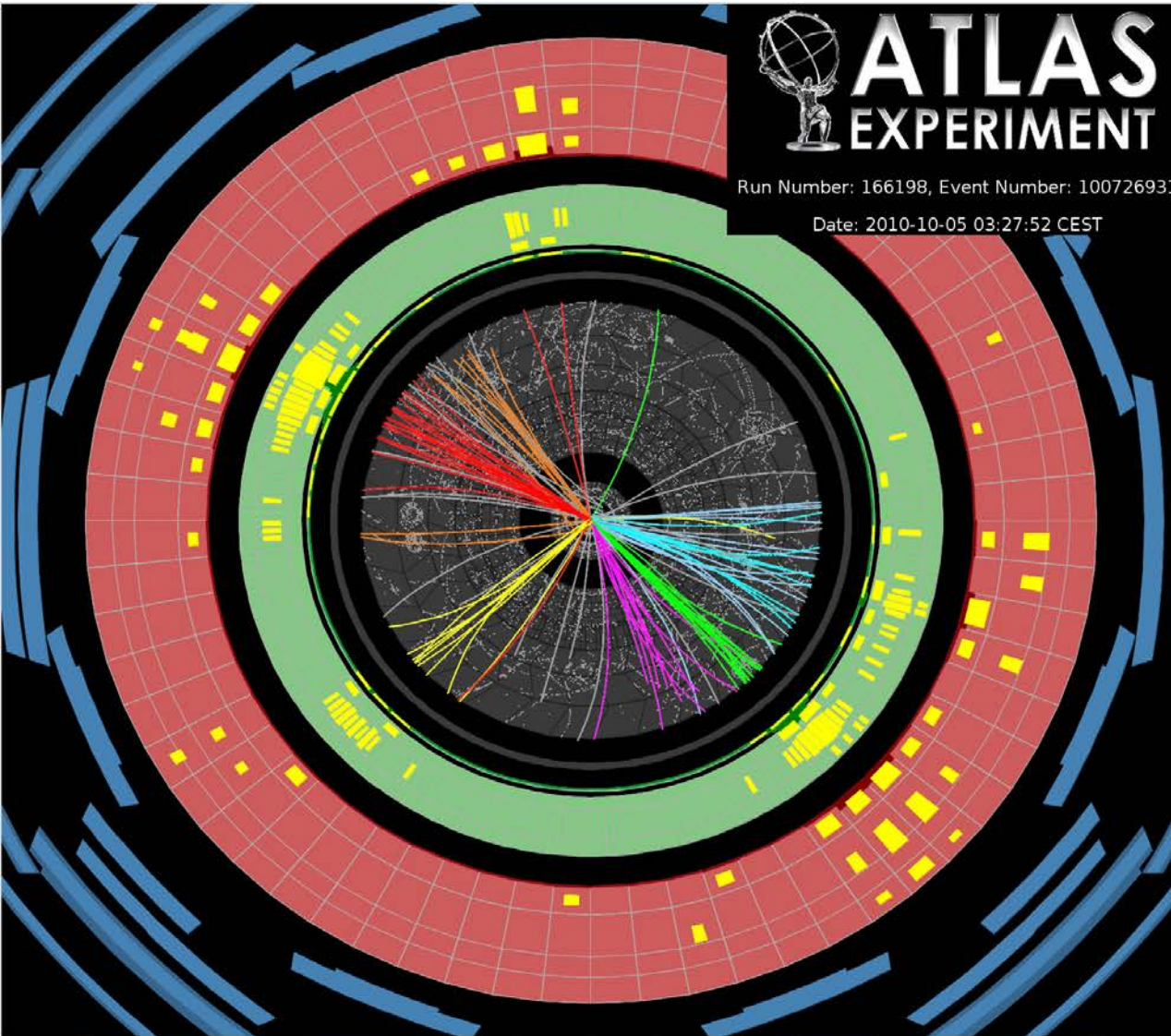
Cross sections for important hard scattering Standard Model processes at the Tevatron and the LHC colliders

# High $p_T$ jet events at the LHC



Event display that shows the highest-mass central dijet event collected during 2010, where the two leading jets have an invariant mass of 3.1 TeV. The two leading jets have  $(p_T, y)$  of (1.3 TeV, -0.68) and (1.2 TeV, 0.64), respectively. The missing  $E_T$  in the event is 46 GeV. From [ATLAS-CONF-2011-047](#).

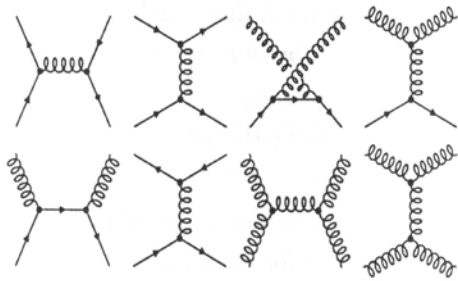
# An event with a high jet multiplicity at the LHC



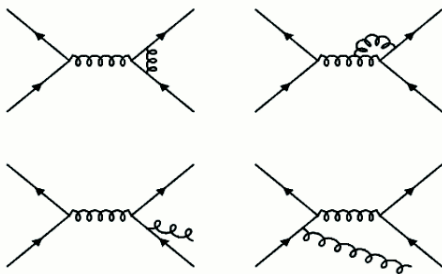
The highest jet multiplicity event collected by the end of October 2010, counting jets with  $p_T$  greater than 60 GeV: this event has eight. 1st jet (ordered by  $p_T$ ):  $p_T = 290$  GeV,  $\eta = -0.9$ ,  $\phi = 2.7$ ; 2nd jet:  $p_T = 220$  GeV,  $\eta = 0.3$ ,  $\phi = -0.7$  Missing  $E_T = 21$  GeV,  $\phi = -1.9$ , Sum  $E_T = 890$  GeV. The event was collected on 5 October 2010.

# Theoretical calculations

## Leading order



## ...some NLO contributions

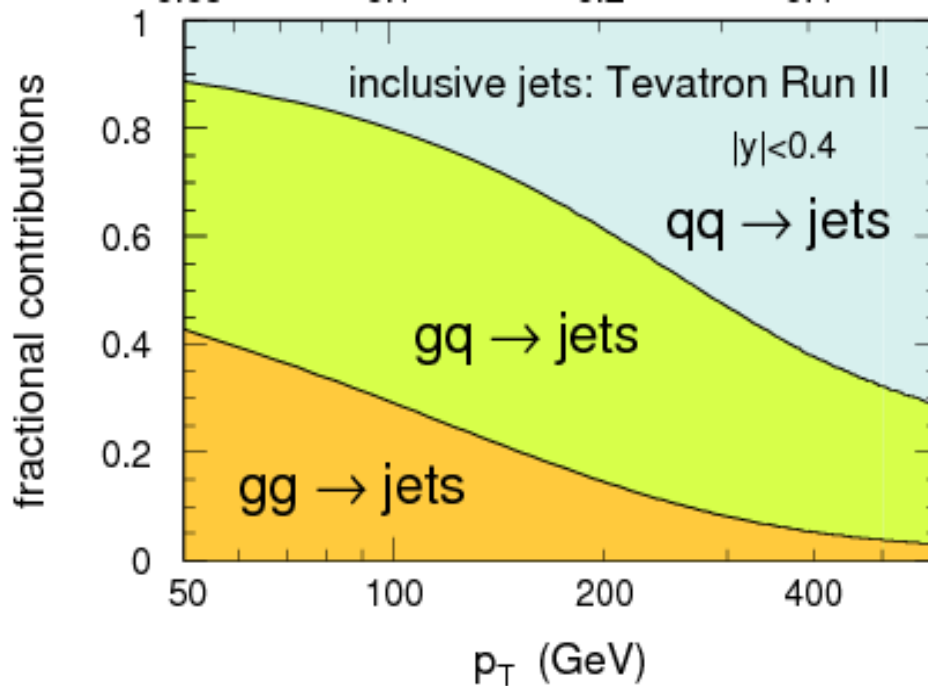


$$\frac{d\hat{\sigma}}{d\hat{t}}(ab \rightarrow cd) = \frac{|M|^2}{(16\pi\hat{s}^2)}$$

Subprocess	$ M ^2/g_s^4$	$ M(90^\circ) ^2/g_s^4$
$qq' \rightarrow qq'$ $q\bar{q}' \rightarrow q\bar{q}'$	$\frac{4}{9} \frac{\hat{s}^2 + \hat{u}^2}{\hat{t}^2}$	2.2
$qq \rightarrow qq$	$\frac{4}{9} \left( \frac{\hat{s}^2 + \hat{u}^2}{\hat{t}^2} + \frac{\hat{s}^2 + \hat{t}^2}{\hat{u}^2} \right) - \frac{8}{27} \frac{\hat{s}^2}{\hat{u}\hat{t}}$	3.3
$q\bar{q} \rightarrow q'\bar{q}'$	$\frac{4}{9} \frac{\hat{t}^2 + \hat{u}^2}{\hat{s}^2}$	0.2
$q\bar{q} \rightarrow q\bar{q}$	$\frac{4}{9} \left( \frac{\hat{s}^2 + \hat{u}^2}{\hat{t}^2} + \frac{\hat{t}^2 + \hat{u}^2}{\hat{s}^2} \right) - \frac{8}{27} \frac{\hat{u}^2}{\hat{s}\hat{t}}$	2.6
$q\bar{q} \rightarrow gg$	$\frac{32}{27} \frac{\hat{u}^2 + \hat{t}^2}{\hat{u}\hat{t}} - \frac{8}{3} \frac{\hat{u}^2 + \hat{t}^2}{\hat{s}^2}$	1.0
$gg \rightarrow q\bar{q}$	$\frac{1}{6} \frac{\hat{u}^2 + \hat{t}^2}{\hat{u}\hat{t}} - \frac{3}{8} \frac{\hat{u}^2 + \hat{t}^2}{\hat{s}^2}$	0.1
$qg \rightarrow qg$	$\frac{\hat{s}^2 + \hat{u}^2}{\hat{t}^2} - \frac{4}{9} \frac{\hat{s}^2 + \hat{u}^2}{\hat{u}\hat{s}}$	6.1
$gg \rightarrow gg$	$\frac{9}{4} \left( \frac{\hat{s}^2 + \hat{u}^2}{\hat{t}^2} + \frac{\hat{s}^2 + \hat{t}^2}{\hat{u}^2} + \frac{\hat{u}^2 + \hat{t}^2}{\hat{s}^2} + 3 \right)$	30.4

- Right: Results of the LO matrix elements for the various scattering processes, expressed in terms of the Mandelstam variables  $s$ ,  $t$  and  $u$ . (Kripfganz et al, 1974);
- $gg$  scattering is the dominant contribution under  $\eta = 0$ ;  
(sensitivity to gluons, sensitivity to gluon self-coupling, as predicted by QCD)
- NLO predictions have meanwhile been calculated (2002).

The composition of the partons involved as function of the  $p_T$  of the jet at the Tevatron:

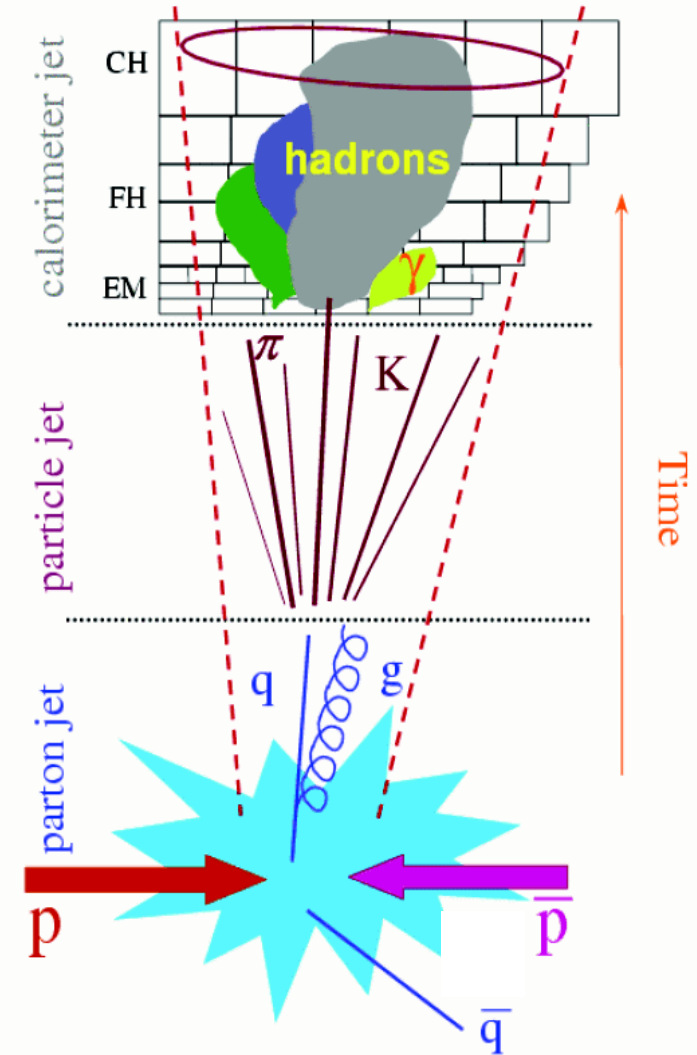


Tevatron,  
ppbar,  $\sqrt{s} = 1.96$  TeV,  
central region  $|\eta| < 0.4$

- $qq$  scattering dominates at high  $p_T$
- However, gluons contribute over the full range

# Jet reconstruction and energy measurement

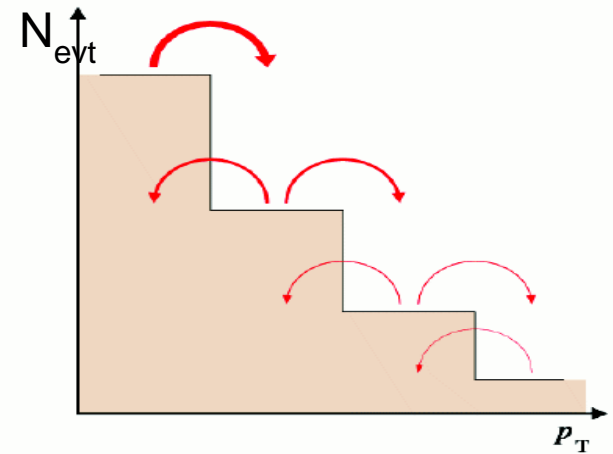
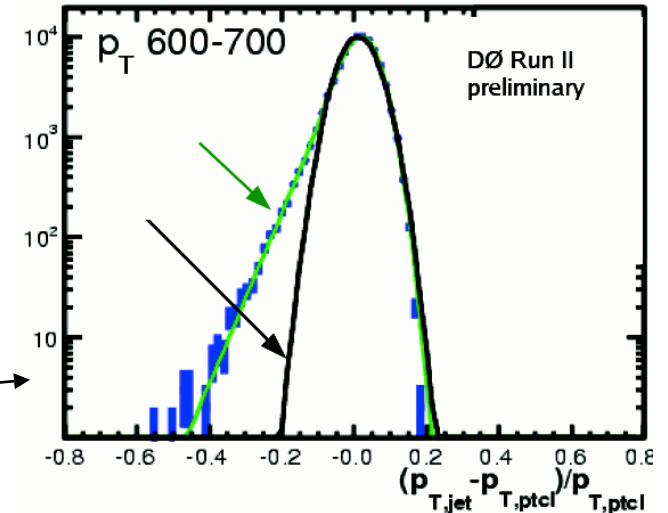
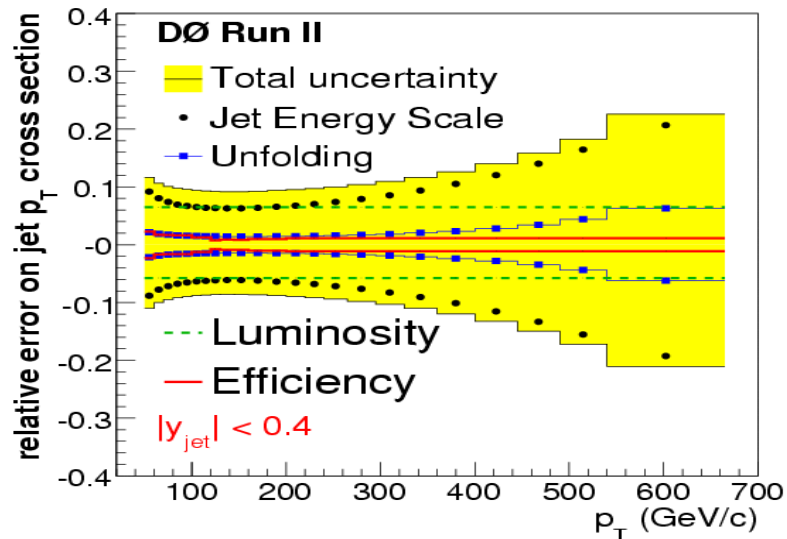
- A jet is NOT a well defined object  
(fragmentation, gluon radiation, detector response)
- The detector response is different for particles interacting electromagnetically ( $e, \gamma$ ) and for hadrons  
→ for comparisons with theory, one needs to correct back the calorimeter energies to the „particle level“ (particle jet)  
*Common ground between theory and experiment*
- One needs an algorithm to define a jet and to measure its energy  
*conflicting requirements between experiment and theory (exp. simple, e.g. cone algorithm, vs. theoretically sound (no infrared divergencies))*
- Energy corrections for losses of fragmentation products outside jet definition and underlying event or pileup energy inside



# Experimental issues

$$d^2\sigma / dp_T d\eta = N / (\epsilon \cdot L \cdot \Delta p_T \cdot \Delta\eta)$$

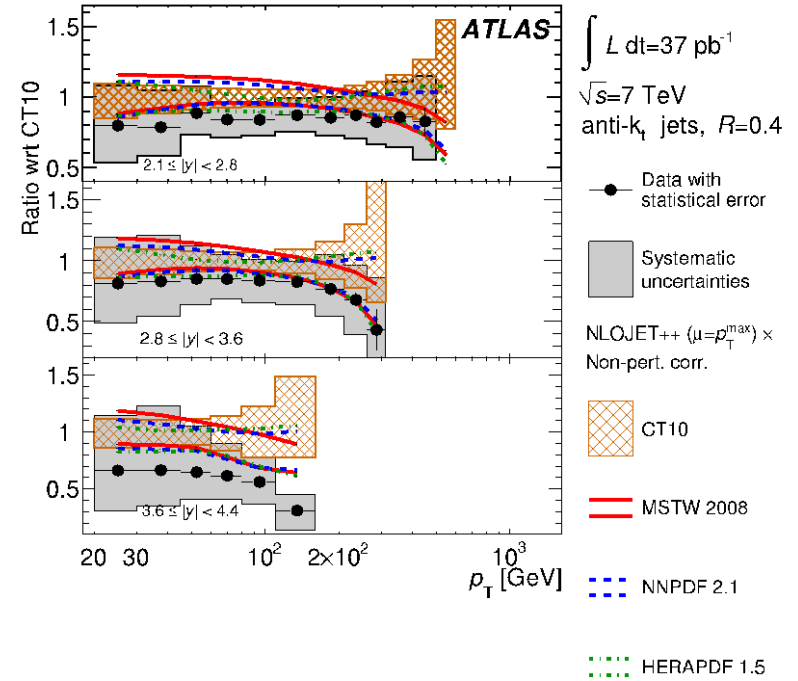
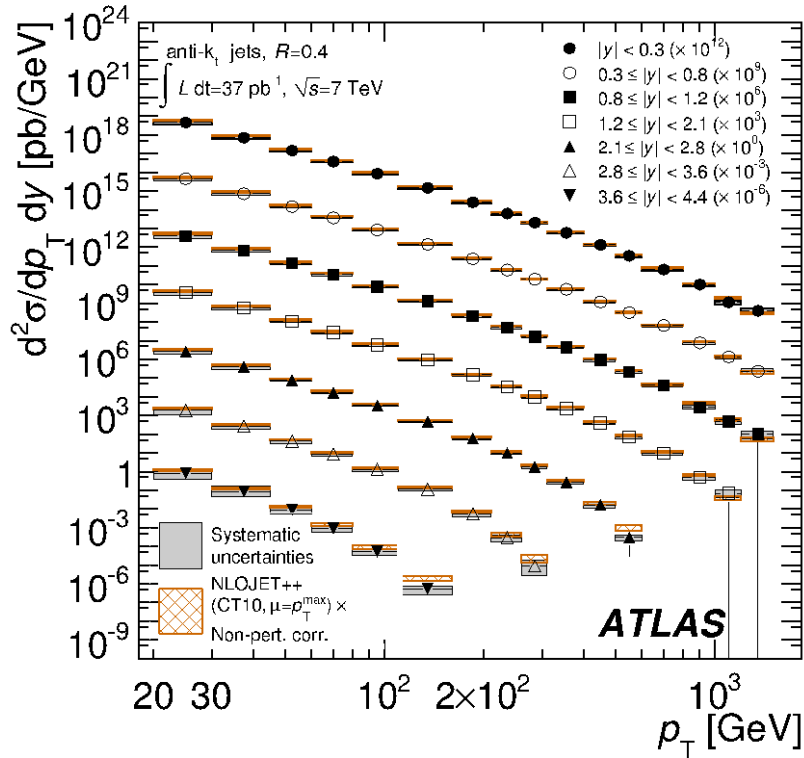
- In principle a simple counting experiment
- However, steeply falling  $p_T$  spectra are sensitive to jet energy scale uncertainties and resolution effects (migration between bins) → corrections (unfolding) to be applied
- Sensitivity to jet energy scale uncertainty:  
 DØ: 1% energy scale error → 10% cross section uncert. at  $|\eta| < 0.4$



Major exp. errors:  
 energy scale, luminosity (6%),...



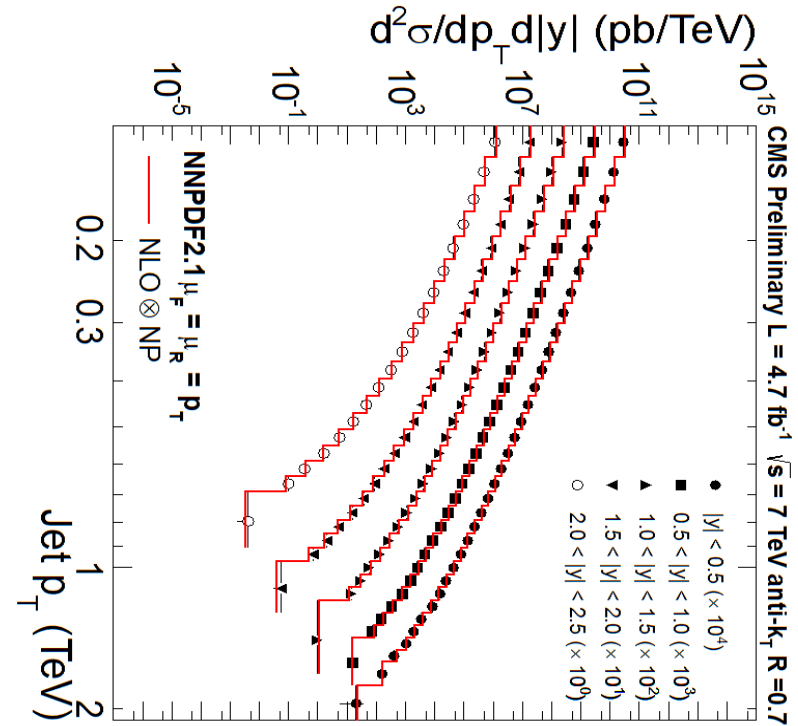
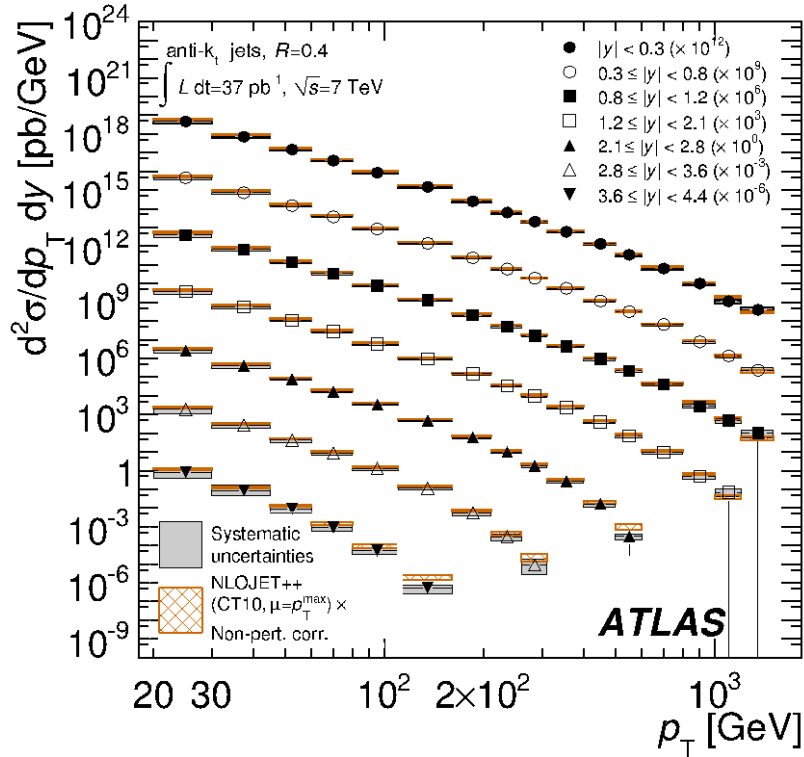
# Double differential cross sections, as function of $p_T$ and rapidity $y$ (full 2010 data set)



somewhat larger deviations in the forward region

- Data are well described by NLO pert. QCD calculations
- Experimental systematic uncertainty is dominated by jet energy scale uncertainty
- Theoretical uncertainties: unknown higher order corrections, parton density functions,  $\alpha_s$ , ...

# Double differential cross sections, as function of $p_T$ and rapidity $y$ : (full 2010 data set)

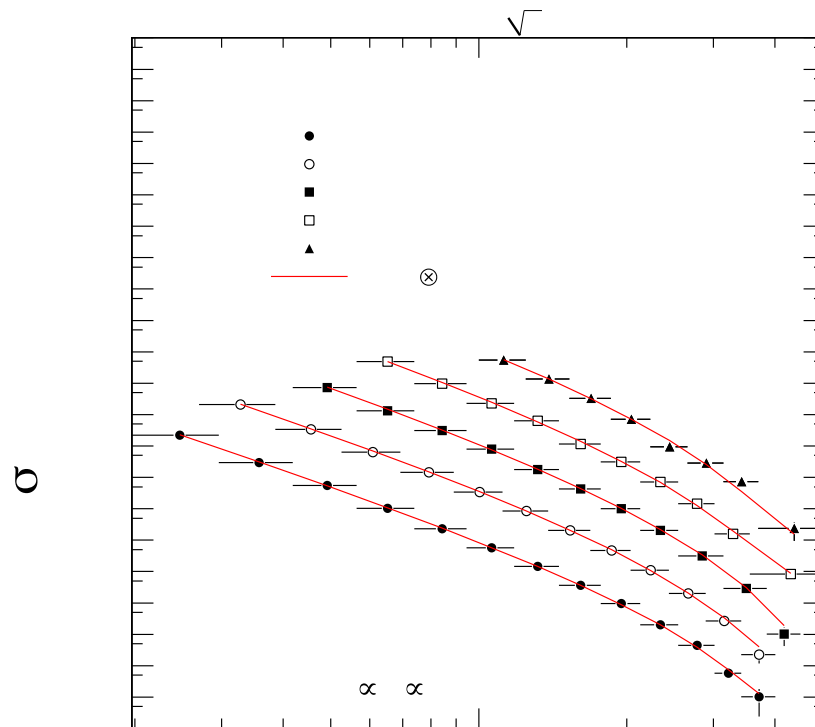
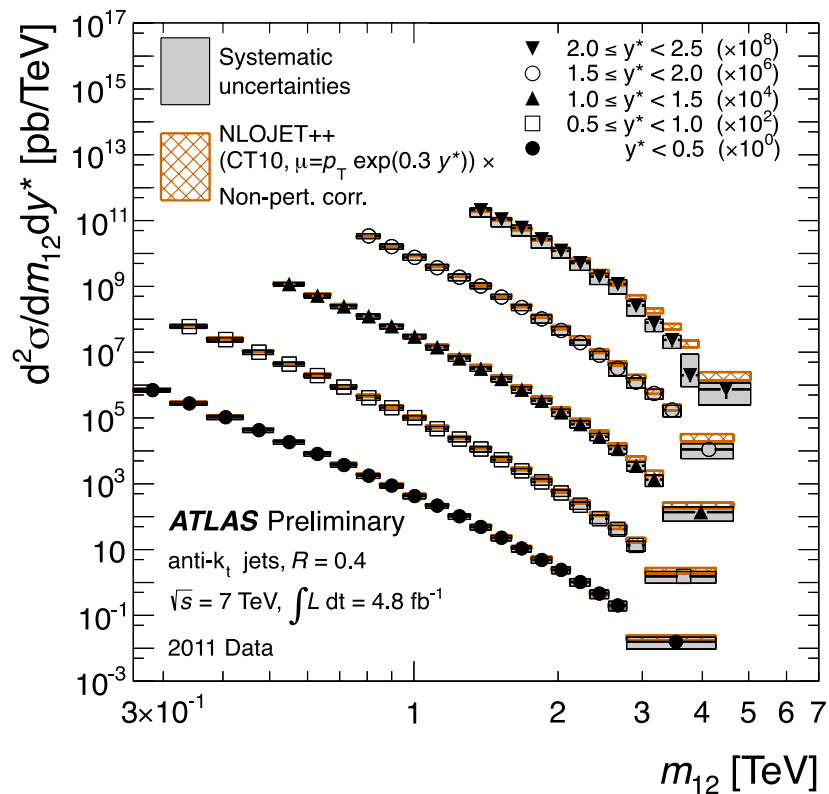


CMS: include full 2011 data set;  
comparison up to 2 TeV (central rapidities)

- Data are well described by NLO pert. QCD calculations
- Experimental systematic uncertainty is dominated by jet energy scale uncertainty
- Theoretical uncertainties: unknown higher order corrections, parton density functions,  $\alpha_s$ , ...



# Invariant di-jet mass spectra

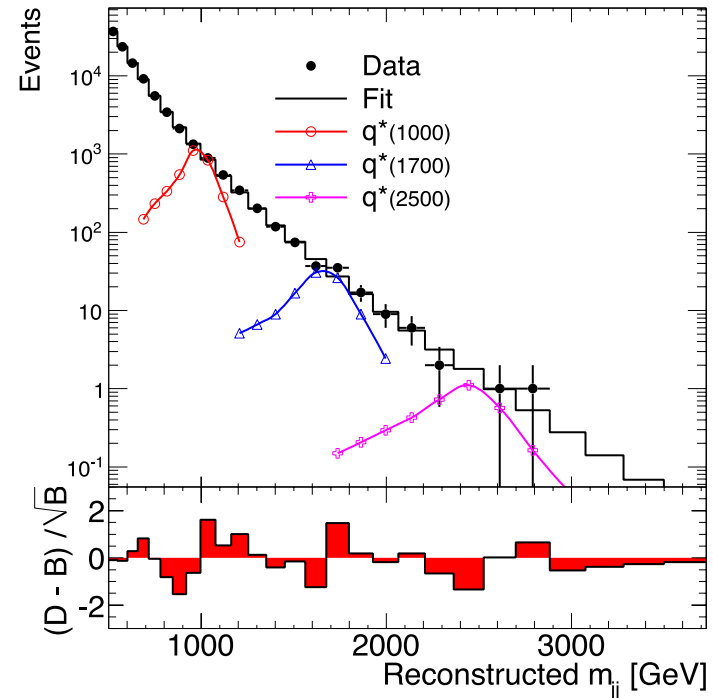


- Important for:
- Test of QCD
  - Search for new resonances decaying into two jets ( $\rightarrow$  next slide)



# In addition to QCD test: Sensitivity to New Physics

- Di-jet mass spectrum provides large sensitivity to new physics  
e.g. Resonances decaying into  $qq$ , excited quarks  $q^*$ , .....
- Search for resonant structures in the di-jet invariant mass spectrum

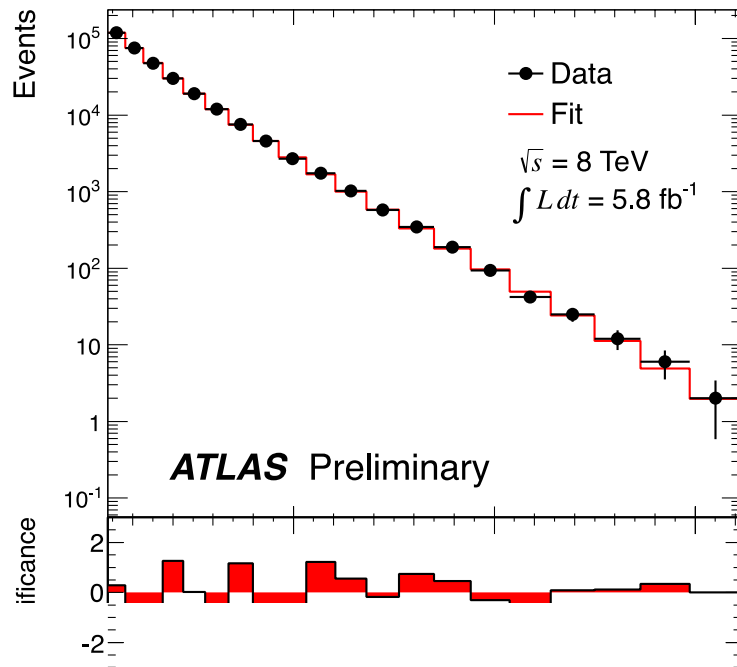


CDF (Tevatron),  $L = 1.13 \text{ fb}^{-1}$ :  $0.26 < m_{q^*} < 0.87 \text{ TeV}$

ATLAS (LHC),  $L = 0.000315 \text{ fb}^{-1}$  exclude (95% C.L)  $q^*$  mass interval  
 $0.30 < m_{q^*} < 1.26 \text{ TeV}$   
 $L = 0.036 \text{ fb}^{-1}$ :  $0.60 < m_{q^*} < 2.64 \text{ TeV}$



- Include new data at  $\sqrt{s} = 8$  TeV (2012)
- Invariant di-jet masses up to 4.1 TeV



CDF (Tevatron),  $L = 1.13 \text{ fb}^{-1}$ :

$0.26 < m_{q^*} < 0.87 \text{ TeV}$

ATLAS (LHC),  $L = 0.000315 \text{ fb}^{-1}$

exclude (95% C.L)  $q^*$  mass interval

$0.30 < m_{q^*} < 1.26 \text{ TeV}$

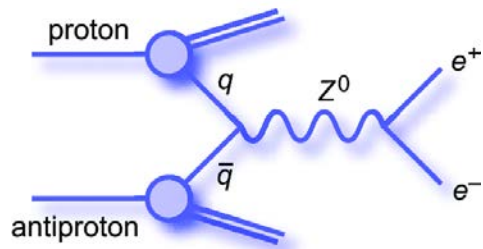
$L = 0.036 \text{ fb}^{-1}$ :

$0.60 < m_{q^*} < 2.64 \text{ TeV}$

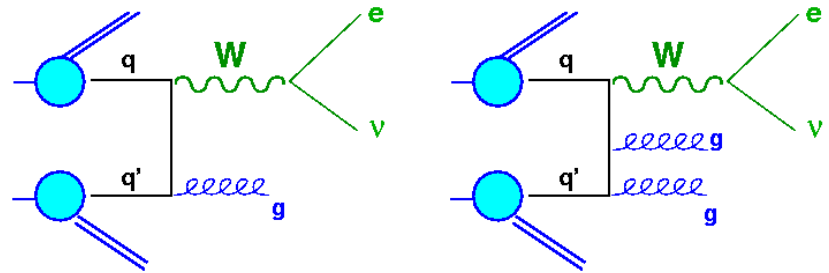
ATLAS (LHC),  $L = 5.8 \text{ fb}^{-1}$ , 8 TeV:

$m_{q^*} < 3.66 \text{ TeV}$

# QCD aspects in $W/Z$ (+ jet) production

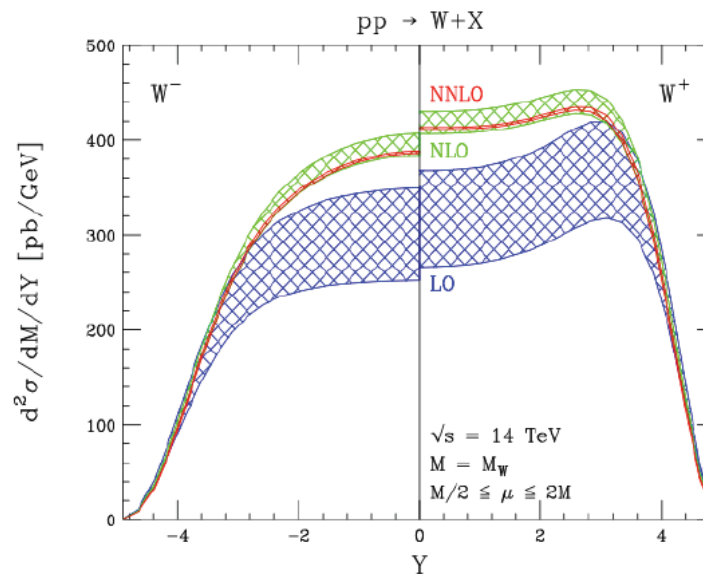
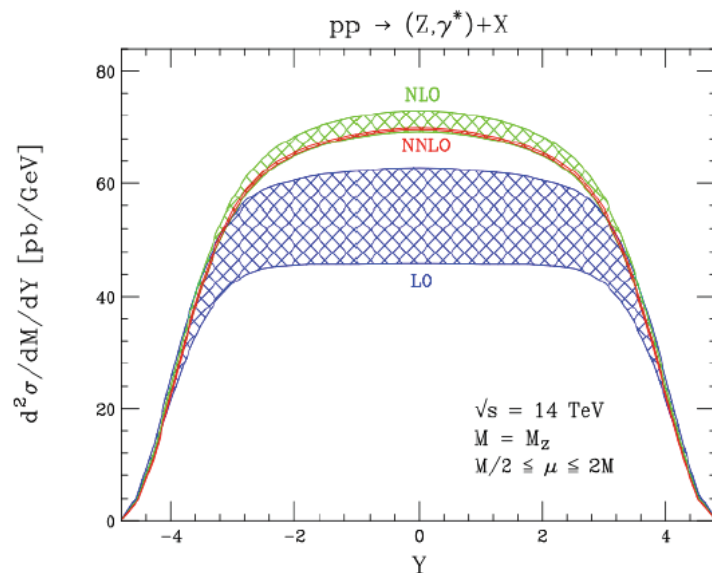
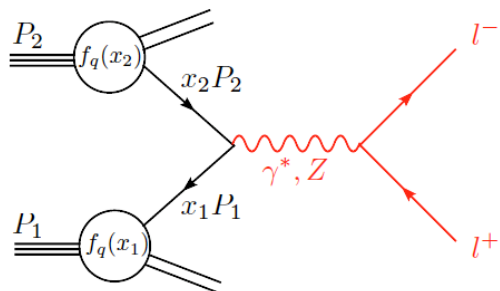


QCD at work

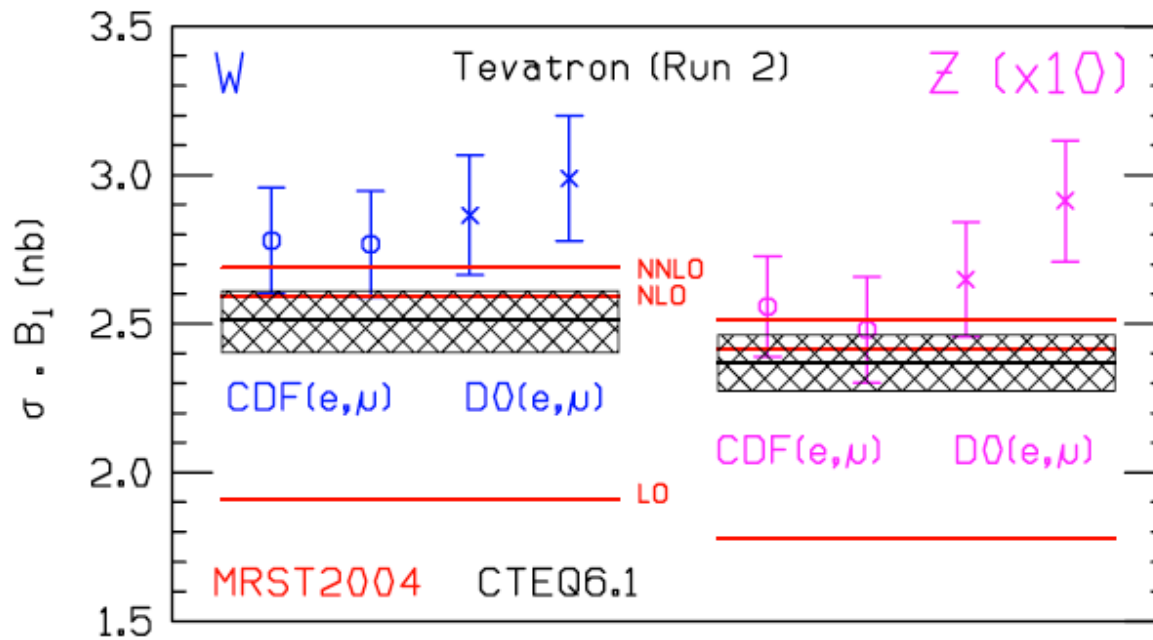


- Important test of NNLO Drell-Yan QCD prediction for the total cross section
- Test of perturbative QCD in high  $p_T$  region (jet multiplicities,  $p_T$  spectra,....)
- Tuning and „calibration“ of Monte Carlos for background predictions in searches at the LHC

# Example: Drell-Yan production of W/Z bosons



*Rapidity distributions for Z and  $W^\pm$  production at LO, NLO, and NNLO*



Predictions for the W and Z total cross section at the Tevatron, using MRST2004 and CTEQ6.1 pdfs, compared with measurements from the CDF and D0 experiments. The MRST predictions are shown at LO, NLO and NNLO. The CTEQ6.1 NLO predictions are shown together with the accompanying error band resulting from pdf uncertainties.

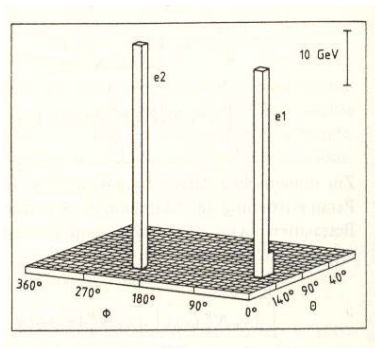
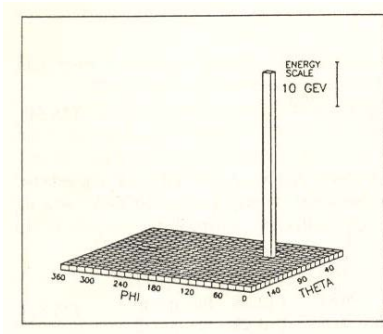
# How do W and Z events look like ?

As explained, leptons, photons and missing transverse energy are key signatures at hadron colliders

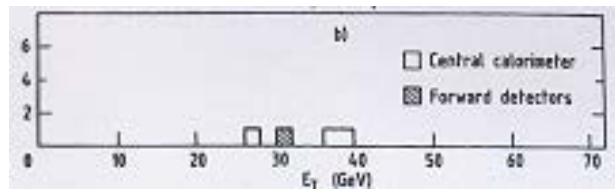
→ Search for leptonic decays:  $W \rightarrow \ell \nu$  (large  $P_T(\ell)$ , large  $E_T^{\text{miss}}$ )  
 $Z \rightarrow \ell \ell$

A bit of history: one of the first W events seen;  
UA2 experiment

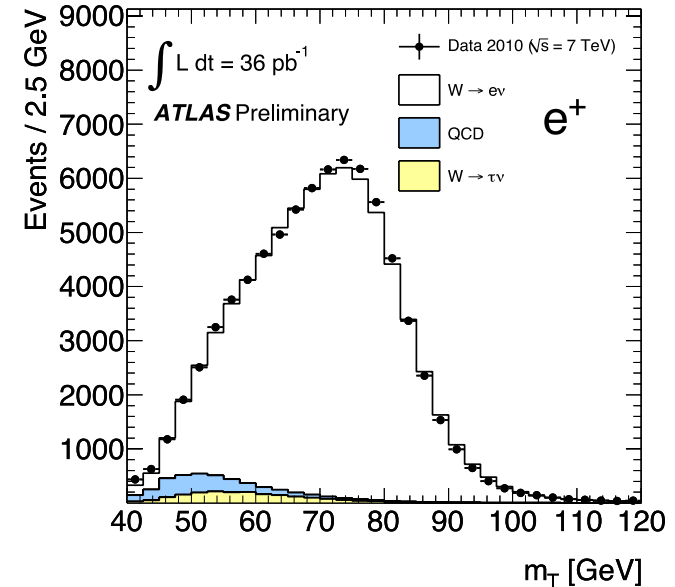
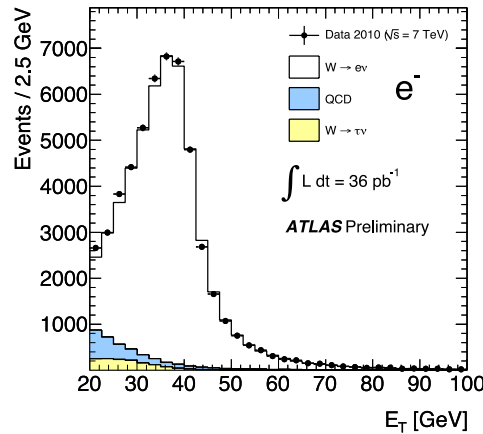
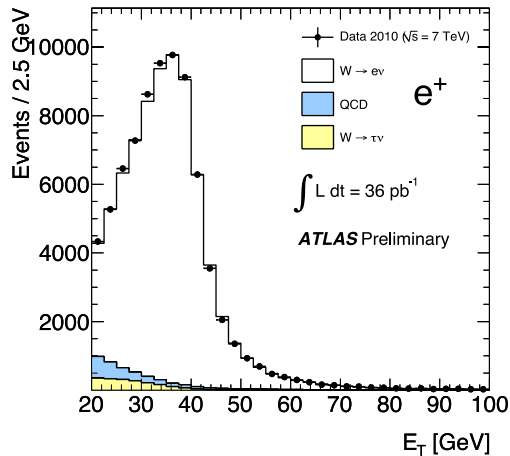
W/Z discovery by the UA1 and UA2 experiments at CERN  
(1983/84)



Transverse momentum of  
the electrons



# W/Z selections in the ATLAS / CMS experiments



## Electrons:

- Trigger: high  $p_T$  electron candidate in calorimeter
- Isolated el.magn. cluster in the calorimeter
- $P_T > 20$  GeV/c
- Shower shape consistent with expectation for electrons
- Matched with a track

## Z $\rightarrow$ ee

- $76 \text{ GeV}/c^2 < m_{ee} < 106 \text{ GeV}/c^2$

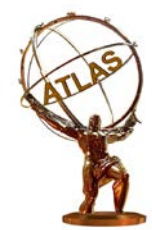
## W $\rightarrow$ ev

- Missing transverse momentum  $> 20$  GeV/c
- Transverse mass  $M_T > 40$  GeV

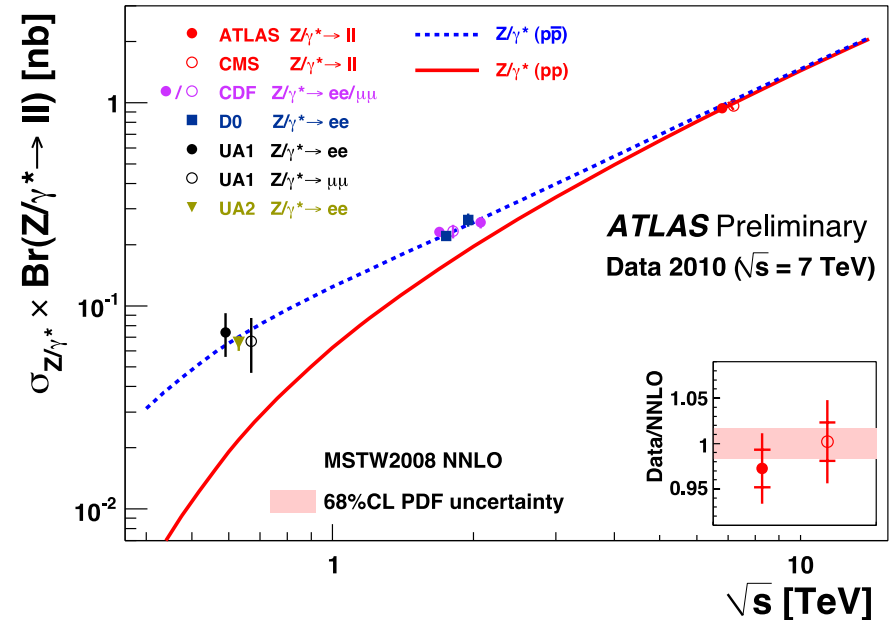
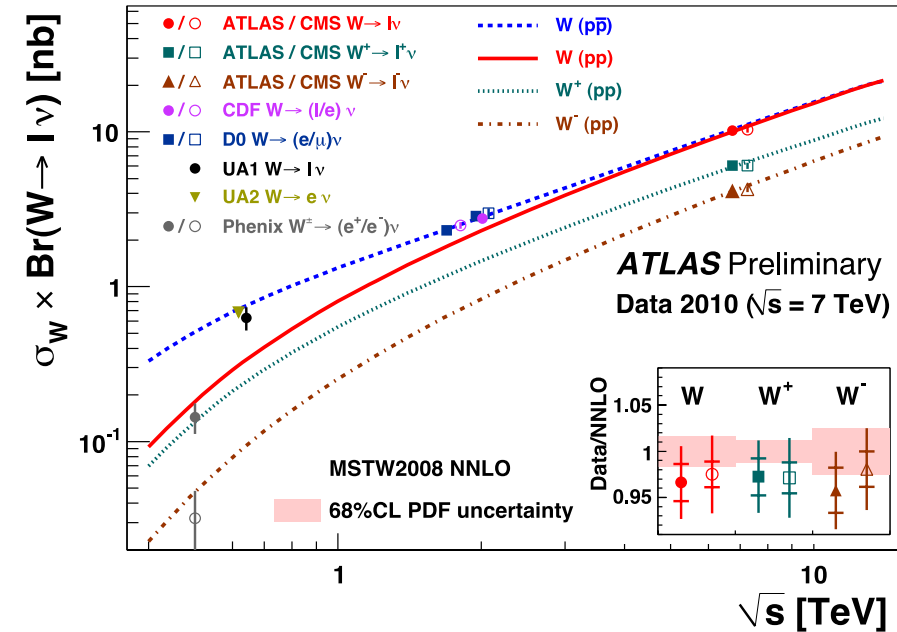
$$M_W^T = \sqrt{2 \cdot P_T^l \cdot P_T^{\nu} \cdot (1 - \cos \Delta\phi^{l,\nu})}$$

Transverse mass

(longitudinal component of the neutrino cannot be measured)



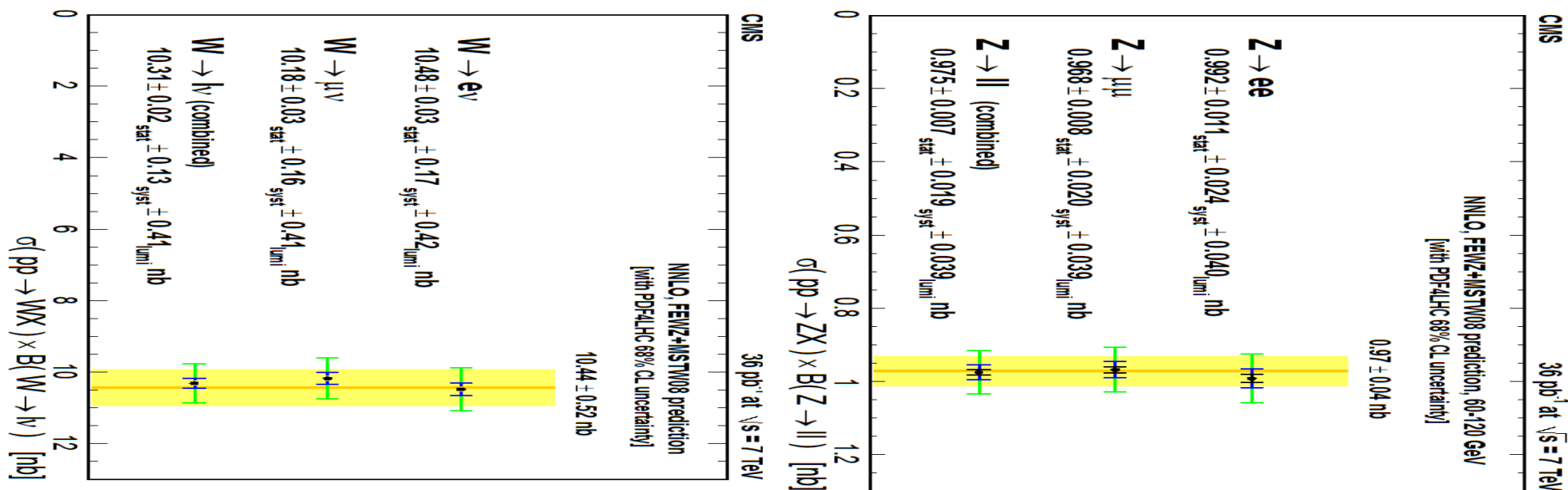
# W and Z production cross sections at hadron colliders



- Theoretical NNLO predictions in very good agreement with the experimental measurements (for pp, p p-bar and as a function of energy)
- Good agreement as well between the ATLAS and CMS experiments

# W and Z production cross sections at the LHC

Measured cross section values in comparison to NNLO QCD predictions:



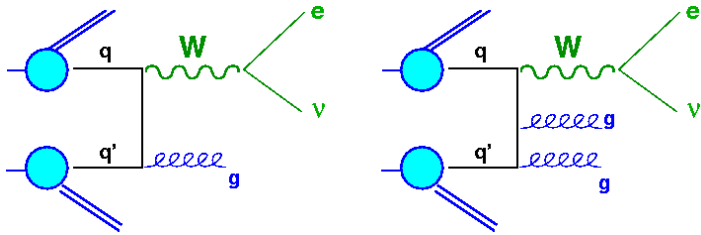
Data are well described by NNLO QCD calculations

C.R.Hamberg et al, Nucl. Phys. B359 (1991) 343.

Precision is already dominated by systematic uncertainties

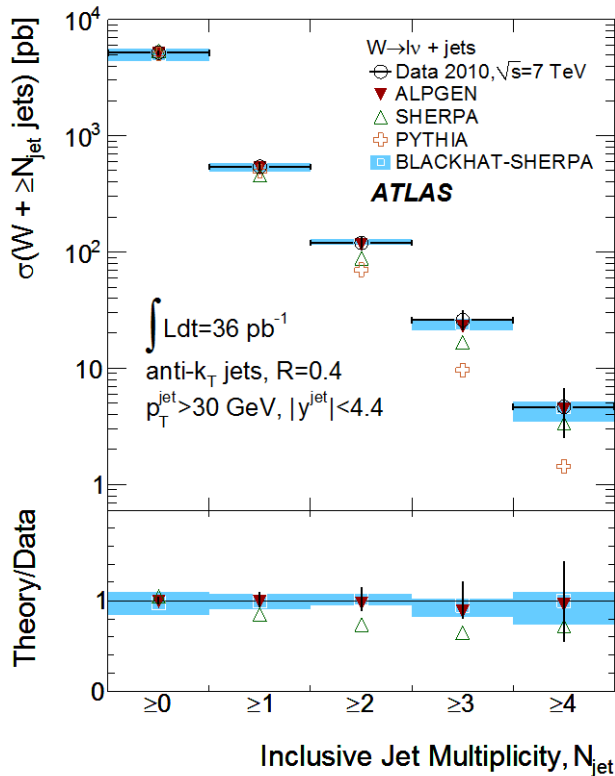
[The error bars represent successively the statistical, the statistical plus systematic and the total uncertainties (statistical, systematic and luminosity). All uncertainties are added in quadrature.]

# W/Z + jet cross section measurements

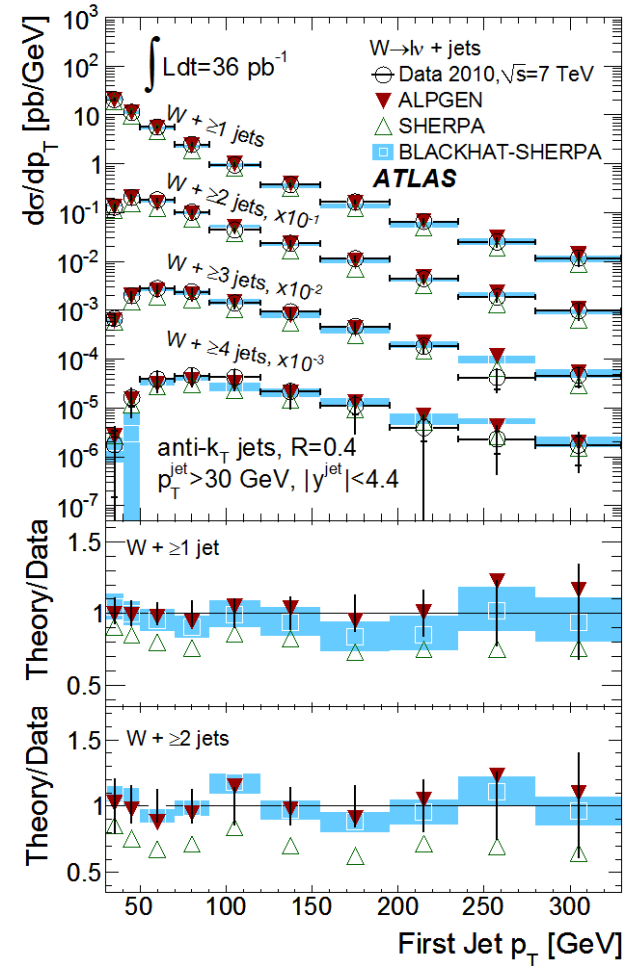


- LO predictions fail to describe the data;
- Jet multiplicities and  $p_T$  spectra in agreement with NLO predictions within errors;

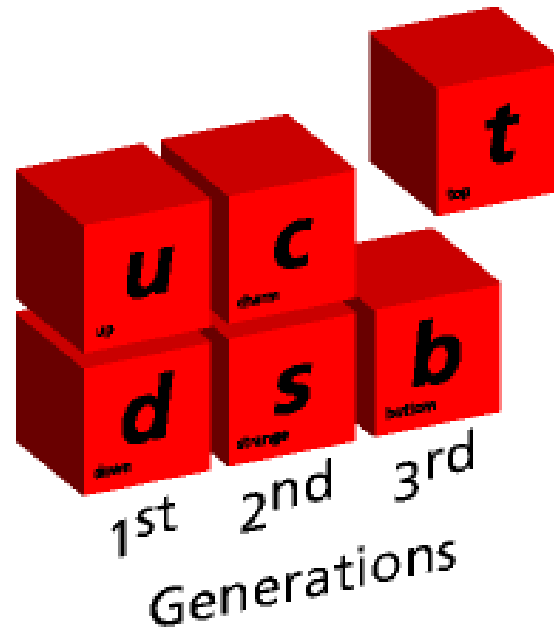
## Jet multiplicities in W+jet production



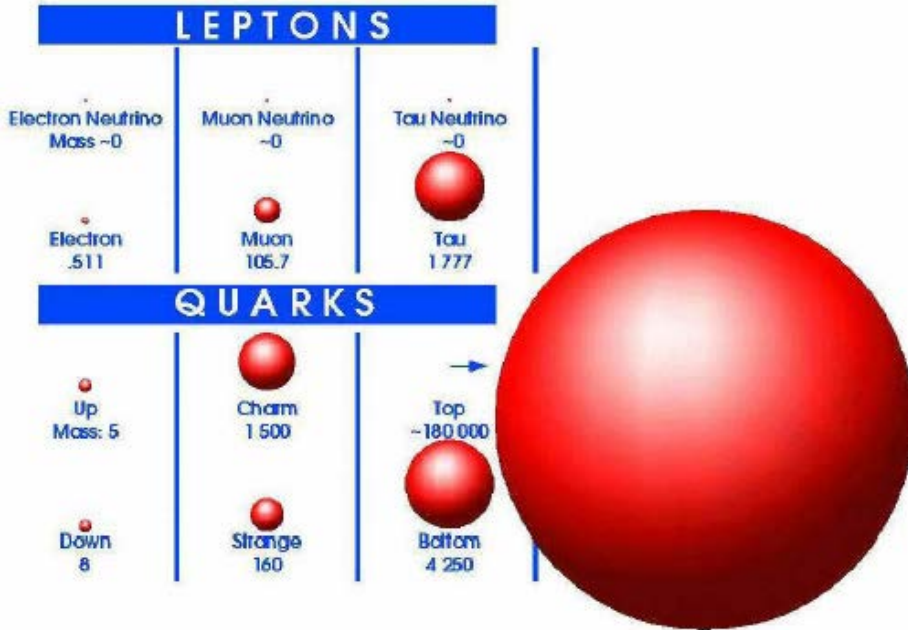
## $p_T$ spectrum of leading jet



# Top Quark Physics



# Why is Top-Quark so important ?



The top quark may serve as a window to **New Physics** related to the electroweak symmetry breaking;

Why is its Yukawa coupling  $\sim 1$  ??

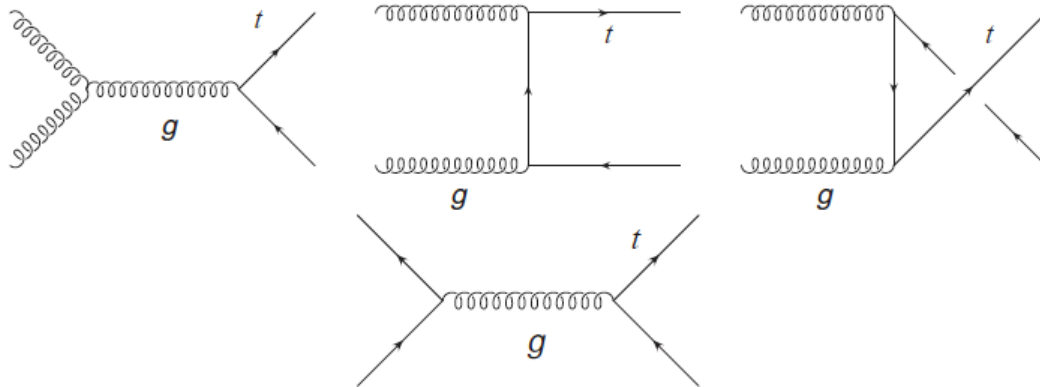
$$M_t = \frac{1}{\sqrt{2}} \lambda_t v$$

$$\Rightarrow \lambda_t = \frac{M_t}{173.9 \text{ GeV} / c^2}$$

- A unique quark: decays before it hadronizes, lifetime  $\sim 10^{-25}$  s  
no “toponium states”  
remember: bb, bd, bs..... cc, cs..... bound states (mesons)
- We still know little about the properties of the top quark:  
mass, spin, charge, lifetime, decay properties (rare decays), gauge couplings, Yukawa coupling,...

# Top Quark Production

Pair production: qq and gg-fusion



Top-quark pair production in the Born approximation.

- NLO corrections completely known
- NNLO partly known

approximate NNLO results:

$$\sigma_{\text{LHC}} = (887_{-33}^{+9} (\text{scale})_{-15}^{+15} (\text{PDF})) \text{ pb} \quad (14 \text{ TeV}),$$

$$\sigma_{\text{TeV}} = (7.04_{-0.36}^{+0.24} (\text{scale})_{-0.14}^{+0.14} (\text{PDF})) \text{ pb} \quad (1.96 \text{ TeV}).$$

# Top Quark Decays

BR ( $t \rightarrow Wb$ )  $\sim 100\%$

Dilepton channel:

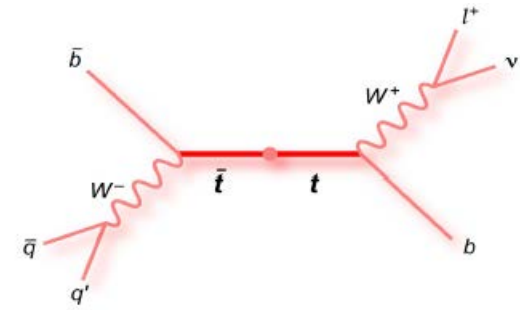
Both  $W$ 's decay via  $W \rightarrow \ell\nu$  ( $\ell=e$  or  $\mu$ ; 4%)

Lepton + jet channel:

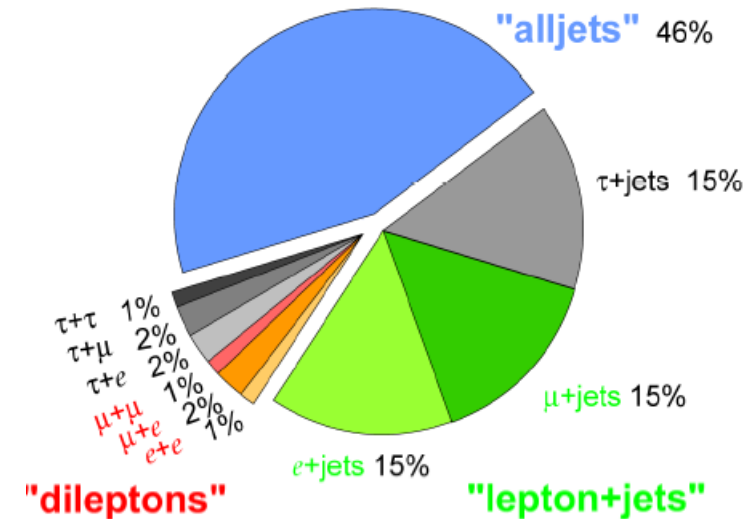
One  $W$  decays via  $W \rightarrow \ell\nu$  ( $\ell=e$  or  $\mu$ ; 30%)

Full hadronic channel:

Both  $W$ 's decay via  $W \rightarrow qq$  (46%)



Top Pair Branching Fractions

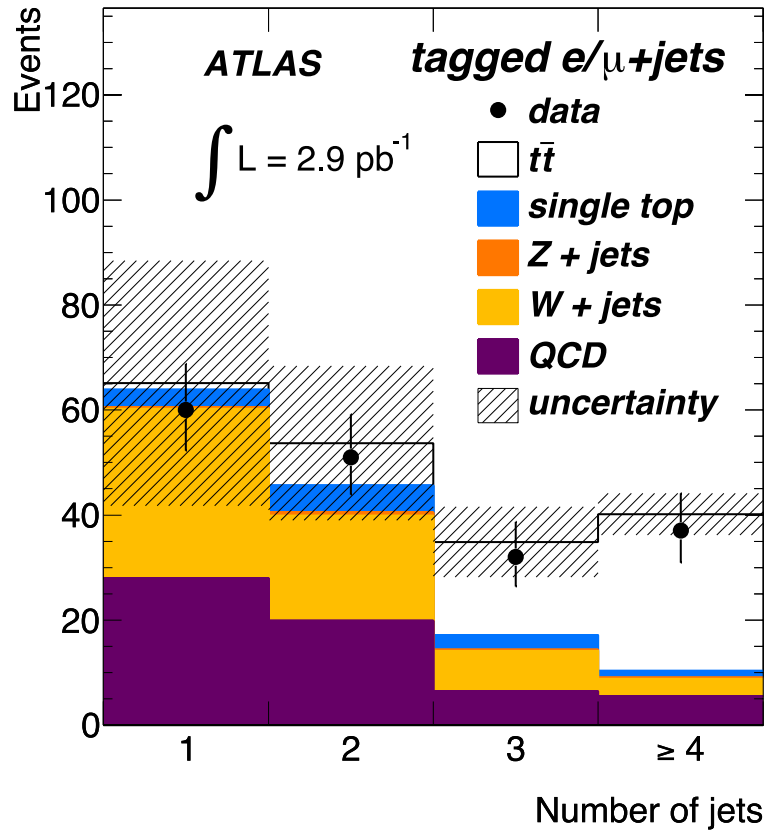


Important experimental signatures: - Lepton(s)

- Missing transverse momentum
- b-jet(s)



# First results on top production from the LHC



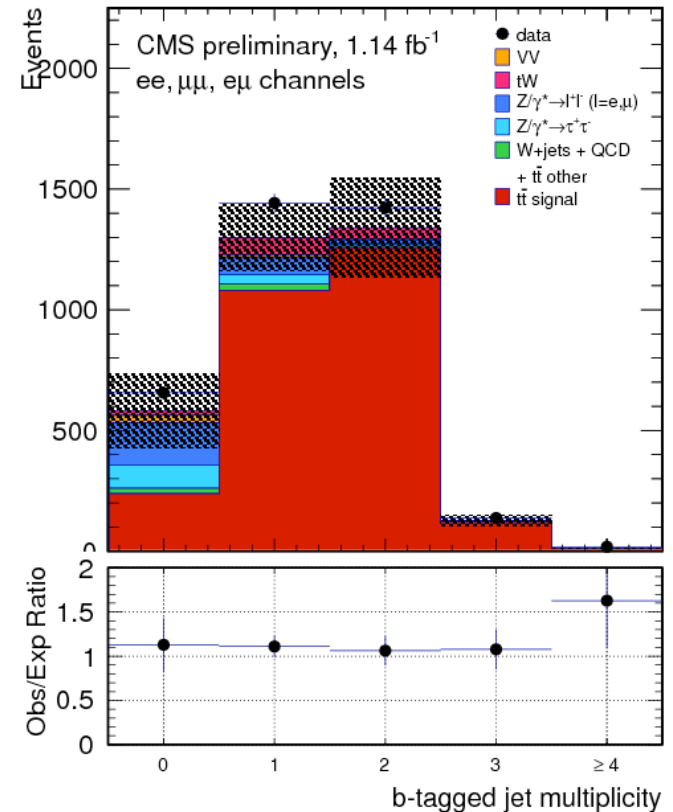
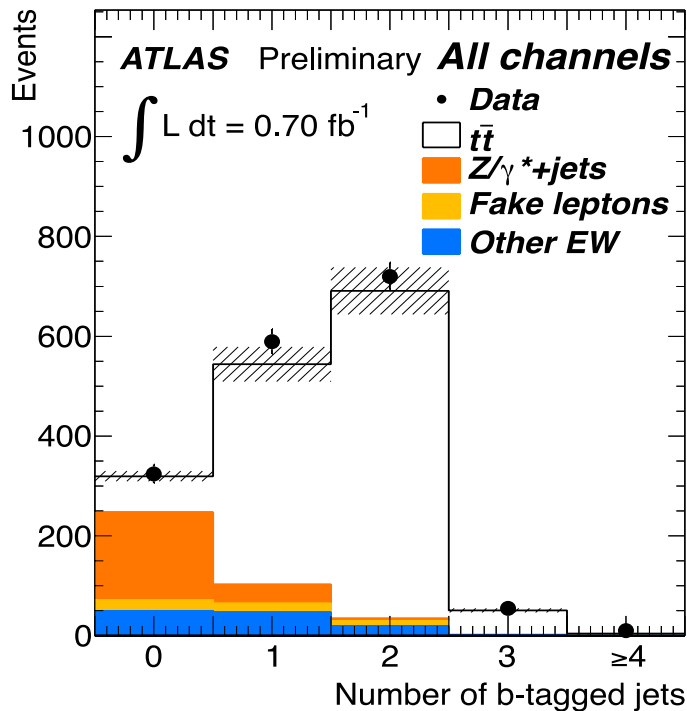
## Event Selection:

- Lepton trigger
- One identified lepton ( $e, \mu$ ) with  $p_T > 20 \text{ GeV}$
- Missing transverse energy:  $E_T^{\text{miss}} > 35 \text{ GeV}$  (significant rejection against QCD events)
- Transverse mass:  $M_T(l, \nu) > 25 \text{ GeV}$  (lepton from  $W$  decay in event)
- One or more jets with  $p_T > 25 \text{ GeV}$  and  $\eta < 2.5$

# Top-quark production measured in many different decay modes

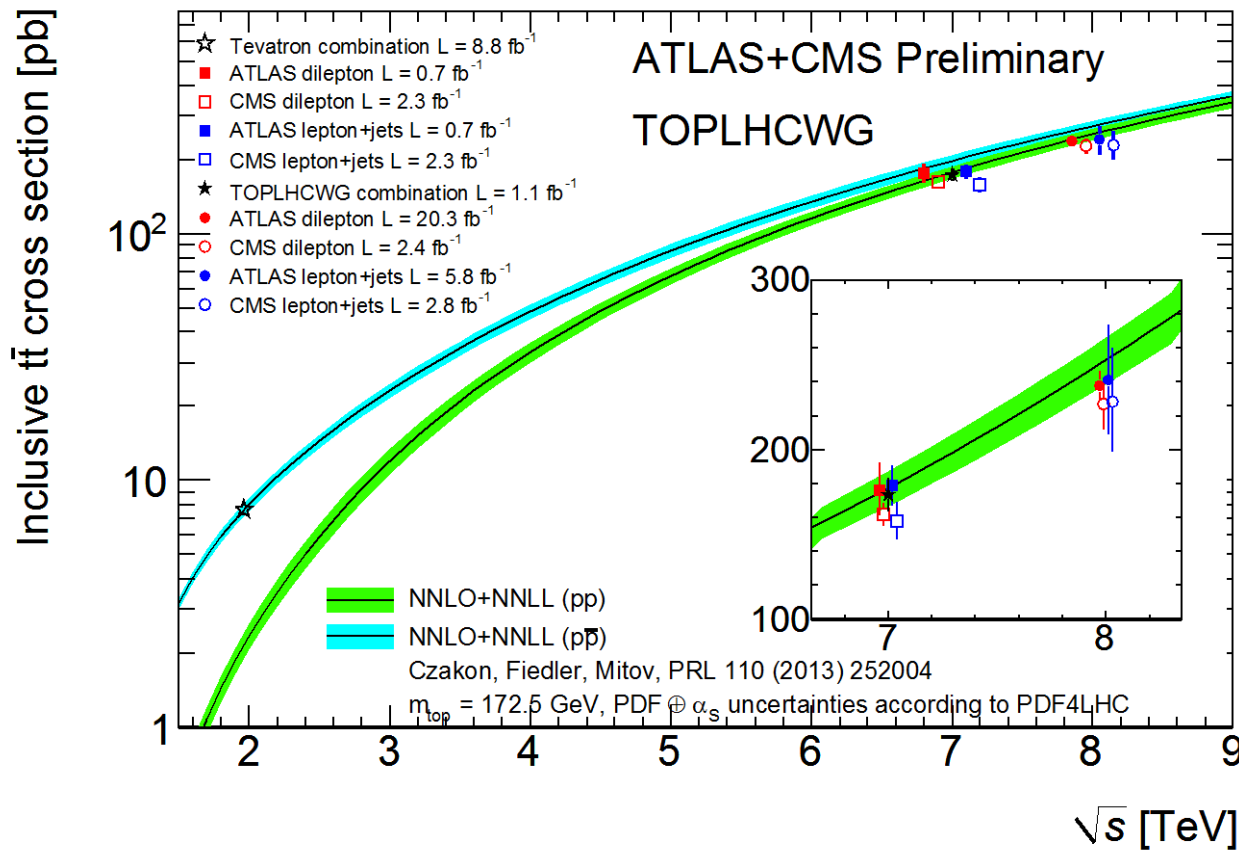
(i) Di-lepton selection in both ATLAS and CMS (0.7 fb<sup>-1</sup> – 1.14 fb<sup>-1</sup>)

Multiplicity distributions of b-tagged jets  
(small backgrounds, mainly from Z+jet production)





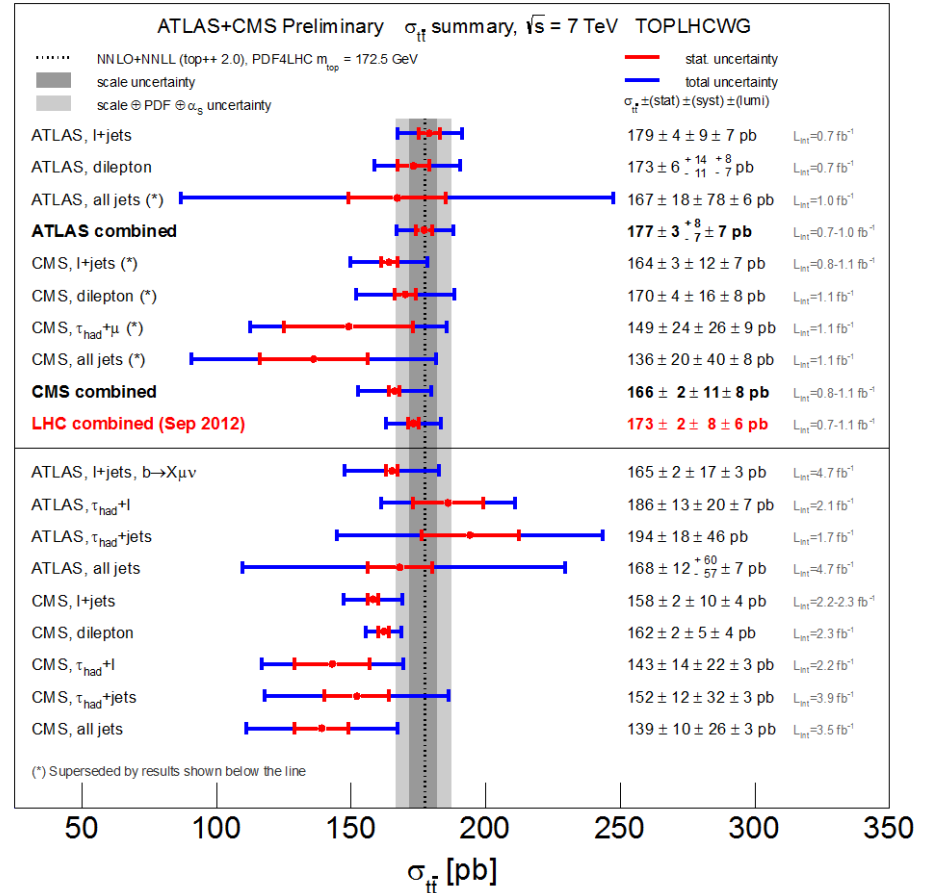
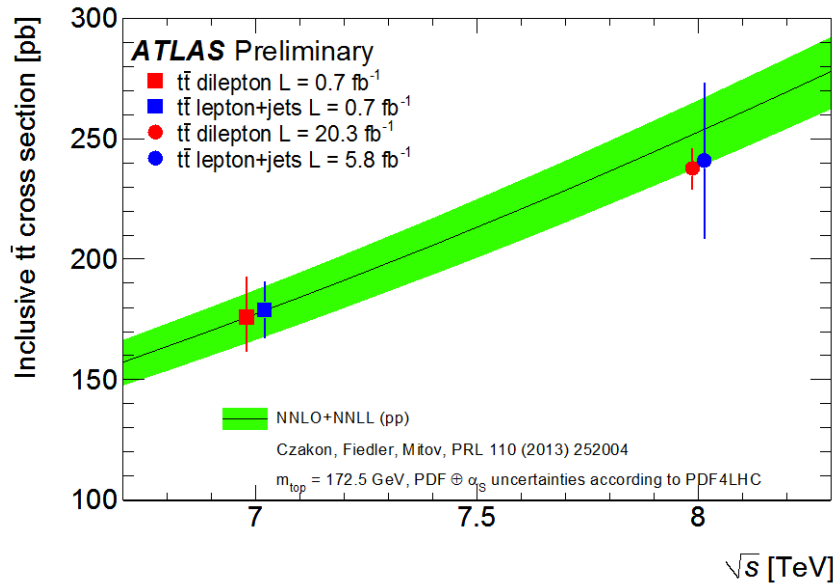
# Top pair production cross section measurements



- Perturbative QCD calculations (approx. NNLO) describe the data well;
- The two LHC experiments agree within the systematic uncertainties

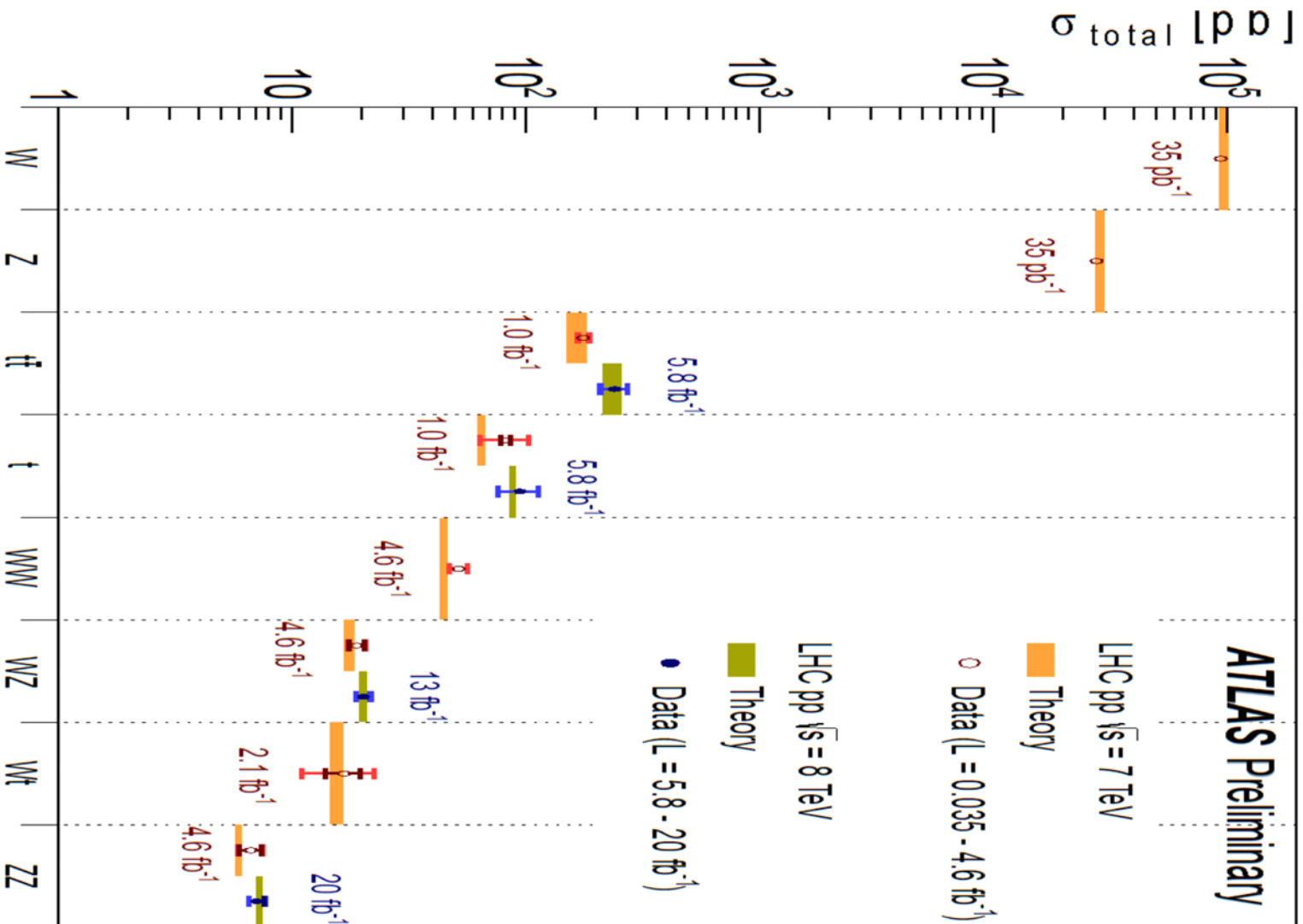


# Results on top pair production cross section measurements in various final states

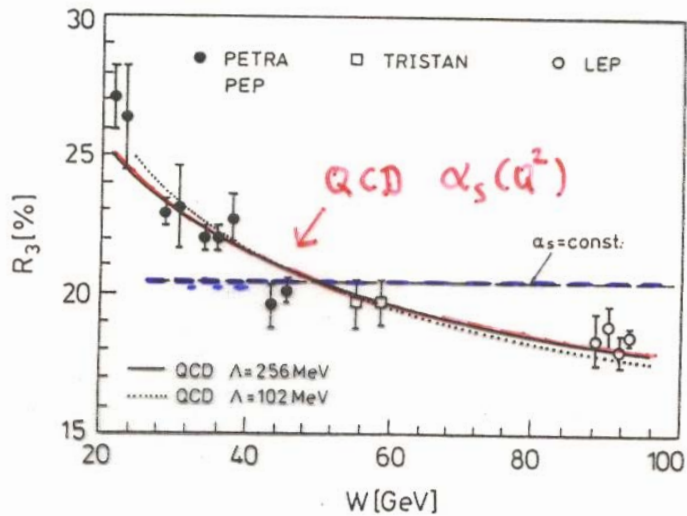


- Good agreement between the various channels and between the two experiments

# The Standard Model at the LHC



## 8.4 Bestimmung der starken Kopplungskonstanten $\alpha_s$



Energieabhängigkeit des relativen Anteils von Drei-Jet-Ereignissen

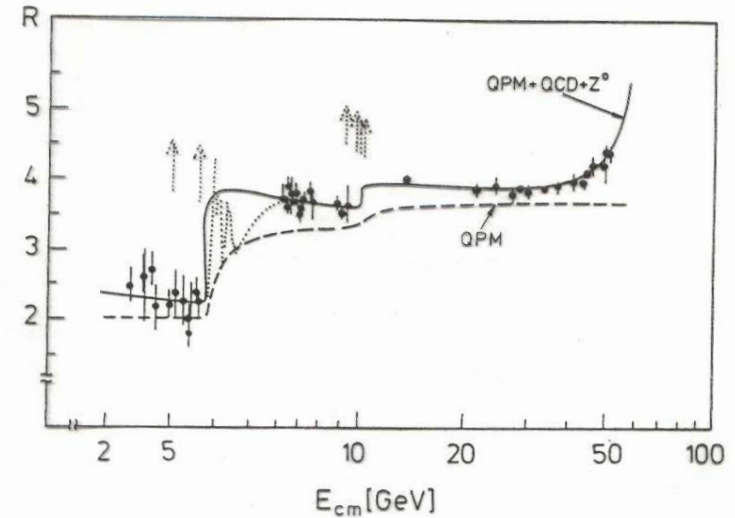
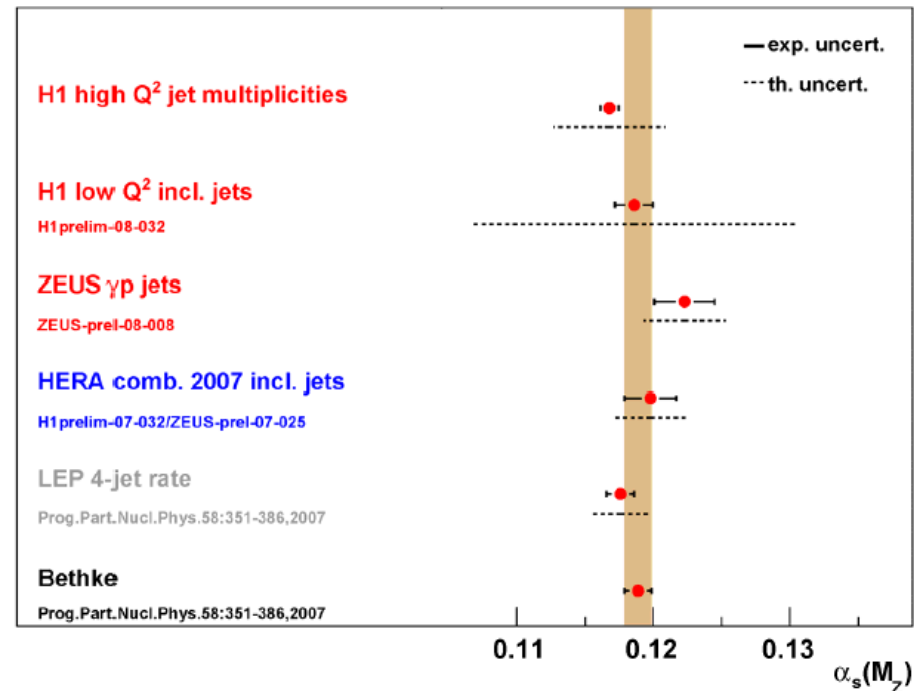
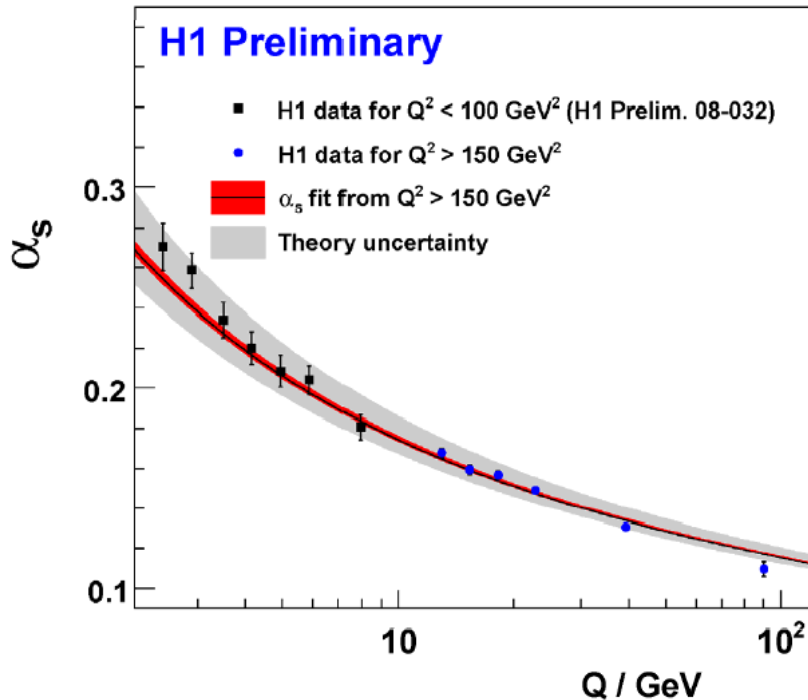


Abb. 12.20. Daten für das Verhältnis  $R$  und die Vorhersagen des Quark-Parton-Modells (QPM) und der QCD. Die  $\psi$ - und  $\Upsilon$ -Resonanzen sind gestrichelt angedeutet. (Marshall 1989).

# $\alpha_s$ from Deep Inelastic Scattering

- Inclusive jet and 2/3 jet production allow for a precise test of the running of  $\alpha_s$  over two orders of magnitude
- Values are compatible with LEP and the world average (precision at level of 3-4%)



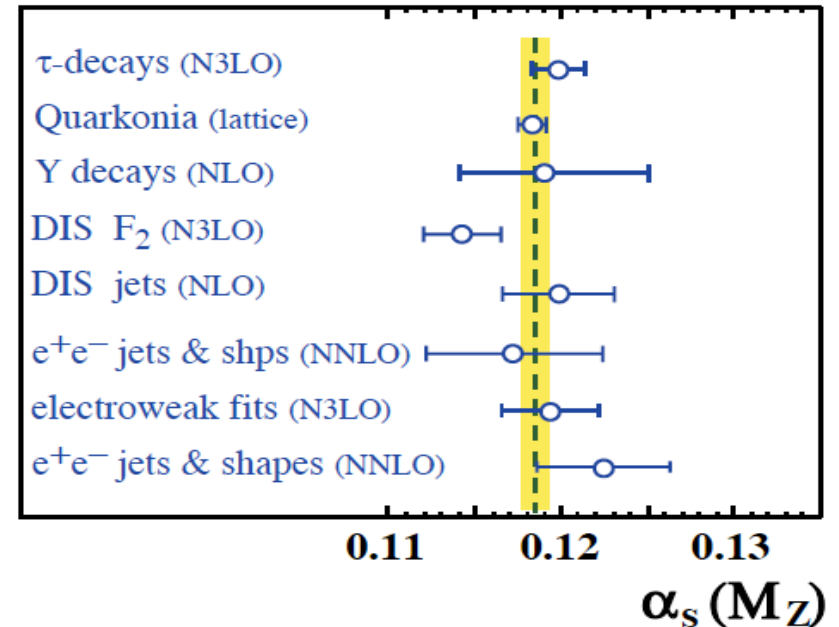
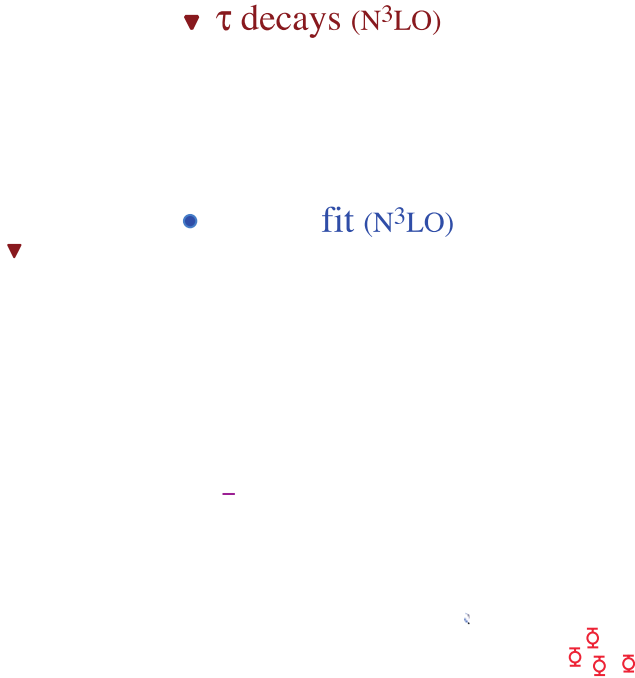
**Jets in DIS ( $Q^2 > 150 \text{ GeV}^2$  - H1):**

$$\alpha_s(M_Z) = 0.1168 \pm 0.0007(\text{exp.})^{+0.0046}_{-0.0030}(\text{th.}) \pm 0.0016(\text{PDF})$$

**Jets in  $\gamma p$  (ZEUS):**

$$\alpha_s(M_Z) = 0.1123 \pm 0.0022(\text{exp.}) \pm 0.0030(\text{th.})$$

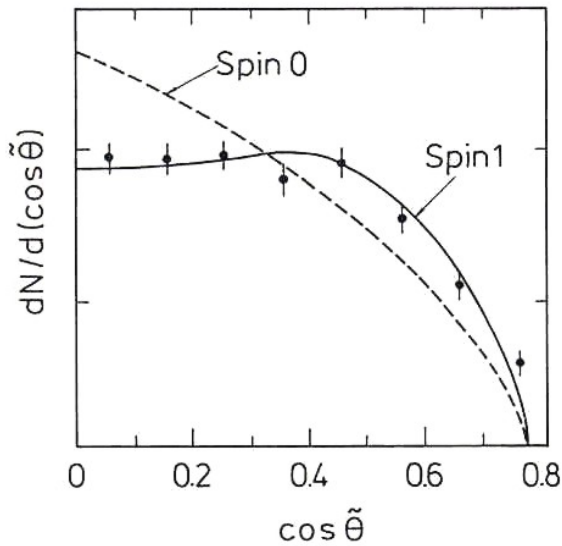
# Messergebnisse von $\alpha_s$ in verschiedenen Experimenten



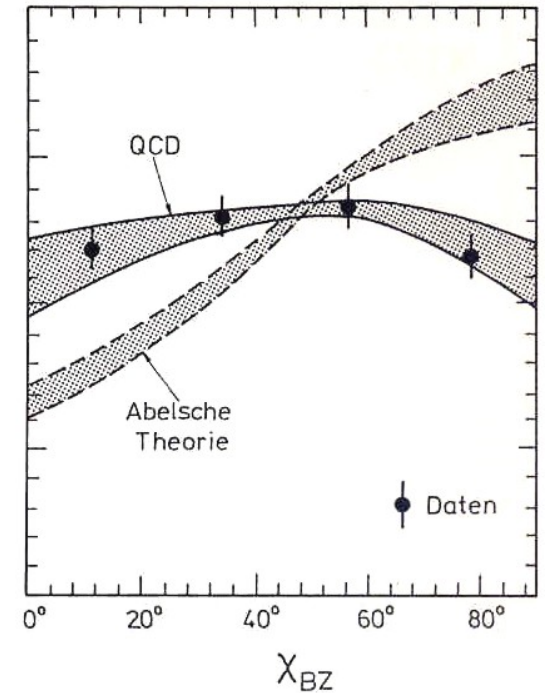
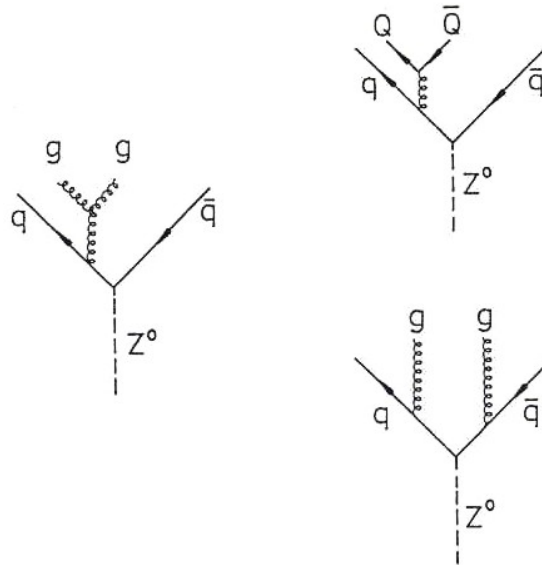
Summary of measurements of  $\alpha_s$  as a function of the respective energy scale  $Q$  (from Particle Data Group).

Summary of measurements of  $\alpha_s(m_Z^2)$ , used as input for the world average value (from Particle Data Group).

## 8.5 Evidenz für Spin-1 und Selbstkopplung der Gluonen



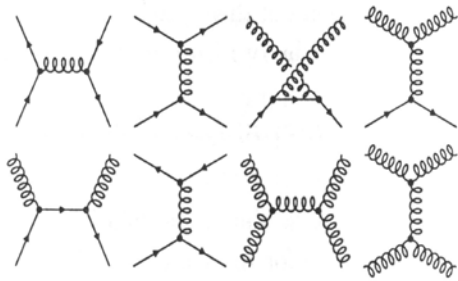
Verteilung des Ellis-Karliner-Winkels in Drei-Jet-Ereignissen (TASSO 1980).



Graphen für die Vier-Jet-Produktion und die experimentell bestimmte Verteilung des Bengtsson-Zerwas-Winkels im Vergleich zur QCD-Rechnung und zu Modellen ohne Gluon-Selbstkopplung (Zerwas 1992).

# Theoretical calculations of two-jet production in ppbar collisions

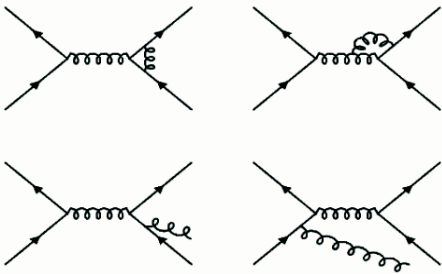
## Leading order



$$\frac{d\hat{\sigma}}{d\hat{t}}(ab \rightarrow cd) = \frac{|M|^2}{(16\pi\hat{s}^2)}$$

Subprocess	$ M ^2/g_s^4$	$ M(90^\circ) ^2/g_s^4$
$qq' \rightarrow qq'$ $q\bar{q}' \rightarrow q\bar{q}'$	$\frac{4}{9} \frac{\hat{s}^2 + \hat{u}^2}{\hat{t}^2}$	2.2
$qq \rightarrow qq$	$\frac{4}{9} \left( \frac{\hat{s}^2 + \hat{u}^2}{\hat{t}^2} + \frac{\hat{s}^2 + \hat{t}^2}{\hat{u}^2} \right) - \frac{8}{27} \frac{\hat{s}^2}{\hat{u}\hat{t}}$	3.3
$q\bar{q} \rightarrow q'\bar{q}'$	$\frac{4}{9} \frac{\hat{t}^2 + \hat{u}^2}{\hat{s}^2}$	0.2
$q\bar{q} \rightarrow q\bar{q}$	$\frac{4}{9} \left( \frac{\hat{s}^2 + \hat{u}^2}{\hat{t}^2} + \frac{\hat{t}^2 + \hat{u}^2}{\hat{s}^2} \right) - \frac{8}{27} \frac{\hat{u}^2}{\hat{s}\hat{t}}$	2.6
$q\bar{q} \rightarrow gg$	$\frac{32}{27} \frac{\hat{u}^2 + \hat{t}^2}{\hat{u}\hat{t}} - \frac{8}{3} \frac{\hat{u}^2 + \hat{t}^2}{\hat{s}^2}$	1.0
$gg \rightarrow q\bar{q}$	$\frac{1}{6} \frac{\hat{u}^2 + \hat{t}^2}{\hat{u}\hat{t}} - \frac{3}{8} \frac{\hat{u}^2 + \hat{t}^2}{\hat{s}^2}$	0.1
$qg \rightarrow qq$	$\frac{\hat{s}^2 + \hat{u}^2}{\hat{t}^2} - \frac{4}{9} \frac{\hat{s}^2 + \hat{u}^2}{\hat{u}\hat{s}}$	6.1
$gg \rightarrow gg$	$\frac{9}{4} \left( \frac{\hat{s}^2 + \hat{u}^2}{\hat{t}^2} + \frac{\hat{s}^2 + \hat{t}^2}{\hat{u}^2} + \frac{\hat{u}^2 + \hat{t}^2}{\hat{s}^2} + 3 \right)$	30.4

## ...some NLO contributions



- Right: Results of the LO matrix elements for the various scattering processes, expressed in terms of the Mandelstam variables  $s$ ,  $t$  and  $u$ . (Kripfganz et al, 1974);
- $gg$  scattering is the dominant contribution under  $\eta = 0$ ;  
(sensitivity to gluons, sensitivity to gluon self-coupling, as predicted by QCD)
- NLO predictions have meanwhile been calculated (2002).